OCEAN TIDE LOADING, BODY TIDE AND POLAR MOTION EFFECTS ON VERY LONG BASELINE INTERFEROMETRY

SPIROS D. PAGIATAKIS

December 1982

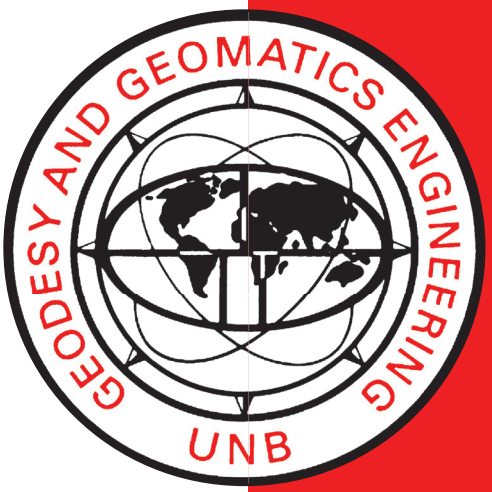

TECHNICAL REPORT
NO. 92

PREFACE

In order to make our extensive series of technical reports more readily available, we have scanned the old master copies and produced electronic versions in Portable Document Format. The quality of the images varies depending on the quality of the originals. The images have not been converted to searchable text.

OCEAN TIDE LOADING, BODY TIDE AND POLAR MOTION EFFECTS ON VERY LONG BASELINE INTERFEROMETRY

SPIROS D. PAGIATAKIS

PREFACE

This report is an unaltered printing of the author's M.Sc.E. thesis, entitled "Ocean Tide Loading, Body Tide and Polar Motion effects on Very Long Baseline Interferometry", submitted to this Department in December, 1982.

The principle thesis advisor for this research was Dr. Petr Vaníček. Details of financial support and other assistance rendered are given in the acknowledgements.

ABSTRACT

Response functions for radial and horizontal displacements, gravity perturbations and tilt due to ocean tide loading were derived, using Green's functions computed by Farrell for the Gutenberg-Bullen A earth model. The general procedure of convolving response functions with an ocean tide model was used in this study. The ocean tide model used was that developed by Schwiderski, using the six leading constituents of the tidal spectrum.

The derived response functions for gravity perturbations were tested against existing determinations of the effect from actual data, at eight stations covering the whole earth. This comparison yielded a mean of the absolute differences between the observed gravity perturbations and those obtained in this study of 0.32 μGal with a root-mean-square scatter of 0.19 μGal.

A body tide model was also developed. The ephemerides of the moon and the sun were based on approximate formulae. Tests performed on the above approximate formulae indicated that the right ascension and declination of the moon and the sun can be obtained with an accuracy of the order of one minute of arc with respect to the values obtained in the astronomical ephemerides. This uncertainty affects the evaluation of

the radial displacement of the terrain by less than 1 cm.

The mathematical models for terrain deformations due to body tide and ocean loading as well as an interpolation procedure for polar motion were added to the Canadian VLBI software package. VLBI data pertaining to the observing period May 1977, obtained by a 3-station VLBI array were used to test the above models. Due to the large standard errors of these data, there is little that can be concluded from the analysis at this time. There is an improvement in the distribution of the delay-rate residuals. Their root-mean-square scatter decreases by 9.2×10^{-5} picoseconds/second while the root-mean-square scatter of the group-delay residuals increases by 3 picoseconds. Co-range and co-tidal charts for north America were also produced, showing the radial and the horizontal displacements of the terrain due to load for the six leading tidal constituents.

TABLE OF CONTENTS

LIST OF TABLES

LIST OF FIGURES

ACKNOWLEDGEMENTS

This research was financially supported in part by the Earth Physics Branch, Ottawa (EMR grants #7-3-80 and #70-3-82). Financial assistance to the author has been also provided by the Surveying Engineering Department, through graduate teaching and research assistantships.

I wish to thank my supervisor Prof. Dr. Petr Vaníček for introducing me to the fascinating field of ocean tide loading, for his guidance, constant support and encouragement. His rigorous and detailed criticism of the manuscript has been of great profit to me.

I am sincerely grateful to Prof. Dr. Richard Langley for his continuous help when Prof. Vaníček was on leave from U.N.B. His constant supply of references and his patience in listening to the various problems as well as his demonstration of the use of the Canadian VLBI software package are greatfully acknowledged.

Thanks are also extended to Mrs. Laura Mills and the staff of the Computing Centre of the University of New Brunswick for their valuable assistance.

Dr. Jim Merriam of the Physics Department, Memorial University of Newfoundland and Dr. Clyde Goad of NGS/NOS/NOAA have also given assistance to this work.

I wish to extend my appreciation to my colleagues of the Geodesy Group in the Department of Surveying Engineering and particularly to my friends Niko Christou and Tom Inzinga, who took the time and trouble to discuss with me all my problems.

Last but not least I wish to express my sincere thanks to my wife Roula for her encouragement and understanding.

CHAPTER I

INTRODUCTION

1.1. General Background and Outline of the Present Study.

The earth within the system of all celestial bodies is influenced by varying gravitational forces which produce deformations, generally called tides. The moon and the sun exert the most predominant forces whereas the forces due to the other celestial bodies are very small and can be neglected without any loss of accuracy. Concentrating on the deformations of the solid earth one talks about body tides, whereas tidal variations of sea level are called ocean tides.

The body tide is rather well understood. Part of the deformation of the earth's crust under time varying forces is also due to the variations coming from the varying ocean tide which produces the so called "load tide". As does the body tide, the load tide influences geodetic quantities observed on the surface of the earth such as gravity, tilt and terrain level. The body tide is a rather smoothly-varying phenomenon, depending upon the overall elastic properties of the earth, whereas the load

tide is more irregular due to the local features of the driving forces and the irregularities of the earth's lithosphere. Using the recent achievements in space geodesy, such as VLBI (very long baseline interferometry) and laser ranging, one can obtain repeatabilities of the order of a few centimetres for continental or transcontinental baseline lengths.

The deformation of the terrain due to ocean tide loading is of the order of a few centimetres depending on the locality and therefore it may play an important role for increasing the accuracy of VLBI baselines to the centimetre level.

The primary objective of this study was to develop a mathematical model which would evaluate the radial and horizontal displacements of the terrain due to ocean tide loading, to derive an improved approximation procedure for polar motion using existing data coming mainly from BIH (Bureau International de l' Heure) Circular D tables and to update the Canadian VLBI software package to account for the above effects.

As a mathematical model for the ocean tide loading, the general procedure of convolving a known ocean tide model with appropriate Green's functions was used in this study. The ocean tide model used, is that developed by Schwiderski (1978), who uses empirical tidal constants

coming from about 2,000 tide gauges scattered all over the globe. These empirical data were used as boundary conditions for the solution of the Navier-Stokes tidal equations on a 1°x1° spherical grid system in connection with hydrodynamically-defined bathymetry recognizing barrier effects of large boundary and bottom anomalies. The tidal equations were augmented by turbulent friction terms with novel mesh-area, eddy-viscosity and bottom-friction coefficients (Schwiderski, 1978).

In this study, the six leading constituents of the tidal spectrum were used. Schwiderski's ocean tide model predicts the tidal height with an accuracy of better than 5 cm anywhere in the open oceans for each of the leading tidal constituents. This estimate is based upon the worldwide agreement of the computed tidal constants with empirical data, which have the same accuracy. The accuracy for the coastal waters is expected to be worse due to local effects such as roughness of the sea bottom and a-priori resolution limits of 1°x1° imposed on the solution of the discrete tidal equations.

The Green's functions were derived from the geometry of the load effect and they involve the infinite summation of the load deformation coefficients with the Legendre polynomials. This infinite summation was evaluated indirectly using the Green's functions computed

by Farrell (1972).

Although gravity perturbations do not affect VLBI observations directly, Green's functions were derived for gravity, to indirectly test the present technique against existing actual determinations of gravity perturbations.

Lagrange interpolation was used to determine the position of the earth's pole of rotation using BIH Circular D smoothed values. The software, which exists at the Department of Surveying Engineering was provided by the M.I.T. Department of Earth and Planetary Sciences and was integrated into the Canadian VLBI software package to give an improved estimate of the pole position. Data for the position of the pole are stored on tape and include information for the time span January 1969-April 1981.

1.2. Green's Functions and Load Deformation Coefficients.

The evaluation of the load effect can be done through a convolution integral by convolving an ocean tide model with appropriate Green's functions (integration kernels). The geometry of the effect dictates the shape of such Green's functions. These functions include infinite summation of the load deformation coefficients multiplied by the Legendre polynomials. To evaluate this infinite series one must know the infinitely many load deformation

coefficients. A direct evaluation of these would require infinitely many observations of the load effect, which clearly are not available. Instead, an earth model must be postulated and the load deformation coefficients can be evaluated theoretically through the numerical solution of the equations of equilibrium of the earth. Such a solution is given by Longman (1962; 1963). Longman evaluated the load deformation coefficients up to order 40. Farrell (1972) determined these coefficients up to order 10,000 considering the Gutenberg-Bullen A earth model and tabulated (ibid, Table A3) Green's functions for different effects.

1.3. General Context and Contributions of This Study.

The Canadian VLBI software package GEOAIM (GEOdetic Analysis of Interferometric Measurements), which was developed initially at York University, Toronto, Ontario (Langley, 1979), accounted only for the body tide component of the earth tide. The correction for polar motion assumed a constant value for a whole observing period. As mentioned earlier, corrections of VLBI observations due to ocean tide loading and an interpolation routine for polar motion are necessary to increase the accuracy of the determination of the baselines to the centimetre level. Methods used in

previous studies of this kind have had varying degrees of success. In this work, an alternative approach is developed for the evaluation of the load effects. Green's functions for terrain deformations and gravity perturbations are derived, using Green's functions computed by Farrell (1972) (Chapter III). A Green's function for the relative tilt of the terrain is also derived (Appendix B).

A contribution is also made in the evaluation of load response directly beneath the load where there is a singularity in the formulation of Green's functions. Although not of concern in evaluating displacements of VLBI stations, this problem is treated for completeness in Appendix C based on the theory of Boussinesq (1885).

Another contribution is made by drawing co-range and co-tidal charts for the radial and horizontal displacements of the terrain due to ocean loading for North America, which represents a new source of information for deformations of this kind (Appendix A).

In terms of improving the computational efficiency of GEOAIM, a contribution is made by developing a mathematical model for body tide deformations (Chapter IV). The ephemerides of the moon and the sun are determined through approximate formulae rather than from tables (e.g. Merriam, 1978).

Another contribution is made by modifying an existing routine (Chapter IV) for the determination of polar motion.

Finally, so that the software developed here can easily be applied by others as separate routines, it has been documented and is now readily available from the Surveying Engineering Department at U.N.B. (Appendix G).

CHAPTER II

LOAD EFFECTS DUE TO OCEAN TIDE

2.1. General Considerations.

As the water masses of the ocean move under the gravitational attraction of the moon and the sun, they load and unload periodically the ocean floor. This action brings about displacements as well as changes in the gravity field not only on the ocean floor but also on land. The deformations can be described by the following three distinct but by no means independent phenomena (Vaníček, 1980):

a) Deformation of the lithosphere under the weight of the additional water masses.

b) Gravitational attraction of the tidal waters.

c) Gravitational attraction of the crustal deformation caused by the load (indirect effect).

The most conspicuous effect is the first one. The amount of deformation depends upon the characteristics of the

lithosphere, i.e. thickness and rheological properties. Also, the closer a point is to the load the more it is affected. Due to the attraction of the additional water masses, the gravitational potential is disturbed and a deformation of the lithosphere as well as a change of the gravity field occur. This is the second phenomenon. As a consequence of the first two deformations a redistribution of masses is induced. This redistribution of masses changes the gravitational potential and therefore a new deformation comes about. Since the third phenomenon acts indirectly through the tidal potential the description as "indirect effect" is used in the literature (e.g. Vaníček and Krakiwsky, 1982).

All three effects are inter-related and must be considered simultaneously. The magnitude of the total effect depends upon the rheology of the earth, which therefore has to be taken into account. Rheology can be regarded as the study of the deformation and flow of matter under stress. It is the theory which relates the relative deformation (strain) of a medium due to stress. Stress is the acting force per unit area and may be thought of as being composed of normal (σ) and tangential (τ) components (Eirich, 1950). The rheology of the earth can be taken into consideration through the load deformation coefficients introduced by Munk and MacDonald (1960), which are similar to the ordinary Love numbers.

2.2. Load Deformation Coefficients.

The elastic behaviour of the earth was first recognized by Kelvin in 1876. It is expressed through dimensionless quantities called Love numbers defined as follows (Vaníček and Krakiwsky, 1982): The ratio of the elastic radial displacement of a mass element of the real earth to the radial displacement of the corresponding element of a hypothetical fluid earth is the first Love number and is denoted by h. The changes of the shape of the earth under the tidal forces cause redistribution of masses within the earth and subsequently changes in its gravity field. These changes in the gravity field can be expressed as changes in the potential, briefly called deformation potential. The ratio of the deformation potential to the potential which produces it (i.e. tidal potential) is the second Love number and is denoted by k. The ratio of the horizontal elastic displacement of an actual mass element to the horizontal displacement of the corresponding element of the hypothetical fluid earth is the third Love number (or Shida's number) and is denoted by ℓ.

The load deformation coefficients or load numbers, like the Love numbers, are dimensionless quantities. They depend on the extent of the load and on the depth of the deformation. To distinguish between the load and Love

numbers a prime will be used for the former. Let u'_ℓ denote the vertical displacement of the earth's surface due to the load, u'_a the displacement of a gravity equipotential surface caused by the attraction of water masses and u'_i the indirect effect on the vertical displacement. The load deformation coefficients are defined as follows (Vaníček, 1980):

$$\left.\begin{aligned} h' &= u'_\ell/u'_a \,, \\ k' &= u'_i/u'_a \,, \\ \ell' &= v'_\ell/v'_a \,, \end{aligned}\right\} \qquad (2.1)$$

where v'_ℓ denotes the horizontal displacement of a mass element under the load and v'_a the horizontal displacement of a gravity equipotential surface caused by the attraction of additional water masses. The above definitions refer only to the geometry of the deformations. Expressing the radial displacement of the gravity equipotential surface under the load as a function of potential one obtains (Vaníček and Krakiwsky, 1982)

$$(u'_a)_n = \frac{w^L_n}{g} \,. \qquad (2.2)$$

The subscript of the potential denotes the wave number i.e. the spatial extent of the load. Taking into

consideration the extreme values for n, n=0 describes a load that covers the whole earth, whereas for $n \to \infty$ one deals with point mass load. Substituting (2.2) into the first two of the equations (2.1) yields

$$\left.\begin{aligned} (u'_\ell)_n &= h'_n \frac{W_n^L}{g}, \\ (u'_i)_n &= k'_n \frac{W_n^L}{g}. \end{aligned}\right\} \qquad (2.3)$$

The determination of the load numbers can be done through the numerical integration of the equations of equilibrium of a deformed earth, derived from the equations of free oscillations of the earth given by Pekeris and Jarosch (1958). The equations of equilibrium (Longman, 1962; Farrell, 1972) are differential equations of second order described in a geocentric spherical coordinate system. For the solution of these differential equations (Longman, 1962) a Green's function (in a closed form) can be derived for a certain earth model in which the Lamé coefficients (λ, μ) and density ρ are given as functions of the radius of the earth. The Lamé elasticity constant μ expresses the rigidity of a medium. Constant λ has no direct physical interpretation.

Using the derived Green's function which depends on the Lamé coefficients λ, μ and density ρ, the equations

of equilibrium can be solved by numerical integration. Such a solution was attempted by Longman (1963) considering a point mass load on the surface of the earth.

It is obvious that the load numbers are intimately related to a Green's function which, in turn, is dependent on the chosen density model. Different sets of load numbers can be obtained by assuming different density and elasticity models for the earth.

The load numbers obtained by Longman (1963) are not sufficient since the evaluation of the load effects includes infinite summation of the load numbers with the Legendre polynomials (Chapter III). Farrell (1972) obtained numerical values for all three load numbers up to n=10,000 (Fig. 2.1).

The Gutenberg-Bullen A earth model belongs to the family of A-type models developed in late 30's. An earth model can be generally considered as specified when numerical values of the set of variables (λ, μ, ρ) or some equivalent set are specified for all depths. The basic assumption for constructing the A-type models is that the density of the layer below the crust (approximate depth 0-30 km) as well as the values for the velocities of p and s waves have to be assumed (Bullen, 1975). The seismic waves p and s travel through the earth's interior

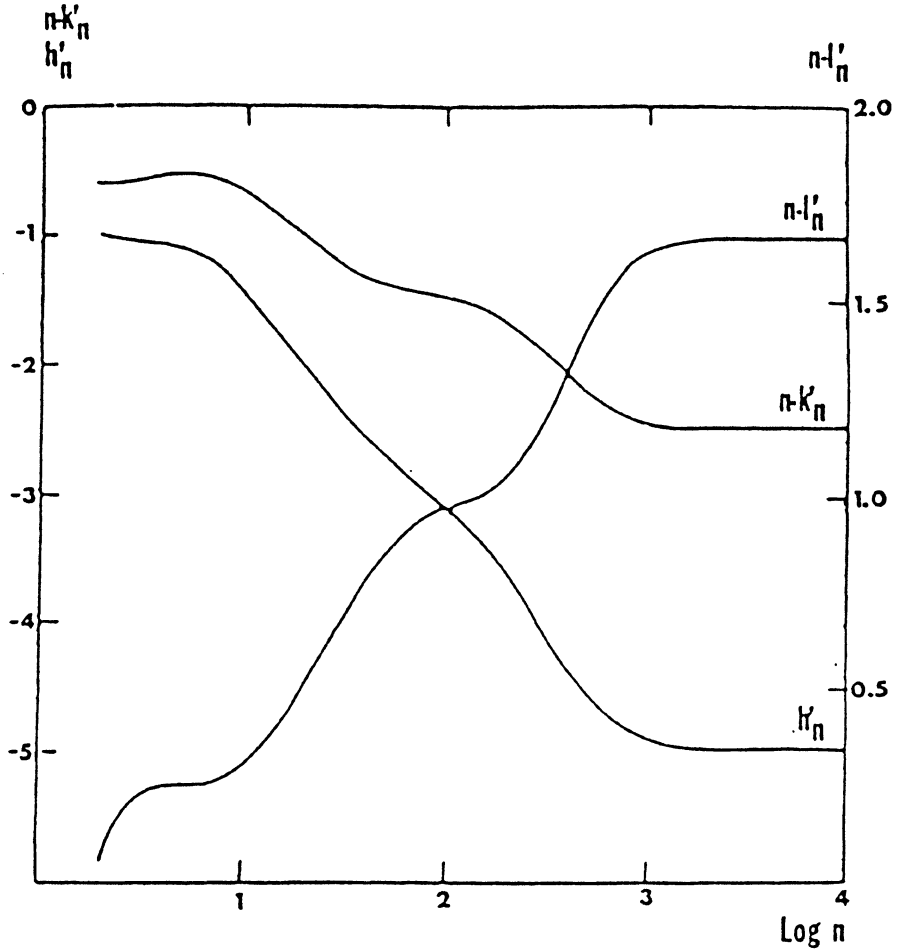

Fig. 2.1

Load deformation coefficients (Farrell, 1972).

rather than around the surface and they are called body waves. The primary (p) wave is a compressional wave travelling with about twice the speed of the secondary (s) wave which is a transverse wave. In addition to the density ρ and the Lamé coefficients λ; μ, these models include a distribution of the earth's incompressibility (expressed through the bulk modulus); pressure and gravitational intensity (Bullen, 1975).

2.3. Simplifying Assumptions.

The load tide has different features from the body tide. It is more irregular than the body tide in respect of amplitude and phase and this is generally due to the local rheological characteristics of the lithosphere as well as to the features of the coastal waters. For points more than about 1° inland (from the coast) the response of the lithosphere does not depend on the fine geological structure. For coastal points the local geology as well as the local tide govern the response. So, a global model is insufficient for such points. Also, the response of the earth is not purely elastic and a dissipation of energy will occur. The earth's response to harmonic surface loads will lag behind the driving force and the lag will vary with distance from the load as well as with frequency (Farrell, 1972).

In this study, the following simplifying assumptions were made:

a) The point at which one wants to determine the load effect must be an inland point i.e. a point which lies at least 100 km from the coast.

b) The response of the earth to loading is considered to be elastic.

For the first of the simplifying assumptions a distance of about 50 km might be sufficient, depending on the thickness of the lithosphere. Other investigators assume that points can be considered as inland points when they are 300 km to 500 km from the coast (Zschau, 1976), or 500 km to 1000 km (Beaumont and Lambert, 1972), or 100 km (Farrell, 1972). The differences among the different models, beyond about 100 km are only a few percent.

2.4. Loading Potential on a Rigid Earth.

For the formulation of the load effects it is expedient to use the potential of the load. Considering a spherical earth, the loading potential induced at a point A by an infinitesimal water mass dm, ψ distant from A (Fig. 2.2) can be written as

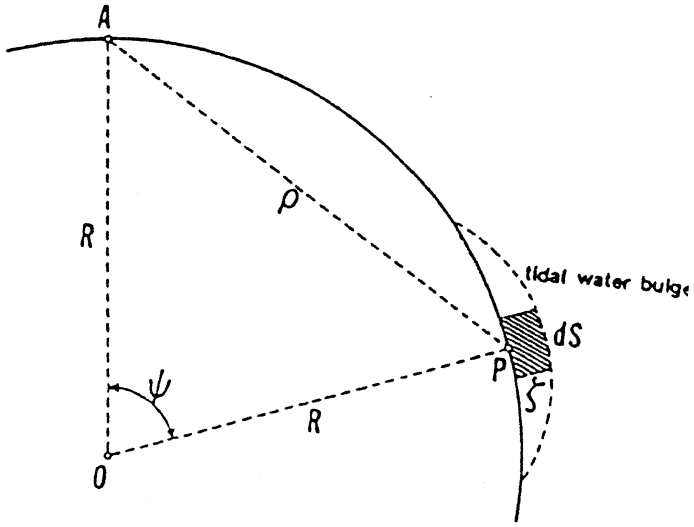

Fig. 2.2
Geometry of the attraction effect of load.

$$dw_A^L = G \frac{dm}{\rho} , \tag{2.4}$$

where G is the gravitational constant and ρ the chord distance between the point of interest A and the point of load P. Further, the infinitesimal mass dm can be written as

$$dm = \zeta \sigma_w dS , \tag{2.5}$$

where ζ is the tidal height above mean sea level, σ_w is the density of sea water and dS the infinitesimal surface element. By substituting (2.5) into (2.4) and integrating (2.4) all over the oceans, the total loading potential at the point of interest is obtained:

$$w_A^L = G\sigma_w \iint_{oceans} \frac{\zeta}{\rho} dS . \tag{2.6}$$

It is expedient to expand the inverse of the chord distance in Legendre polynomials. Using Carnot's formula (cosine law) for the triangle AOP, the inverse of the distance becomes

$$\frac{1}{\rho} = \frac{1}{R} (2-2 \cos \psi)^{-1/2} , \tag{2.7}$$

where ψ is the geocentric angle between the point of interest and the load and R is the radius of the earth. The term in parentheses is the generating function of the Legendre polynomials from which they are uniquely determined (Rectorys, 1969). So, equation (2.7) can be

written as

$$\frac{1}{\rho} = \frac{1}{R} \sum_{n=0}^{\infty} P_n (\cos \psi) \ . \tag{2.8}$$

Substituting (2.8) into (2.6), the total loading potential in terms of Legendre polynomials becomes

$$W_A^L = \frac{G\sigma_w}{R} \iint_{\text{oceans}} \zeta \sum_{n=0}^{\infty} P_n (\cos \psi) dS \ . \tag{2.9}$$

Equation (2.9) can be written further as

$$W_A^L = \iint_{\text{oceans}} K(\psi) \zeta dS \ , \tag{2.10}$$

where $K(\psi)$ is a Green's function (integration kernel) given by

$$K(\psi) = \frac{G\sigma_w}{R} \sum_{n=0}^{\infty} P_n(\cos \psi) \ . \tag{2.11}$$

In the above formulation there is a singularity involved when $\psi \to 0$. This happens when the distance between the point of interest and the load tends to zero and (2.6) is not determined. This singularity does not affect the evaluation of the load effects since all the points under consideration are at least 100 km from the coast. Nevertheless, this singularity is physically meaningless and can be removed (Appendix C).

CHAPTER III

LOAD EFFECTS ON AN ELASTIC EARTH

3.1. Radial Displacement.

The development of the potential of the load on a rigid earth can be combined with the load numbers to give an expression for the radial displacement of the terrain on an elastic earth. Recalling the first of the equations (2.3) and (2.9) one obtains for the radial displacement

$$u'_\ell = \frac{G\sigma_w}{Rg} \iint_{\text{oceans}} \zeta \sum_{n=0}^{\infty} h'_n P_n (\cos \psi) dS \ . \tag{3.1}$$

The integration kernel reads

$$K^{u'_\ell} = \frac{G\sigma_w}{Rg} \sum_{n=0}^{\infty} h'_n P_n (\cos \psi) \ . \tag{3.2}$$

The integration kernel $K^{u'_\ell}$ involves the evaluation of the infinite summation of the product of the first load number h' with the Legendre polynomials. This task is impossible to carry out practically. Instead, the infinite summation in (3.2) was obtained by the Green's functions tabulated by Farrell (1972, Table A3).

Farrell gives the following expression for the radial displacement (ibid, Eq. 37):

$$u'(\psi) = \frac{R}{M_e} \sum_{n=0}^{\infty} h'_n P_n (\cos \psi), \tag{3.3}$$

where R is the radius of the earth and M_e its mass. Furthermore, Farrell tabulates (ibid, Table A3) the following:

$$\tilde{u}'(\psi) = u'(\psi) \cdot 10^{12} (R\psi), \tag{3.4}$$

where $u'(\psi)$ is given by (3.3), R is the radius of the earth in metres and ψ is the geocentric angular distance between the point of interest and the load in radians. By substituting $u'(\psi)$ from (3.3) into (3.4) one gets

$$\tilde{u}'(\psi) = \frac{R^2 \psi}{M_e} 10^{12} \sum_{n=0}^{\infty} h'_n P_n (\cos \psi). \tag{3.5}$$

By solving (3.5) with respect to the infinite summation one obtains

$$\sum_{n=0}^{\infty} h'_n P_n (\cos \psi) = \frac{M_e}{R^2} 10^{-12} \frac{\tilde{u}'(\psi)}{\psi}. \tag{3.6}$$

Equation (3.6) gives an expression for the infinite summation as a function of $\tilde{u}'(\psi)$, which can be taken from Farrell's tables for a certain angle ψ. Combining (3.2) and (3.6) the integration kernel becomes

$$\boxed{K_{\ell}^{u'} = \frac{GM_e \sigma_w}{R^3 g} 10^{-12} \frac{\tilde{u}'(\psi)}{\psi}.} \tag{3.7}$$

The above kernel is plotted in Fig. 3.1. The values of $\tilde{u}'(\psi)$ are tabulated in a form of discrete values for the angle ψ. An analytical expression for $\tilde{u}'(\psi)$ for intermediate values of ψ is necessary for the evaluation of the derived kernel in (3.7). For this reason cubic spline interpolation was used.

3.2. Horizontal Displacement.

The horizontal (lateral) displacement due to an infinitesimal loading mass in the direction of the load can be written as

$$(v'_\ell)_n = \frac{\ell'_n}{g} \frac{\partial W_n^L}{\partial \psi} . \tag{3.8}$$

Differentiating (2.9) with respect to ψ, (3.8) yields

$$v'_\ell = \frac{G\sigma_w}{Rg} \iint_{\text{oceans}} \zeta \sum_{n=0}^{\infty} \ell'_n \frac{\partial P_n(\cos\psi)}{\partial \psi} dS . \tag{3.9}$$

Following the same procedure as in Subsection 3.1, the infinite summation in (3.9) can be written as (Farrell 1972, Eq. 45 and Table A3)

$$\sum_{n=0}^{\infty} \ell'_n \frac{\partial P_n(\cos\psi)}{\partial \psi} = \frac{M_e}{R^2 10^{12}} \frac{\tilde{v}'(\psi)}{\psi} , \tag{3.10}$$

where $\tilde{v}'$ is tabulated in Farrell (1972). Combining (3.9) and (3.10) one obtains

$$v'_\ell = \frac{G\sigma_w}{Rg} \iint_{\text{oceans}} \frac{M_e \tilde{v}'(\psi)}{R^2 10^{12} \psi} \zeta dS , \tag{3.11}$$

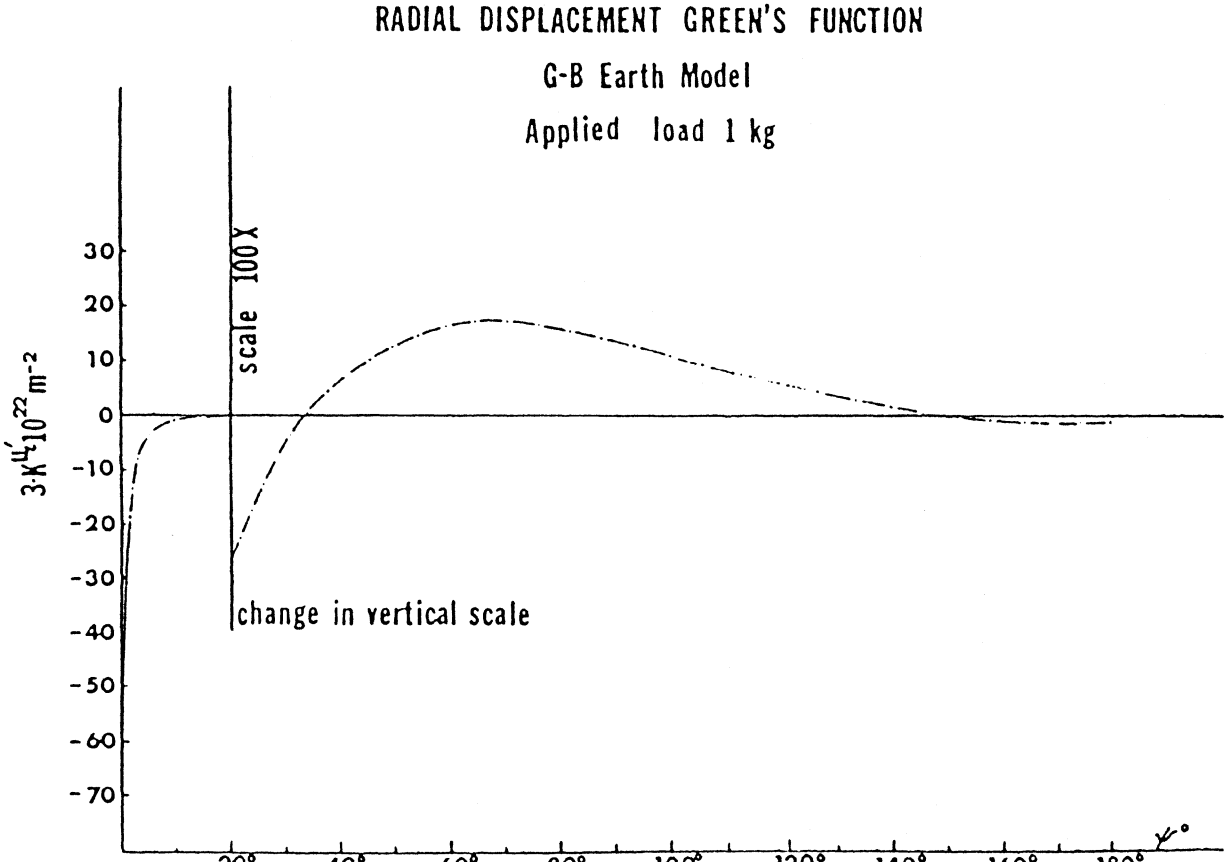
RADIAL DISPLACEMENT GREEN'S FUNCTION
G-B Earth Model
Applied load 1 kg
scale 100 X
change in vertical scale
$3 \cdot K' 4' 10^{22} m^{-2}$
30
20
10
0
-10
-20
-30
-40
-50
-60
-70
20°
40°
60°
80°
100°
120°
140°
160°
180°
ψ°
Fig. 3.1

and the integration kernel becomes

$$K^{v'_\ell} = \frac{-G\sigma_w}{Rg} \frac{M_e}{R^2 \cdot 10^{12}} \frac{\tilde{v}'(\psi)}{\psi} . \qquad (3.12)$$

Since $\tilde{v}'(\psi)$ is always negative the minus sign was used in (3.12) to indicate that a displacement is positive in the direction of the load. The above kernel is plotted in Fig. 3.2.

It is expedient to express the horizontal displacement in terms of north-south and east-west components. The azimuth of the line connecting the point of interest A and the point of load P was used in this study. If (ϕ_A, λ_A) and (ϕ_P, λ_P) are the coordinates of the points A and P respectively, the azimuth of the connecting line PA is (Rectorys, 1969)

$$\cos A_{PA} = \frac{\sin \phi_P - \cos \psi \sin \phi_A}{\sin \psi \cos \phi} . \qquad (3.13)$$

Care is needed when using the above formula. When λ_P is smaller than λ_A, the azimuth is $360^\circ - A_{PA}$ and when λ_P is greater than λ_A the azimuth is A_{PA}. Finally, the north-south and east-west displacements are given by

$$\left.\begin{aligned} v'_\phi &= v' \cos A_{PA} , \\ v'_\lambda &= v' \sin A_{PA} . \end{aligned}\right\} \qquad (3.14)$$

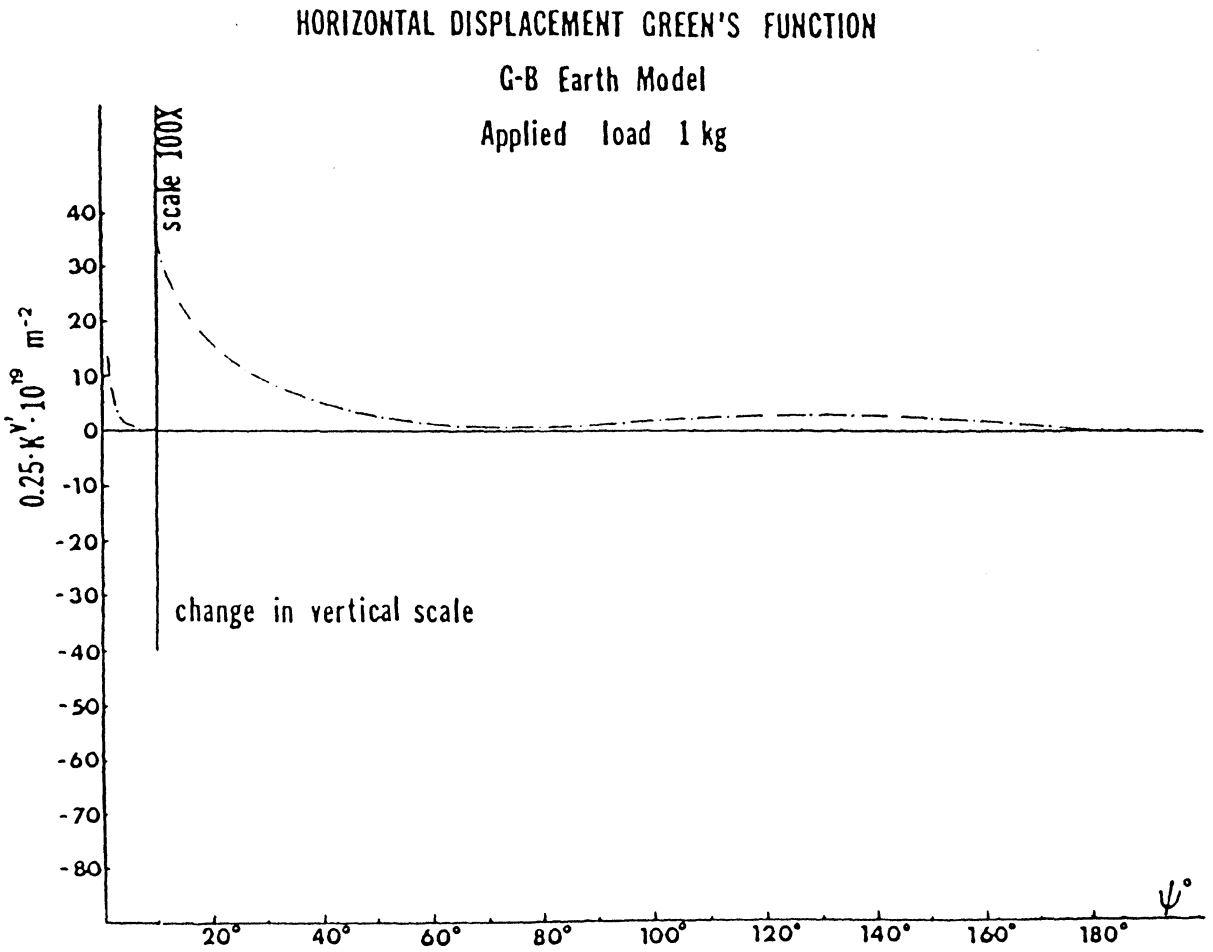
HORIZONTAL DISPLACEMENT GREEN'S FUNCTION
G-B Earth Model
Applied load 1 kg
scale 100X
0.25·K'·10^19 m^-2
40
30
20
10
0
-10
-20
-30
-40
-50
-60
-70
-80
change in vertical scale
20°
40°
60°
80°
100°
120°
140°
160°
180°
ψ°

Fig. 3.2

3.3. Gravity Perturbation.

The gravity perturbation due to load on a rigid earth is

$$\Delta g^L = \frac{\partial W_A^L}{\partial R} . \tag{3.15}$$

Differentiating (2.9) with respect to R yields

$$\Delta g^L = - \frac{G\sigma_w}{R^2} \iint_{oceans} \zeta \sum_{n=0}^{\infty} P_n(\cos \psi) dS . \tag{3.16}$$

The integration kernel becomes

$$K^{\Delta g^L} = - \frac{G\sigma_w}{R^2} \sum_{n=0}^{\infty} P_n (\cos \psi) . \tag{3.17}$$

Using the load numbers (Subsection 2.2), the integration kernel for an elastic earth yields

$$K^{\Delta g^L} = + \frac{G\sigma_w}{R^2} \sum_{n=0}^{\infty} \{n+2h'_n-(n+1)k'_n\} P_n(\cos \psi). \tag{3.18}$$

where the term in brackets is referred to as gravimetric factor and it is explained in Subsection 3.4. Again, in this expression the infinite summation of the load numbers and the Legendre polynomials appears. Farrell (1972) gives the following expression for the gravity perturbation (ibid, Eq. 46):

$$g^F(\psi) = \frac{g}{M_e} \sum_{n=0}^{\infty} \{n+2h'_n-(n+1)k'_n\} P_n (\cos \psi) . \tag{3.19}$$

He also tabulates (ibid, Table A3) the following:

$$\tilde{g}(\psi) = g^E(\psi)\ 10^{18}(R\psi) , \tag{3.20}$$

where $g^E(\psi)$ is the "elastic" perturbation arising from the earth's elastic deformation and is given by (Farrell, 1972)

$$g^E(\psi) = g^F(\psi) - g^N(\psi) \ , \tag{3.21}$$

where $g^F(\psi)$ is the total perturbation due to load given by (3.19) and $g^N(\psi)$ is the perturbation due to the Newtonian attraction of the load only and is given by

$$g^N(\psi) = - \frac{g}{4M_e \sin(\psi/2)} \ . \tag{3.22}$$

From (3.21) and (3.22) one obtains

$$g^F(\psi) = g^E(\psi) - \frac{g}{4M_e \sin(\psi/2)} \ . \tag{3.23}$$

Substituting $g^E(\psi)$ from (3.20) and $g^F(\psi)$ from (3.19), into (3.23) yields

$$\frac{g}{M_e} A = \frac{1}{R} 10^{-18} \frac{\tilde{g}(\psi)}{\psi} - \frac{g}{4M_e \sin(\psi/2)} \ , \tag{3.24}$$

where:

$$A = \sum_{n=0}^{\infty} \{n+2h'_n-(n+1)k'_n\} P_n(\cos\psi) \ . \tag{3.25}$$

Solving (3.24) with respect to A and substituting into (3.18), one obtains:

$$\boxed{K\Delta g^L = +\frac{G\sigma_w}{R^2} \left\{\frac{M_e}{Rg} 10^{-18} \frac{\tilde{g}(\psi)}{\psi} - \frac{1}{4 \sin(\psi/2)}\right\} \ .} \tag{3.26}$$

The gravity perturbation kernel given by (3.26) is a function of ψ and $\tilde{g}(\psi)$ only and is plotted in Fig. 3.3. Again, $\tilde{g}(\psi)$ is obtained from Farrell's tables and a cubic spline interpolation was used for intermediate values of ψ. The units of the integration kernel are $m^{-2}\,sec^{-2}$.

3.4. Complications with the Gravimetric Factor.

The gravimetric factor

$$\delta'_n = \{n+2h'_n-k'_n(n+1)\} \qquad (3.27)$$

was originally derived by Longman (1963) to apply to gravity measurements made at a point situated below the tidal loading sheet (ibid. Eq. 35). Since gravity measurements normally are taken at stations situated above the level of the tides, the question arises as to what formula one should use. Pekeris (1978) states that the gravimetric factor (3.27) is valid only at points right under the loading sheet (Fig. 3.4). For observations made above the tidal level, one must add an additional correction to the one determined using the gravimetric factor given by (3.27) which is $4\pi G\sigma_w\zeta$. This additional correction has to do with the increase in gravity as one crosses the tidal sheet from below. As a result of this correction, the gravimetric factor changes

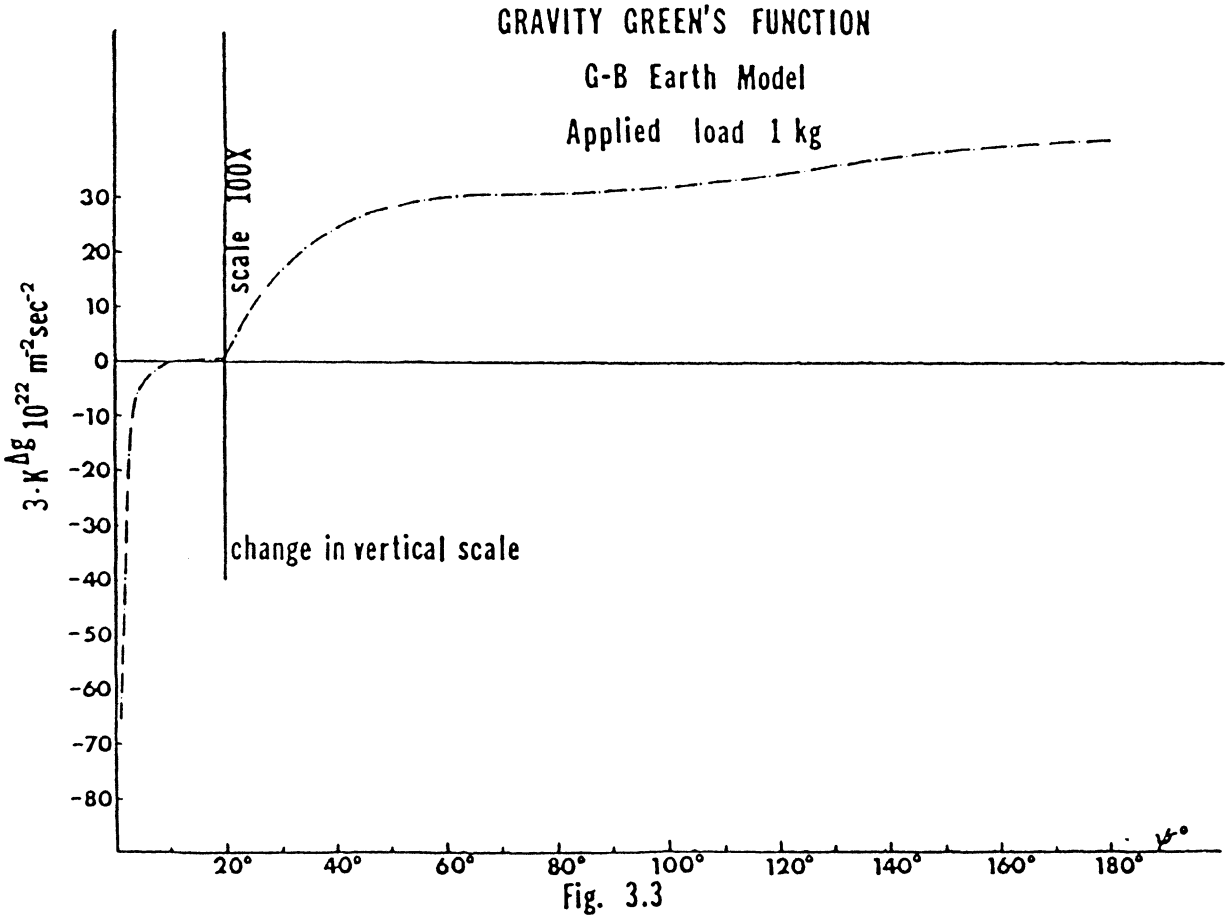
GRAVITY GREEN'S FUNCTION
G-B Earth Model
Applied load 1 kg
scale 100X
change in vertical scale
$3 \cdot K^{\Delta g} 10^{22}\ m^2 sec^{-2}$
30
20
10
0
-10
-20
-30
-40
-50
-60
-70
-80
20°
40°
60°
80°
100°
120°
140°
160°
180°
Fig. 3.3

OCEAN TIDE LOADING SHEET

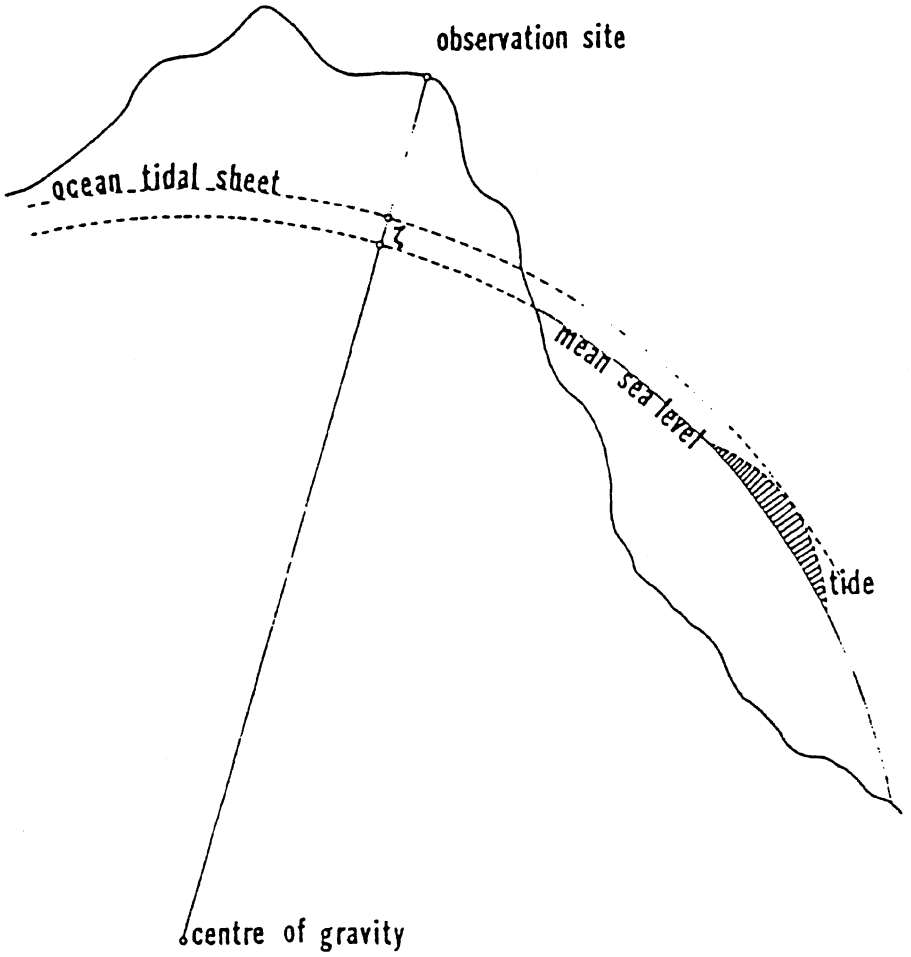

Fig. 3.4

to

$$\delta'_n = \{2h'_n-(n+1)(1+k'_n)\}. \qquad (3.28)$$

According to Pekeris (1978), the gravimetric factor (3.28) applies to gravity measurements made at stations situated right above the level of the tides. Care is needed when one applies (3.28) at island stations if gravity is measured right at the coast.

For gravity measurements made inland or at the bottom of the sea the correction $4\pi G\sigma_w\zeta$ must be put equal to zero (Pekeris, 1978). Other investigators (e.g. Goad, 1980) use the gravimetric factor given by (3.28) for points situated above the tidal sheet, which contradicts the theory. In this study, the gravimetric factor given by (3.27) was used since all the points are situated inland and are above the level of the tides.

3.5. Loads of Degree 0 and 1.

Loads of degree 0 and 1 (n=0, n=1 in the harmonic expansion) deserve special attention. The term n=0 describes a uniform load on the surface of the earth. Thus, if the adopted tidal model preserves water masses, this term disapears. Extensive computer experiments using Schwiderski's model showed that the inclusion or exclusion of the term n=0 has practically no effect on

the results. For gravity a maximum difference of about 0.1 μGals in the amplitudes and 2 in the phases was found. The corresponding effect on displacements would be about 0.2 cm.

Load n=1 is more complicated. Longman (1963) states that the load deformation coefficients are undetermined when n=1 since they depend on the displacement of the earth as a whole, and therefore concludes that load n=1 should not be included in the calculations. Cathles (1971) showed that load n=1 does not move the centre of mass of the earth in respect of surface mass loads such as ocean loading. The concensus appears to be that load n=1 should be included in the evaluation of the loading effects.

Experiments using the present gravity model showed that the effect of including or excluding the term n=1 depends on the locality. For points surrounded by oceans of generally high tides whose antipodes are open oceans, the use of the term n=1 gives erratic results compared to those obtained by actual observations. Alice Springs (Australia) is an example: resulting gravity, excluding load n=1 is very close to the observed value (Chapter V, Table 5.1). A further investigation is needed to consider some other points located, for example, in Australia and Hawaii.

CHAPTER IV

BODY TIDE AND POLAR MOTION

4.1. Radial Displacement.

The absolute radial displacement of the terrain due to body tide for an elastic earth is given by (Vaníček and Krakiwsky, 1982):

$$u_n = h_n \frac{W_n^T}{g} \quad , \tag{4.1}$$

where W_n^T is the tidal potential, g is the magnitude of gravity and h_n the first Love number. The potential due to a celestial body of mass M_* at a point P on the surface of the earth is (Fig. 4.1)

$$U = G \frac{M_*}{r_*} \cdot \tag{4.2}$$

Expanding $1/r_*$ in Legendre series and disregarding the terms of the order n=0 and n=1 (they do not produce any tidal effect), one obtains for the tidal potential

$$W^T = \frac{GM_*}{\rho_*} \sum_{n=2}^{\infty} \left(\frac{R}{\rho_*}\right)^n P_n(\cos z_*) \ . \tag{4.3}$$

where R is the radius of the earth, ρ_* is the apparent

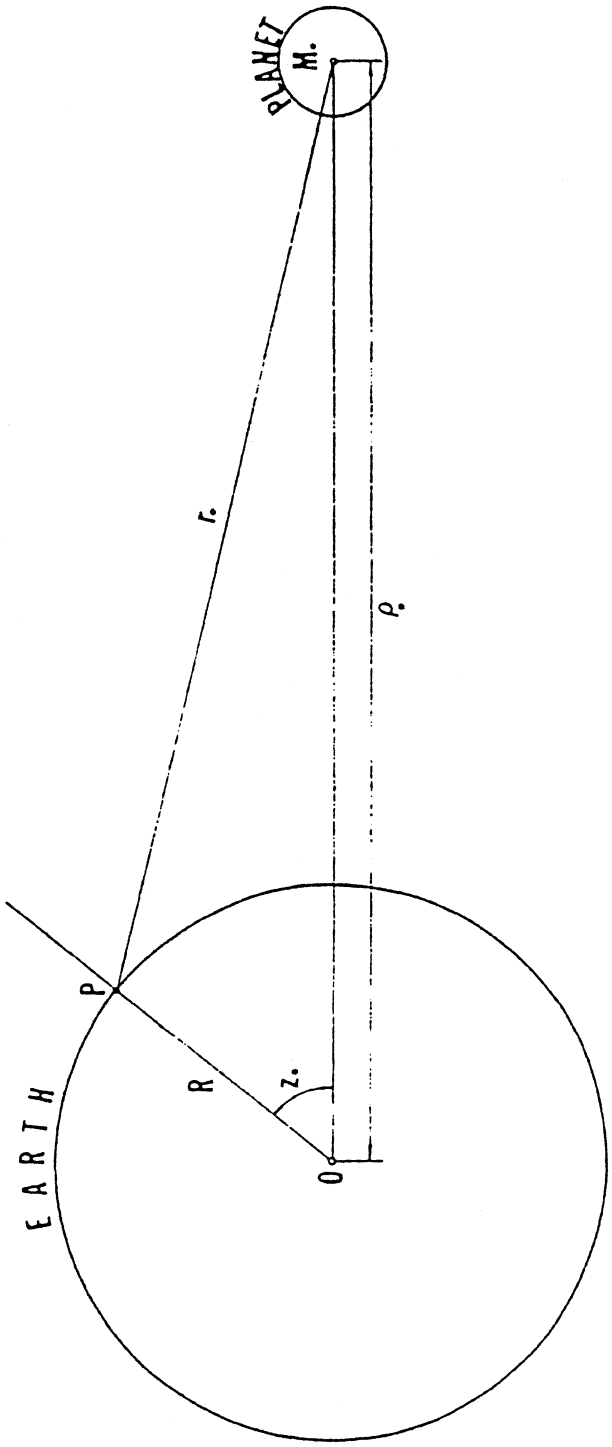

Fig. 4.1. Geometry of the attraction effect of body tides.

distance of the celestial body from the earth and z_* is its apparent zenith distance. Keeping only the term n=2, which is the most predominant and using the mean distance, c_*, between the earth and the celestial body, one obtains

$$W_2^T = \frac{3}{4} \frac{GM_* R^2}{c_*^3} (\cos 2z_* + \frac{1}{3}) \frac{c_*^3}{\rho_*^3} \tag{4.4}$$

and the radial displacement becomes

$$u_* = \frac{3}{4} \frac{GM_* R^2}{g c_*^3} h_2 (\cos 2z_* + \frac{1}{3}) k_*^3 , \tag{4.5}$$

where $k_* = c_*/\rho_*$. Substituting the constant terms in (4.5) for the moon and the sun yields

$$\left.\begin{aligned} u_{\mathfrak{C}} &= 53.6\ h_2 (\cos^2 z_{\mathfrak{C}} - \tfrac{1}{3}) k_{\mathfrak{C}}^3 \quad \text{(cm)}, \\ u_{\odot} &= 24.6\ h_2 (\cos^2 z_{\odot} - \tfrac{1}{3}) k_{\odot}^3 \quad \text{(cm)}. \end{aligned}\right\} \tag{4.6}$$

The total radial displacement due to the moon and the sun yields:

$$u_o = u_{\mathfrak{C}} + u_{\odot} . \tag{4.7}$$

From the ephemerides of the moon and the sun one obtains

$$\left.\begin{aligned} 0.83 < k_{\mathfrak{C}}^3 &< 1.26, \\ 0.95 < k_{\odot}^3 &< 1.05. \end{aligned}\right\} \tag{4.8}$$

4.2. North-South Displacement.

The horizontal displacement due to body tide for an elastic earth in north-south direction is given by (Vaníček, 1980)

$$v_\phi = \frac{\ell_2}{g} \frac{\partial W_2^T}{\partial \phi}, \tag{4.9}$$

where ℓ_2 is Shida's number and W_2^T is given by (4.4). Further, $\cos(z_*)$ is given by

$$\cos z_* = \sin \phi \cdot \sin \delta_* + \cos \phi \cdot \cos \delta_* \cos H_*, \tag{4.10}$$

where δ_* and H_* are the declination and the hour angle of the celestial body respectively. Since the term in parentheses in (4.4) is a function of ϕ, one obtains

$$v_\phi = \frac{3}{2} \ell_2 \frac{GM_* R^2}{g c_*^3} k_*^3 \frac{\partial}{\partial \phi} (\cos^2 z_* - \tfrac{1}{3}). \tag{4.11}$$

Carrying out the differentiation one obtains

$$v_\phi = \frac{3}{2} \ell_2 \frac{GM_* R^2}{g c_*^3} k_*^3 \{\sin 2\phi \, (\sin^2 \delta_* - \cos^2 \delta_* \cos^2 H_*) + \sin^2 2\delta_* \cos H_* \cos 2\phi\}. \tag{4.12}$$

The above formula gives the north-south displacement due to the moon or the sun and it is reckoned positive northwards.

4.3. East-West Displacement.

Similar to the north-south, the east-west displacement is given by (Vaníček, 1980)

$$v_\lambda = \frac{\ell_2}{g} \frac{\partial W_2^T}{\cos \phi \ \partial \lambda} . \tag{4.13}$$

Differentiating (4.4) with respect to λ, yields

$$v_\lambda = \frac{\ell_2}{g} \frac{3}{2} \frac{GM_\star R^2}{c_\star^3 \cos \phi} \{2 \cos^2\phi \cdot \cos^2\delta_\star \cdot \sin H_\star + \frac{1}{2} \sin 2\phi \cdot \sin 2\delta_\star \cdot \sin H_\star\} k_\star^3 . \tag{4.14}$$

The above formula gives the east-west displacement due to the moon or the sun and is reckoned positive eastwards. Note here that in the VLBI software package, the east-west component is considered positive westwards (Merriam, 1978) thus in the VLBI programme, (4.14) is used with opposite sign.

4.4. Ephemerides of the Moon and the Sun.

The zenith distance of the moon at a point P with geographic latitude ϕ is given by

$$\cos z_\mathfrak{C} = \sin \phi \cdot \sin \delta_\mathfrak{C} + \cos \phi \cdot \cos \delta_\mathfrak{C} \cdot \cos H_\mathfrak{C} , \tag{4.15}$$

where $\delta_\mathfrak{C}$ is the declination of the moon and $H_\mathfrak{C}$ its hour angle. For the sun one obtains

$$\cos z_{\odot} = \frac{\sin \delta_{\odot} \cdot \cos (\phi-\omega)}{\sin \omega}, \quad \tan \omega = \frac{\tan \delta_{\odot}}{\cos H_{\odot}}. \tag{4.16}$$

All the angles in the above formulae must be used with proper signs. They can be derived from the astronomical triangles (Explanatory Supplement to the Astronomical Ephemeris and Nautical Almanac, 1978). North latitude is considered positive. The declination of the sun is given approximately by (Melchior, 1966, p.35)

$$\delta_{\odot} \doteq \arcsin (0.406 \sin \alpha_{\odot} + 0.008 \sin 3\alpha_{\odot}). \tag{4.17}$$

The right ascension $\alpha_{\odot}$ of the sun is given by

$$\alpha_{\odot} \doteq x' - 0.043 \cdot \sin(2x') \frac{180°}{\pi} \text{ (degrees)} , \tag{4.18}$$

where

$$x' \doteq h + 0.034 \cdot \sin (h-p') \frac{180°}{\pi} \text{ degrees)} , \tag{4.19}$$

where h is the geometric mean longitude of the sun and p' its paralax. They are given in analytic form in the Explanatory Supplement to the Astronomical Ephemeris and Nautical Almanac (ESAENA) (1978). The ratio $k_{\odot}$ is given by Melchior (1966, p.35):

$$k_{\odot} \doteq 1 + 0.017 \cos (h-p') . \tag{4.20}$$

Ratio $k_{\mathbb{C}}$ is given in Melchior (1978, p. 23).

The orbit of the moon is very complicated. For the derivation of an approximate formula for the ecliptic

latitude, Brown's theory (Improved Lunar Ephemeris 1952-1959, 1954) was used in this study.

The declination of the moon is given by the rigorous formula (ESAENA, 1978)

$$\sin \delta_{\mathbb{C}} = \cos \beta_{\mathbb{C}} \cdot \sin s_{\mathbb{C}} \cdot \sin \varepsilon + \sin \beta_{\mathbb{C}} \cdot \cos \varepsilon, \qquad (4.21)$$

where $\beta_{\mathbb{C}}$ is the ecliptic latitude, $s_{\mathbb{C}}$ is the mean longitude of the moon, measured on the ecliptic from the mean equinox of date to the mean ascending node of the lunar orbit and then along the orbit and ε is the obliquity of the ecliptic. The arguments $s_{\mathbb{C}}$ and ε can be computed using the formulae included in the ESAENA (1978).

The ecliptic latitude of the moon $\beta_{\mathbb{C}}$ is subject to complicated perturbations. It is expressed in Tables I,5 (Improved Lunar Ephemeris 1952-1959, 1954) in the form (ibid. p.398):

$$\beta''_{\mathbb{C}} = (1+C)(\gamma_1 \cdot \sin S + \gamma_2 \cdot \sin 3S + \gamma_3 \cdot \sin 5S + N) + \\ + \text{planetary perturbations}, \qquad (4.22)$$

where C, S and N are trigonometric series and γ_1, γ_2, γ_3 are constants. These constants are given as (ibid. p.398)

$$\gamma_1 = 18519''.7, \quad \gamma_2 = -6''.241, \quad \gamma_3 = 0''.004. \qquad (4.23)$$

C in (4.22) is of the order of 4×10^{-3} (ibid. p.358), γ_2, γ_3 and the planetary perturbations are very small too. Without any significant loss of accuracy, (4.22) can be written as

$$\beta_{\mathbb{C}}'' \doteq 18519''.7 \sin S + N. \qquad (4.24)$$

The principal part of N is (ibid. p.411)

$$N \doteq -526'' \sin (2h - s_{\mathbb{C}} - N_{\mathbb{C}}), \qquad (4.25)$$

where h is the mean geometric longitude of the sun, mean equinox of date, given in the ESAENA (1973).

In (4.24) the argument S is (Improved Lunar Ephemeris 1952-1959, 1954, p.402):

$$S = s_{\mathbb{C}} - N_{\mathbb{C}} + \text{periodic terms}. \qquad (4.26)$$

The most predominant part of the periodic terms in (4.26) is that of N and is given approximately by (ibid. p.407)

$$\delta S \doteq 7''.4 \cos N_{\mathbb{C}} . \qquad (4.27)$$

Combining (4.24, -25, -26, -27) one obtains

$$\beta_{\mathbb{C}}'' \doteq 18519''.7 \sin (s_{\mathbb{C}} - N_{\mathbb{C}} + \delta S) - 526'' \sin (2h - s_{\mathbb{C}} - N_{\mathbb{C}}). \qquad (4.28)$$

Using equations (4.21) and (4.28) the declination of the moon is determined with an accuracy of better than one minute of arc with respect to the values obtained in the

astronomical ephemerides which, in turn, gives an uncertainty in the determination of the radial displacement of the terrain less than 1 cm.

4.5. Hour Angles of the Moon and the Sun.

The hour angle of the moon or the sun can be determined by

$$H_* = ST + \lambda - \alpha_* \ , \tag{4.29}$$

where ST is the mean sidereal time at 00 hours UT, λ is the geographic longitude of the site and α_* is the right ascension of the moon or the sun. The sidereal time is given by (ESAENA, 1978)

$$ST = 99^s.69098333 + 36000^s.76892 \cdot T + 3^s.86708333 . 10^{-4}\ T^2 \ , \tag{4.30}$$

where T is in Julian centuries (of 36525 days) elapsed since 1st January 1900.0 at 12.00 hours of ET. In (4.29) longitude λ is considered positive eastwards.

The right ascension of the sun is given by (4.18) and for the moon by (Melchior, 1966, p.35):

$$\alpha_{\mathbb{C}}^{\circ} = s_{\mathbb{C}}^{\circ} + \frac{180^{\circ}}{\pi}\{-0.043 \sin 2s_{\mathbb{C}} + 0.019 \sin N_{\mathbb{C}} - 0.019 \sin(2s_{\mathbb{C}} - N_{\mathbb{C}})\}. \tag{4.31}$$

Equations (4.15) and (4.31) are used in the software to evaluate radial and horizontal displacements given by (4.6), (4.12) and (4.14).

4.6. Polar Motion.

In 1765 Euler had predicted that if the rotation axis of the earth didn't coincide with the axis of maximum moment of inertia, then the axis of rotation would move with respect to the earth with a period of 10 months. This polar motion was first observed in 1891 and in 1895 the International Union of Geodesy (now International Association of Geodesy) established the International Latitude Service (now under the direction of the International Polar Motion Service, IPMS), consisting of five observatories at the latitude of 39° 08' north, which have been recording the polar motion until today.

The observed polar path is fairly complicated and up to now there is not a clear explanation of it. The mean amplitude of polar motion is about 0".2 but the period is not 10 months as Euler had predicted. Chandler, at the end of the 19th century found that there are two basic periods; one of 14 months and one of 12 months. The period of 14 months has the same origin as Euler's but is longer because of the deformability of the earth. The other one (12 months) seems to have its origin in the seasonal changes in the redistribution of the mass of the atmosphere. Also, there is a suspicion that the pole moves secularly in the direction of the meridian 75° West.

Two of the major sources of information on polar motion are the International Polar Motion Service (IPMS) and the Bureau International de l' Heure (BIH). Also, data are available from the Doppler Polar Motion Service (DPMS). The BIH produces polar motion data from data of the IPMS and from data provided by a large number of independent observatories. The DPMS is a part of the U.S.A. Department of Defense (DoD) and has no official commitments outside the Department (Henriksen, 1977).

In this study, information for polar motion was obtained from BIH Circular D smoothed values of pole position based on the "1979 BIH system". The Circular D publication of BIH is published monthly and contains smoothed and raw values of UT1-UTC, UT2-UTC and coordinates of the pole (BIH Annual Report for 1979, 1980).

Simultaneous computations of UT1 and polar motion were initiated by BIH in 1967, based on available data in 1966-1967. The initial solution was affected by annual errors due to star catalogues, errors in the astronomical constants, refraction and instrumental effects (BIH Annual Report for 1979, 1980). In the BIH annual report for 1978, recommendations were included for corrections to UT1 and pole position from the annual errors. The correction for UT1 was based on EROLD (Earth ROtation by

Lunar Distances) results and the corrections for the coordinates of the pole were based on the results of Doppler observations of TRANSIT satellites. The corrected values of the polar path form the so called "1979 BIH system". The maximum systematic errors remaining in UT1 and polar coordinates in the "1979 BIH system" should be of the order of 0.01 seconds and 0".001 respectively, for the period 1972-1979 (BIH Annual Report for 1979, 1980).

The computational procedure used in the software provided by the M.I.T. Department of Earth and Planetary Sciences, is the Lagrangian interpolation, using cubic polynomials. Each time the pole position is desired, the Lagrange's interpolation is used for four values of the pole position; two before and two after the desired time (R. B. Langley, personal communication). The time interval between the known values is five days, although a monthly separation could be used with less precise results. The values of the pole coordinates x, y are known at four epochs t_1, t_2, t_3, t_4. A cubic polynomial P has to be determined to satisfy the following conditions for the x coordinate:

$$P_x(x_1) = x(t_1),\ P_x(x_2) = x(t_2),\ P_x(x_3) = x(t_3),\ P_x(x_4)=x(t_4) \quad (4.32)$$

and for the y coordinate

$$P_y(t_1) = y(t_1),\ P_y(t_2) = y(t_2),\ P_y(t_3) = y(t_3),\ P_y(t_4) = y(t_4). \quad (4.33)$$

These polynomials, if they exist, are unique (Apostol, 1962) and they are determined by the formulae

$$\left.\begin{aligned} P_x(t) &= \sum_{k=1}^{4} x(t_k)\ L_k(t), \\ P_y(t) &= \sum_{k=1}^{4} y(t_k)\ L_k(t). \end{aligned}\right\} \quad (4.34)$$

Each of the above formulae is called Lagrange's interpolation formula. $L_k(t)$ is determined by

$$L_k(t) = \prod_{\substack{j=1 \\ j\neq k}}^{4} \frac{t-t_j}{t_k-t_j}, \quad (4.35)$$

where t is the desired time for the interpolation, which in the present model, satisfies the inequality

$$t_2 < t < t_3 . \quad (4.36)$$

The above interpolation scheme was used in GEOAIM to give values for the pole position.

CHAPTER V

COMPUTATIONAL RESULTS

5.1. Gravity Perturbations due to Body Tide and Ocean Loading.

The mathematical model for the body tide developed in this study was tested against Merriam's model (Merriam, 1978) and against actual recordings of the gravity perturbation at the University of New Brunswick, using the recording gravimeter LaCoste and Romberg G-28. The comparisons indicated that there are small differences of the order of a few μGals between Merriam's and that developed in this study. Both models gave quite similar results to the actual gravity perturbations (Fig. 5.1).

The mathematical model for the load effects was indirectly tested against existing determinations of the load effect on gravity, based on actual data, since gravity perturbations are the only ones which can be determined with high enough accuracy. Observed gravity perturbations of the semidiurnal principal lunar tide (M_2) were used for comparisons.

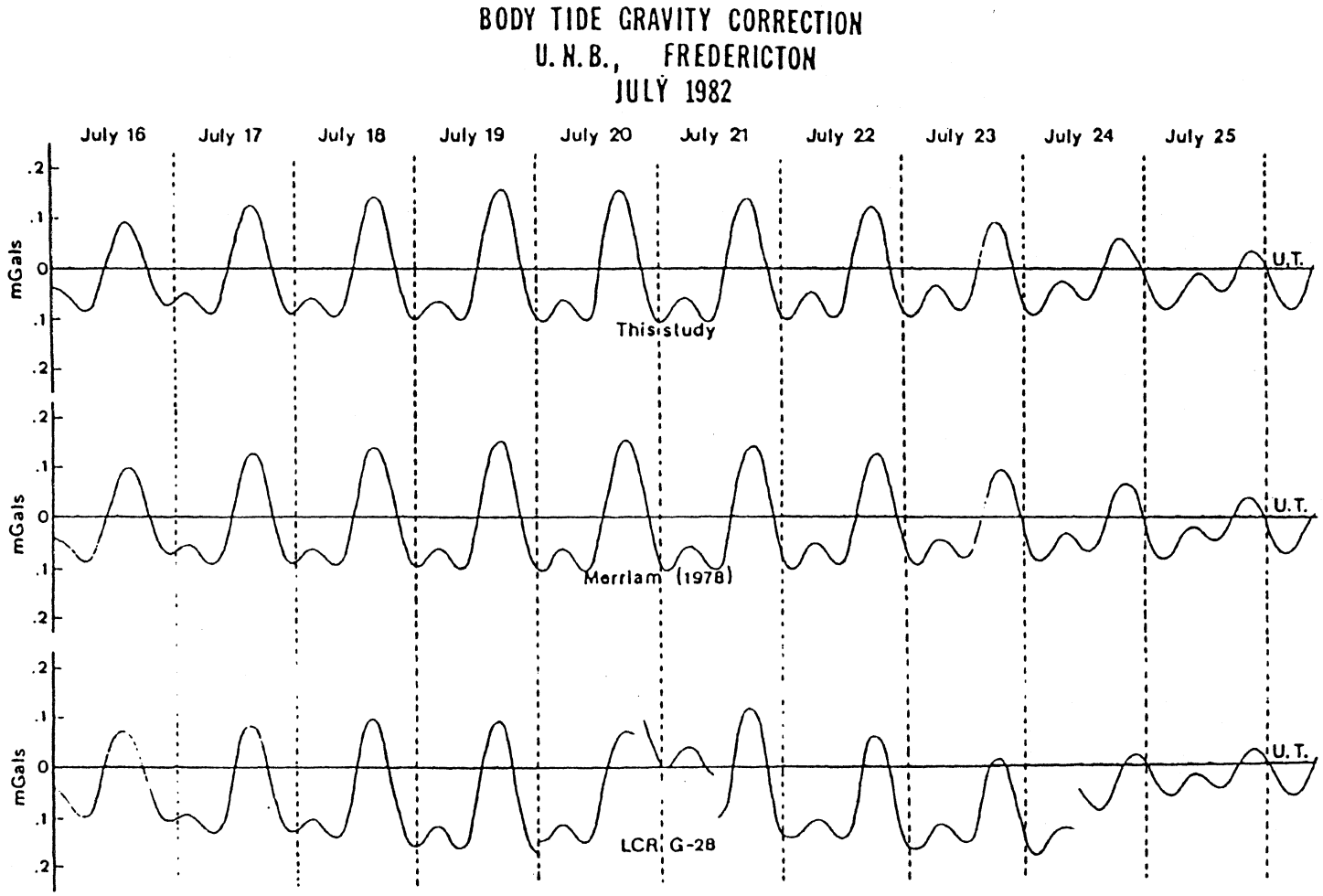
BODY TIDE GRAVITY CORRECTION
U.N.B., FREDERICTON
JULY 1982
July 16
July 17
July 18
July 19
July 20
July 21
July 22
July 23
July 24
July 25
mGals
.2
.1
0
.1
.2
U.T.
This study
Merriam (1978)
LCR G-28

Fig. 5.1

As it can be seen (Table 5.1), the M_2 amplitudes for inland points such as Alice Springs and Potsdam are almost identical with the observed. There is still a very good agreement at the 0.5 μGal level for points situated about 100 km from the coast (Canberra, Brussels, Mizusawa). The predicted phases for these stations are also in good agreement with the observed phases. This agreement appears to be better than that obtained by Goad (1979).

Including all the stations listed in Table 5.1, the mean of the absolute differences of the amplitudes between the observed and those obtained in this study is 0.53 μGal with a root-mean-square (rms) scatter of 0.56 μGal. Excluding La Jolla, which is a coastal point, the mean reduces to 0.32 μGal with an rms scatter of 0.19 μGal. Goad (1979) obtained a mean difference of 0.43 μGal with an rms scatter of 0.36 μGal both including and excluding La Jolla. In other words, the comparison using La Jolla does not affect his results. For the phases, a mean of the absolute differences of 3°.5 with an rms scatter of 5° was obtained in this study (all stations included). Goad (1979) gave 11°.8 for the mean with an rms scatter of 8°.5.

M_2 GRAVIMETRIC TIDAL LOADING

OBSERVATION SITE	OBSERVED		THIS STUDY		GOAD (1979)	
	amp.*	phase	amp.	phase	amp.	phase
La Jolla[4]	3.64	-81[1]	1.68	-84[1]	3.35	-96[1]
Piñon Flat[4]	1.42	-74[1]	0.90	-75[1]	1.74	-107[1]
Alice Springs[5]	0.53	-48[2]	0.60	-46[2]	0.02	41[2]
Canberra[5]	3.57	-41[2]	3.32	-58[2]	2.35	-56[2]
Brussels[6]	2.02	60[3]	1.53	59[3]	2.02	66[3]
Walferdange[7]	1.81	55[3]	1.31	54[3]	1.90	59[3]
Potsdam[8]	0.86	44[3]	0.88	43[3]	1.30	38[3]
Mizusawa[9]	1.82	46[3]	2.21	44[3]	2.23	56[3]

*Amplitudes in μGals

[1]Greenwich phase lag in local time

[2]Local phase lag

[3]Phase lead with respect to the theoretical tide

Sources of observed tide

[4]Warburton et al. (1975)

[5]Melchior (1978)

[6]Melchior et al. (1976)

[7]Torge and Wenzel (1977)

[8]Altmann et al. (1977)

[9]Hosoyama (1977)

Table 5.1

5.2. Terrain Deformations and VLBI.

It was in 1967 that the first successful measurements using very long baseline interferometry (VLBI) were made. Nowadays, it is possible using this technique, to measure transcontinental distances with a precision of a few centimetres. A VLBI system consists of an array of at least two antennae that observe the same set of compact extragalactic radio sources (such as quasars) simultaneously. These radio sources are at a grate enough distance from the earth to allow the assumption of being at infinity with negligible proper motion. The radio source is weak and so large directional antennae of between 20 and 40 metres in diameter have in general been used for reception. Because the signal is coming from sources essentially at infinity, it reaches the earth in the form of plane wave-fronts and it is this property that is used for the VLBI observations (Fig. 5.2).

The basic observables in geodetic VLBI experiments are (i) the difference in times of arrival at two antennae of a signal from the source; and (ii) the rate of change of this time difference. The first one can be a phase-delay difference or a group-delay difference. The phase-delay difference is obtained through phase measurements which generally are very precise but ambiguous (because of the difficulty to resolve the "$2\pi n$" problem), and the group-

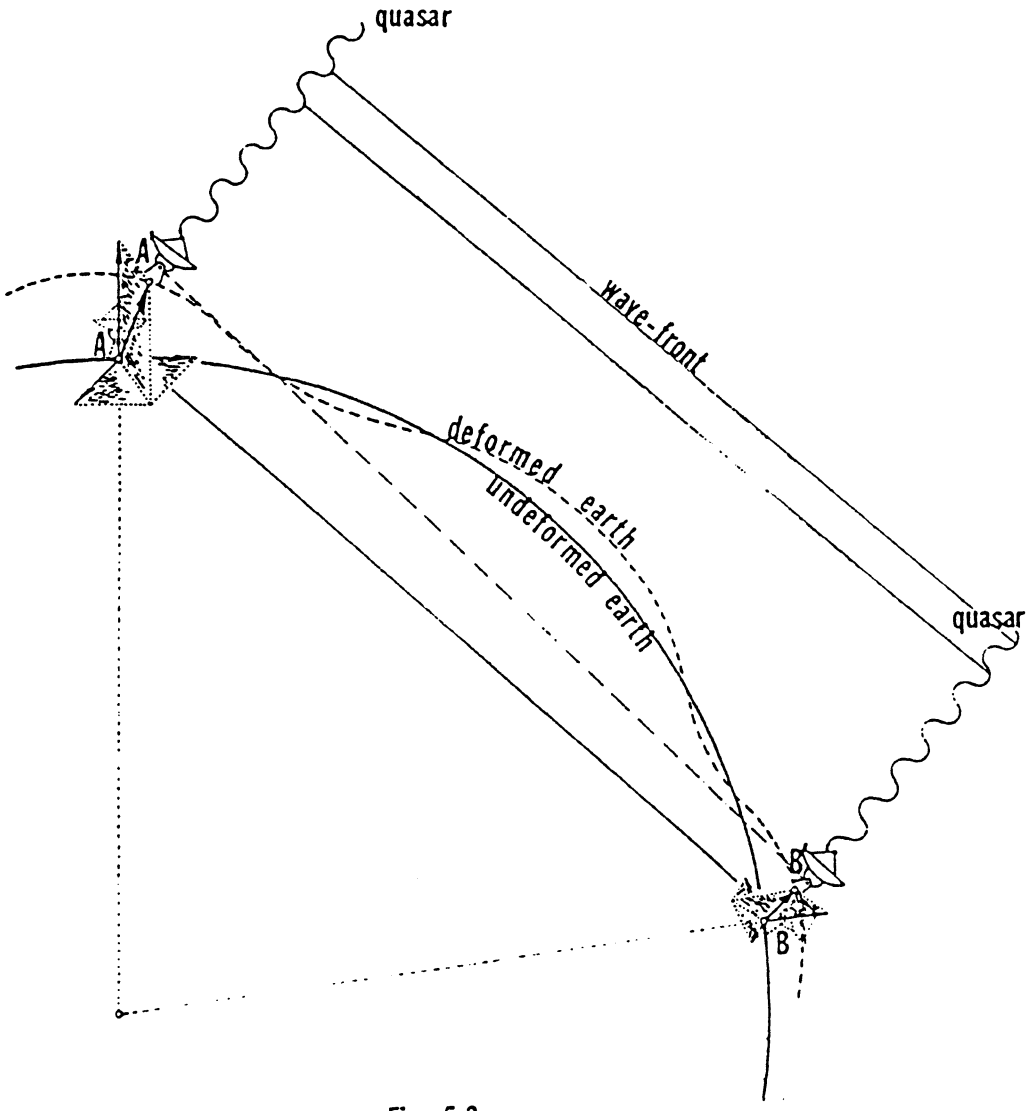

Fig. 5.2

Earth deformation and VLBI geometry.

delay which is less precise but unambiguous, determined by the rate of change of phase-delay with frequency. The rate of change of the phase delay is called fringe frequency and is due principally to the earth's rotation. It is nothing else but the classical differential Doppler shift of the frequency of the signal between the moving antennae (Cannon, 1978).

The situation encountered in VLBI is actually far more complicated than simply observing phase-delays and fringe frequencies. There are a lot of geodynamic phenomena as well as small effects due to the observing systems, which affect the observations and knowledge of them is necessary to reduce the uncertainties of the determination of baselines to the centimetre level. Geodynamic effects include precession and nutation of the earth, crustal motions, body tides, ocean loading, variations in the rate of rotation of the earth and polar motion. In the second category, clock instabilities, source characteristics and propagation medium effects dominate. Under the heading of geodynamic phenomena, only body tides, ocean loading and polar motion are considered in the present study.

Due to the very long distances between the VLBI antennae, the effects of body tide and ocean loading are different at each site. Simultaneous observations of a

radio source give phase-delays and fringe frequencies pertaining to the baseline A'B' (Fig. 5.2, page 51). In Fig. 5.2 the three orthogonal vectors at each site indicate the deformation of the terrain due to both body tide and ocean loading expressed in a local coordinate system. The x-y plane is perpendicular to the local vertical at the site (x- is positive towards west and y- is positive towards north) and z axis along the local vertical (positive outwards). In order to determine the unperturbed length of the baseline AB, the radial as well as the horizontal displacements (north-south, east-west) must be known.

The deformations due to body tide and ocean loading are entered into the VLBI programme in terms of three components as described above, expressed in local coordinate system. This system is rotated so that it becomes parallel to the geocentric coordinate system in which the components of the VLBI baselines are expressed. If $\overrightarrow{\Delta S}_A$ is the vector for the displacement of the terrain at a station $A(\phi_A, \lambda_A)$ due to body tide and ocean loading expressed in the geocentric coordinate system, one can write

$$\overrightarrow{\Delta S}_A = \begin{bmatrix} \Delta X_A \\ \Delta Y_A \\ \Delta Z_A \end{bmatrix} = \left[\begin{array}{c|c|c} \sin\phi_A \cdot \cos\lambda_A & -\sin\lambda_A & \cos\phi_A \cdot \cos\lambda_A \\ \hline \sin\phi_A \cdot \sin\lambda_A & \cos\lambda_A & \cos\phi_A \cdot \sin\lambda_A \\ \hline -\cos\phi_A & 0 & \sin\phi_A \end{array}\right] \begin{bmatrix} v^A_{N-S} \\ v^A_{E-W} \\ u^A \end{bmatrix}, \qquad (5.1)$$

where v^A_{N-S}, v^A_{E-W} are the horizontal displacements of the terrain due to body tide and ocean loading in north-south and east-west directions respectively and u^A is the radial displacement. All three displacements are expressed in a local left-handed coordinate system (Subsection 4.3) and can be obtained by

$$\left.\begin{aligned} v^A_{N-S} &= v_\phi + v'_\phi, \\ v^A_{E-W} &= v_\lambda + v'_\lambda, \\ u^A &= u_o + u'_\ell, \end{aligned}\right\} \tag{5.2}$$

where u_o, v_ϕ and v_λ are given by (4.7), (4.12) and (4.14) respectively. The displacements u'_ℓ, v'_ϕ and v'_λ due to load can be written as a superposition of six harmonic terms as follows:

$$\left.\begin{aligned} u'_\ell &= \sum_{i=1}^{6} \xi_i^\ell \cos(\omega_i t + V_i - \delta_i^\ell), \\ v'_\phi &= \sum_{i=1}^{6} \xi_i^\phi \cos(\omega_i t + V_i - \delta_i^\phi), \\ v'_\lambda &= \sum_{i=1}^{6} \xi_i^\lambda \cos(\omega_i t + V_i - \delta_i^\lambda), \end{aligned}\right\} \tag{5.3}$$

Subscript i in the above formulae denotes the constituent, superscripts ℓ, ϕ, λ denote radial, north-south and east-west displacements respectively, ξ and δ are the amplitude and the Greenwich phase lag of the deformation obtained by the software developed in this study (Appendix G), ω_i and V_i are the frequency and the

astronomical argument of the constituents respectively and t the universal time (UT). In order to derive an analytical expression for the effect of load on the baseline length it is expedient to express radial, north-south and east-west displacements in the direction of the baseline. For simplicity, only one of the loading constituents is considered for the derivation of the analytic expression. For the rest of the constituents the same formulae can be used by changing only the frequency. Consider a 3-D Cartesian coordinate system parallel to the geocentric system with origin at one end of the baseline (Fig. 5.3). Let X, Y and Z be the components of the baseline, α the direction angle of the projection of the baseline onto the X-Y plane with respect to X axis and β the direction angle of the baseline with respect to Z axis. Let δx_A, δy_A and δz_A be the variations of the coordinates of point A of the baseline due to load and δS_x, δS_y, δS_z the projections of the above variations on the baseline. From Fig. 5.3 one can write

$$\left.\begin{aligned} \delta S_x &= \frac{\delta x_A}{\sin\beta \cdot \cos\alpha}, \\ \delta S_y &= \frac{\delta y_A}{\sin\alpha \cdot \sin\beta}, \\ \delta S_z &= \frac{\delta z_A}{\cos\beta}, \end{aligned}\right\} \qquad (5.4)$$

where

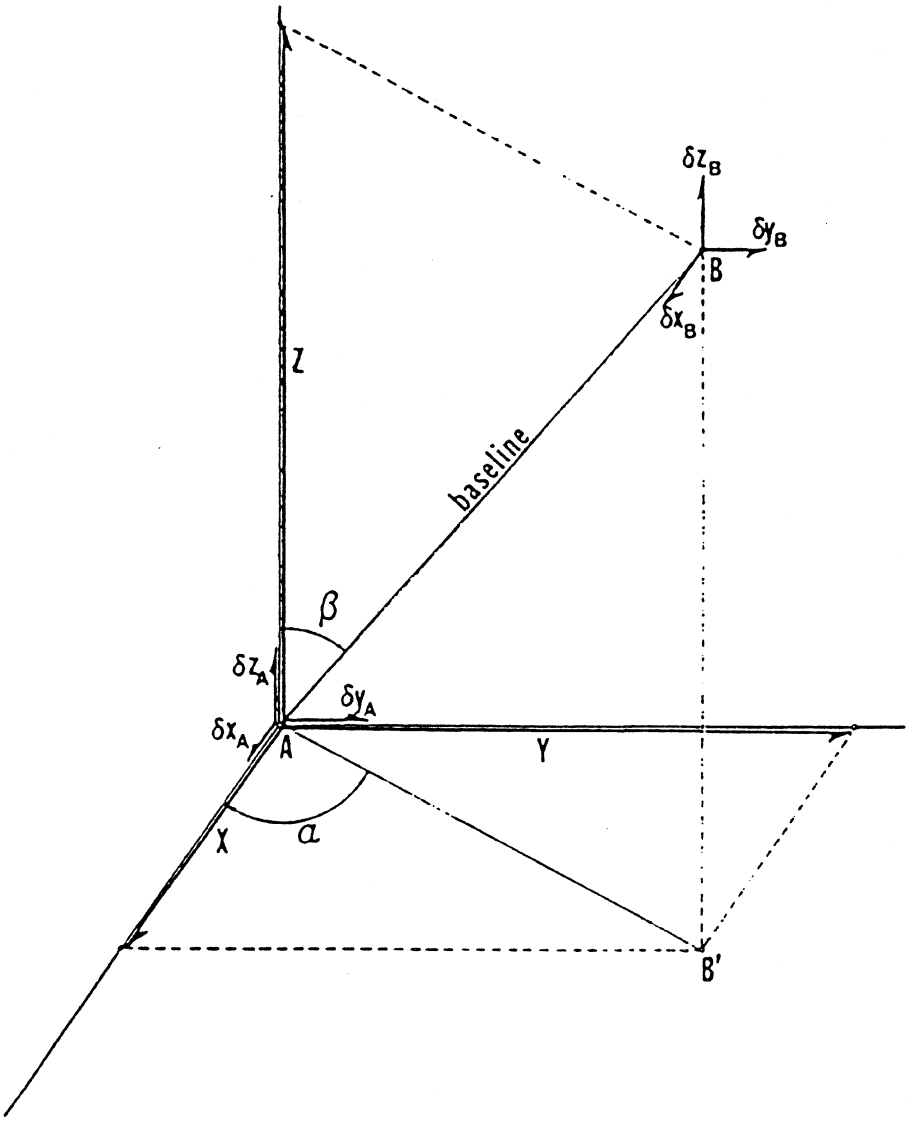

Fig. 5.3. Load effect on baseline length. Coordinate system parallel to geocentric system.

$$\left.\begin{aligned} \tan\alpha &= \frac{Y}{X}\ , \\ \tan\beta &= \frac{(X^2+Y^2)^{1/2}}{Z}\cdot \end{aligned}\right\} \qquad (5.5)$$

From (5.1) one gets

$$\left.\begin{aligned} \delta x_A &= \sin\phi_A \cos\lambda_A v'_\phi - \sin\lambda_A v'_\lambda + \cos\phi_A \cdot\cos\lambda_A u'_\ell\ , \\ \delta y_A &= \sin\phi_A \sin\lambda_A v'_\phi + \cos\lambda_A v'_\lambda + \cos\phi_A \sin\lambda_A u'_\ell\ , \\ \delta z_A &= -\cos\phi_A v'_\phi + \sin\phi_A u'_\ell\ . \end{aligned}\right\} \qquad (5.6)$$

Setting

$$\left.\begin{aligned} a &= \sin\phi_A \cos\lambda_A\ , \\ b &= -\sin\lambda_A\ , \\ c &= \cos\phi_A \cos\lambda_A\ , \\ d &= \sin\phi_A \sin\lambda_A\ , \\ e &= \cos\lambda_A\ , \\ f &= \cos\phi_A \sin\lambda_A\ , \\ k &= -\cos\phi_A\ , \\ p &= \sin\phi_A\ , \end{aligned}\right\} \qquad (5.7)$$

one obtains from (5.6)

$$\left.\begin{aligned} \delta x_A &= a v'_\phi + b v'_\lambda + c u'_\ell, \\ \delta y_A &= d v'_\phi + e v'_\lambda + f u'_\ell, \\ \delta z_A &= k v'_\phi + p u'_\ell. \end{aligned}\right\} \qquad (5.8)$$

Equations (5.8) describe harmonic motions along X, Y and Z axes. Considering only one constituent of the load effect, (5.3) can be written as

$$\left.\begin{aligned} u'_\ell &= \xi^\ell \cos(\omega t + V - \delta^\ell), \\ v'_\phi &= \xi^\phi \cos(\omega t + V - \delta^\phi), \\ v'_\lambda &= \xi^\lambda \cos(\omega t + V - \delta^\lambda). \end{aligned}\right\} \qquad (5.9)$$

Combining (5.8) and (5.9) one obtains

$$\left.\begin{aligned} \delta x_A &= a'\cos(\omega t+V-\delta^\phi) + b'\cos(\omega t+V-\delta^\lambda) + c'\cos(\omega t+V-\delta^\ell), \\ \delta y_A &= d'\cos(\omega t+V-\delta^\phi) + e'\cos(\omega t+V-\delta^\lambda) + f'\cos(\omega t+V-\delta^\ell), \\ \delta z_A &= k'\cos(\omega t+V-\delta^\phi) + p'\cos(\omega t+V-\delta^\ell), \end{aligned}\right\} \qquad (5.10)$$

where

$$\left.\begin{aligned} a' &= a\xi^\phi, \quad e' = e\xi^\lambda, \\ b' &= b\xi^\lambda, \quad f' = f\xi^\ell, \\ c' &= c\xi^\ell, \quad k' = k\xi^\phi, \\ d' &= d\xi^\phi, \quad p' = p\xi^\lambda. \end{aligned}\right\} \qquad (5.11)$$

The first of the equations (5.10) can be written as

$$\delta x = \delta x_1 + c'\cos\ (\omega t+V-\delta^{\ell}) \ , \tag{5.12}$$

where

$$\delta x_1 = a'\cos\ (\omega t+V-\delta^{\phi}) + b'\cos\ (\omega t+V-\delta^{\lambda}) , \tag{5.13}$$

Equation (5.13) expresses a superposition of two harmonic motions with the same frequency and direction but with different phase. The result is a harmonic motion of the same frequency but with different amplitude and phase and can be written as

$$\delta x_1 = a''\cos\ (\omega t+V-\theta_1) \ , \tag{5.14}$$

where

$$a'' = \{(a')^2+(b')^2 + 2a'b'\cos\ (\delta^{\phi}-\delta^{\lambda})\}^{1/2} \tag{5.15}$$

and

$$\tan\ \theta_1 = \frac{a'\sin\ \delta^{\phi}+b'\sin\ \delta^{\lambda}}{a'\cos\ \delta^{\phi}+b'\cos\ \delta^{\lambda}} \ . \tag{5.16}$$

Substituting (5.14) into (5.12) and following the same procedure one obtains

$$\delta x = A_x\cos(\omega t+V-\theta_x) \tag{5.17}$$

where

$$A_x = \{(a'')^2+(c')^2+2a''c'\cos\ (\theta_1-\delta^{\ell})\}^{1/2} \tag{5.18}$$

and

$$\tan \theta_x = \frac{a''\sin \theta_1 + c' \sin \delta^{\ell}}{a''\cos \theta_1 + c' \cos \delta^{\ell}} . \qquad (5.19)$$

Equation (5.17) gives the effect of loading along the X axis corresponding to one component. Combining the first of the equations (5.4) with (5.17) one obtains for the effect of load along the baseline due to the X component of load:

$$\delta S_x = \frac{A_x \cos (\omega t + V - \theta_x)}{\sin \beta \cos \alpha} . \qquad (5.20)$$

Similarly, one obtains for δS_y

$$\delta S_y = \frac{A_y \cos (\omega t + V - \theta_y)}{\sin \alpha \sin \beta} . \qquad (5.21)$$

A_y and θ_y can be obtained from (5.15), (5.18) and (5.19) by changing a', b', c' with d', e', f' respectively. For δS_z one obtains

$$\delta S_z = \frac{A_z \cos (\omega t + V - \theta_z)}{\cos \beta} , \qquad (5.22)$$

where

$$A_z = \{k'^2 + p'^2 + 2k'p' \cos (\delta^{\phi} - \delta^{\ell}) \}^{1/2} , \qquad (5.23)$$

$$\tan \theta_z = \frac{k' \sin \delta^{\phi} + p' \sin \delta^{\ell}}{k' \cos \delta^{\phi} + p' \cos \delta^{\ell}} . \qquad (5.24)$$

The total load effect at one station, along the baseline is given by the superposition of (5.20), (5.21) and (5.22):

$$\delta S = A \cos(\omega t+V-\theta), \tag{5.25}$$

where

$$A = \{A'^{2}_{xy}+A'^{2}_{xy}+2A'_{xy}A'_{z} \cos(\theta_{xy}-\theta_{z})\}^{1/2}, \tag{5.26}$$

$$\tan \theta = \frac{A'_{xy} \sin \theta_{xy}+A'_{z} \sin \theta_{z}}{A'_{xy} \cos \theta_{xy}+A'_{z} \cos \theta_{z}} \tag{5.27}$$

and

$$\begin{aligned} A'_{xy} &= \{A'^{2}_{x}+A'^{2}_{y}+2A'_{x}A'_{y} \cos (\theta_{x}-\theta_{y})\}^{1/2} \\ \tan \theta_{xy} &= \frac{A'_{x} \sin \theta_{x}+A'_{y} \sin \theta_{y}}{A'_{x} \cos \theta_{x}+A'_{y} \cos \theta_{y}}, \end{aligned} \tag{5.28}$$

where

$$\begin{aligned} A'_{x} &= \frac{A_{x}}{\sin \beta \cos \alpha}, \\ A'_{y} &= \frac{A_{y}}{\sin \alpha \sin \beta}, \\ A'_{z} &= \frac{A_{z}}{\cos \beta}. \end{aligned} \tag{5.29}$$

Using equation (5.25) for both ends of the baseline one obtains

$$\begin{aligned} \delta S_{A} &= A_{A} \cos (\omega t+V-\theta_{A}), \\ \delta S_{B} &= A_{B} \cos (\omega t+V-\theta_{B}). \end{aligned} \tag{5.30}$$

Combining equations (5.30) yields

$$\delta S_{AB} = A_{AB} \cos (\omega t+V-\theta_{AB}) , \tag{5.31}$$

where

$$A_{AB} = \{A_A^2+A_B^2+2A_A A_B \cos (\theta_A-\theta_B)\}^{1/2} ,$$

$$\tan \theta_{AB} = \frac{A_A \sin \theta_A+A_B \sin \theta_B}{A_A \cos \theta_A+A_B \cos \theta_B} . \tag{5.32}$$

Equations (5.31) and (5.32) give the effect of load on the baseline length due to one constituent. Similar equations hold for the rest of the constituents. As an example of the effect of load on baseline length, baseline Chilbolton-Owens Valley Radio Observatory was selected (Subsection 5.3, Table 5.2). For this particular baseline, the effect of loading on its length can reach 2.33 cm (M_2:1.19, S_2:0.23, K_1:0.30, O_1:0.25, N_2:0.25, P_1:0.11) due to radial displacement, 0.43 cm (M_2:0.22, S_2:0.08, K_1:0.06, O_1:0.02, N_2:0.03, P_1:0.02) due to north-south displacement and 0.78 cm (M_2:0.36, S_2:0.10, K_1:0.11, O_1:0.11, N_2:0.07, P_1:0.03) due to east-west displacement.

The uncertainty in polar motion affects only the direction of the baseline, which is usually expressed by declination and longitude. This is because polar motion affects only the orientation of the orthogonal coordinate system.

OCEAN TIDE LOADING DEFORMATIONS

CANADIAN VLBI ARRAY

	A R O						O V R O						C H I L					
	VERTICAL[1]		N-S[2]		E-W[3]		VERTICAL[1]		N-S[2]		E-W[3]		VERTICAL[1]		N-S[2]		E-W[3]	
	Amp	Phase	Amp	Phase	Amp	Phase	Amp	Phase	Amp	Phase	Amp	Phase	Amp	Phase	Amp	Phase	Amp	Phase
M2	0.54	158.87	0.06	169.05	0.16	350.40	0.57	39.29	0.37	272.94	0.17	44.43	1.92	302.13	0.07	342.53	0.64	303.75
S2	0.20	194.02	0.02	223.26	0.03	333.31	0.04	131.69	0.14	286.46	0.04	118.28	0.40	349.94	0.02	11.50	0.19	0.51
K1	0.26	7.17	0.02	308.87	0.04	98.59	0.88	42.24	0.13	8.33	0.24	61.04	0.51	194.36	0.06	239.84	0.19	190.22
O1	0.16	0.21	0.01	6.62	0.02	64.52	0.52	26.07	0.07	357.54	0.14	50.76	0.53	160.62	0.03	147.89	0.18	159.10
N2	0.09	155.33	0.01	160.23	0.05	326.06	0.13	346.20	0.08	256.94	0.03	359.36	0.36	269.38	0.02	78.12	0.12	273.52
P1	0.10	11.57	0.01	304.88	0.01	94.78	0.31	41.82	0.04	5.46	0.08	62.12	0.17	195.74	0.02	233.80	0.07	195.58

[1] Positive upwards
[2] Positive northwards
[3] Positive westwards

Table 5.2

Amplitudes (in centimetres)
and Greenwich Phases

The coordinates of the pole are entered into the VLBI programme in terms of x and y, in milliarcseconds. Then the Wobble matrix, which is used in the programme, reads (Langley, 1979):

$$W = \begin{bmatrix} 1 & 0 & -x \\ 0 & 1 & y \\ x & -y & 1 \end{bmatrix} \qquad (5.33)$$

In the wobble matrix, x and y are in radians and they are determined by equations (4.34). The wobble matrix transforms coordinates expressed in the earth-fixed coordinate system to coordinates in a system defined by the instantaneous pole of rotation and the Greenwich mean astronomic meridian (GMAM).

5.3. The Canadian VLBI Array.*

The Canadian VLBI array consists of three stations: Algonquin Radio Observatory (ARO), Lake Traverse, Ontario; Owens Valley Radio Observatory (OVRO), Big Pine,

---

*The name "Canadian VLBI Array" is used in this study only.

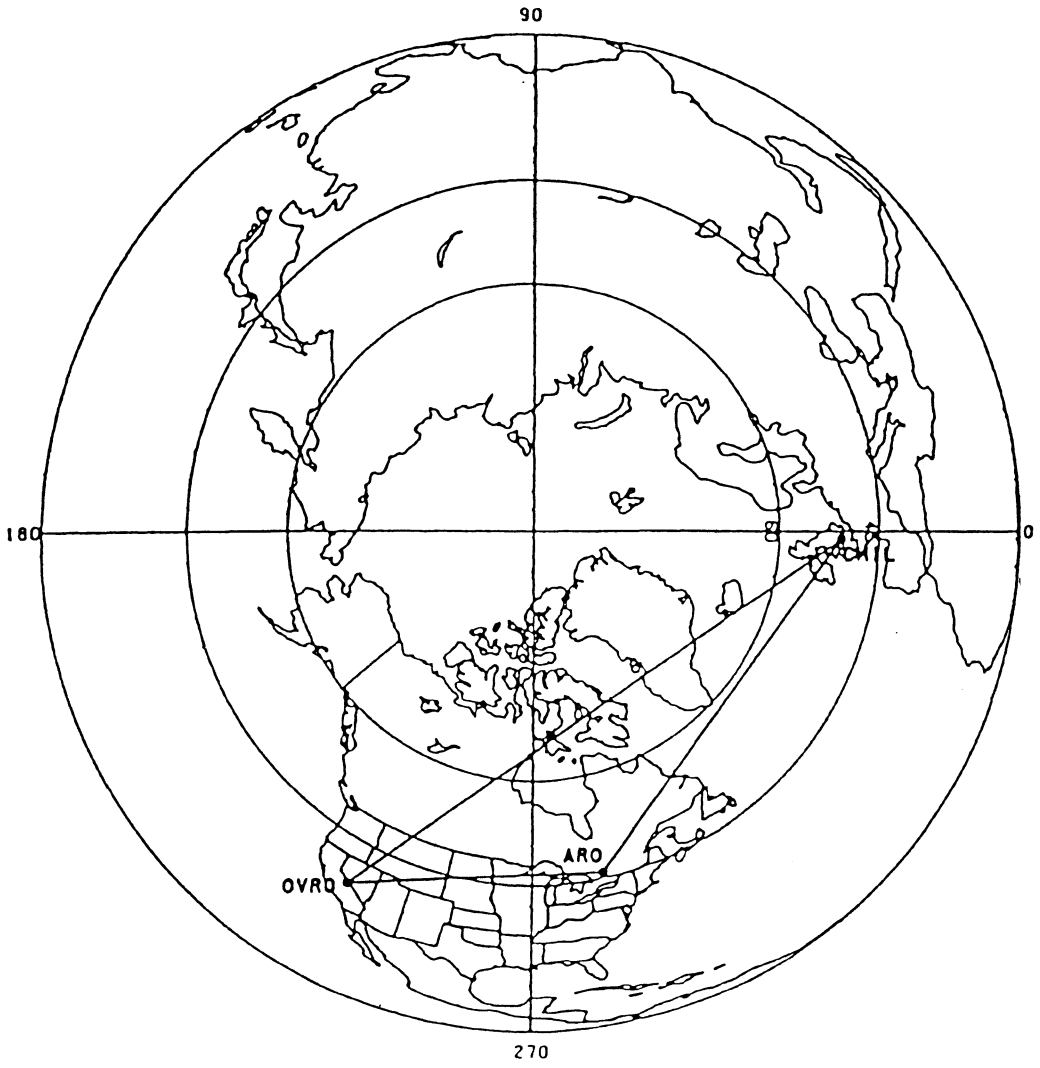

Fig. 5.4

An equatorial projection of the Canadian VLBI array (Langley, 1979).

California; and Chilbolton Observatory (CHIL), Chilbolton, England (Fig. 5.4). This system was used in seven observing sessions between February 1975 and January 1978 (Langley, 1979). The observations were made at frequencies near 10 GHz. Two of the observing sessions yielded good quality data (fringe frequency and delay) and have been analysed in the past. The observing session in May 1977 was used to test the body tide, ocean loading and polar motion models developed in this study. Unfortunately very little can be concluded because of the noisy data and the resulting large standard errors of the baseline lengths which vary from 43 cm (CHIL-ARO) to 80 cm (OVRO-ARO).

Applying only the body tide model developed in this study, there is a considerable difference in the components of the baselines with those obtained by Merriam's model (Langley, 1979), ranging from -47 cm to +14 cm (Figures 5.5, -6, -7) and for the baseline lengths from +4 cm (OVRO-ARO) to +11 cm (CHIL-OVRO) (Fig. 5.8). The rms scatter of the delay-rate residuals decreases by 9.2×10^{-5} picoseconds/sec and of the group-delay residuals increases by 3 picoseconds (1 cm). There is an improvement in the distribution of the standardized delay rate residuals when one applies the present body tide model. The χ^2 test on the standardized delay rate residuals passes while previously it failed. The

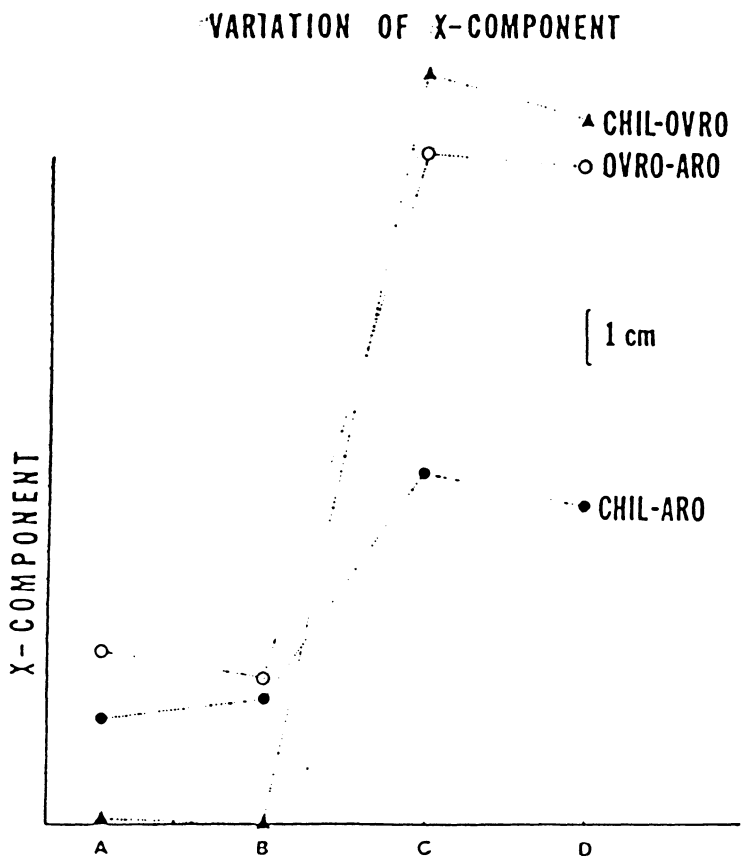

Fig. 5.5. Canadian VLBI Array.

A--No Tidal Correction applied.

B--Body Tide Correction applied (previous model).

C--Body Tide Correction applied (present study).

D--Body Tide and Ocean Loading Corrections applied.

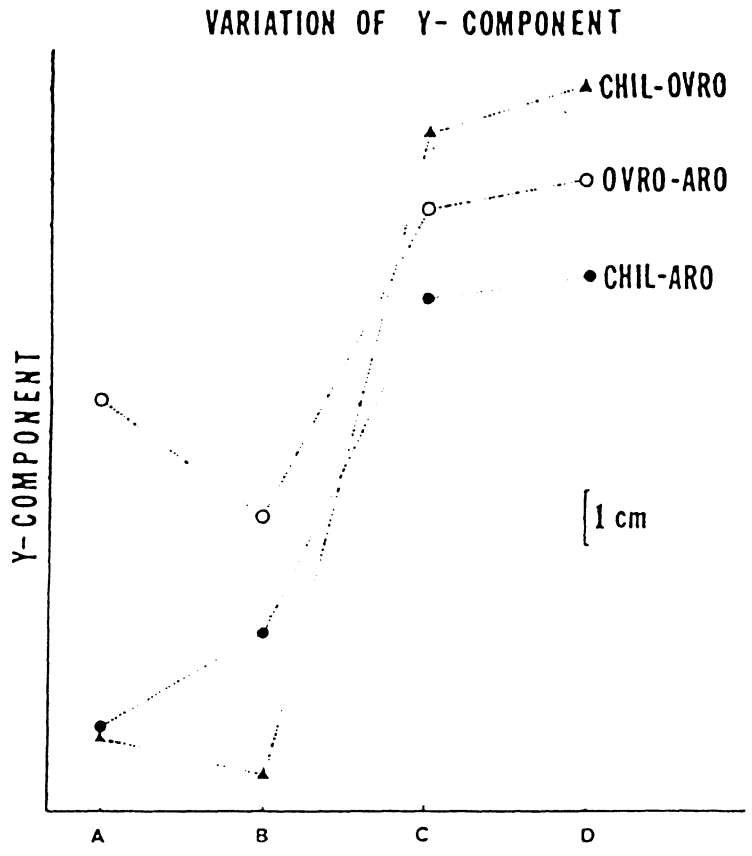

Fig. 5.6. Canadian VLBI Array.

A--No Tidal Correction applied.

B--Body Tide Correction applied (previous model).

C--Body Tide Correction applied (present study).

D--Body Tide and Ocean Loading Corrections applied.

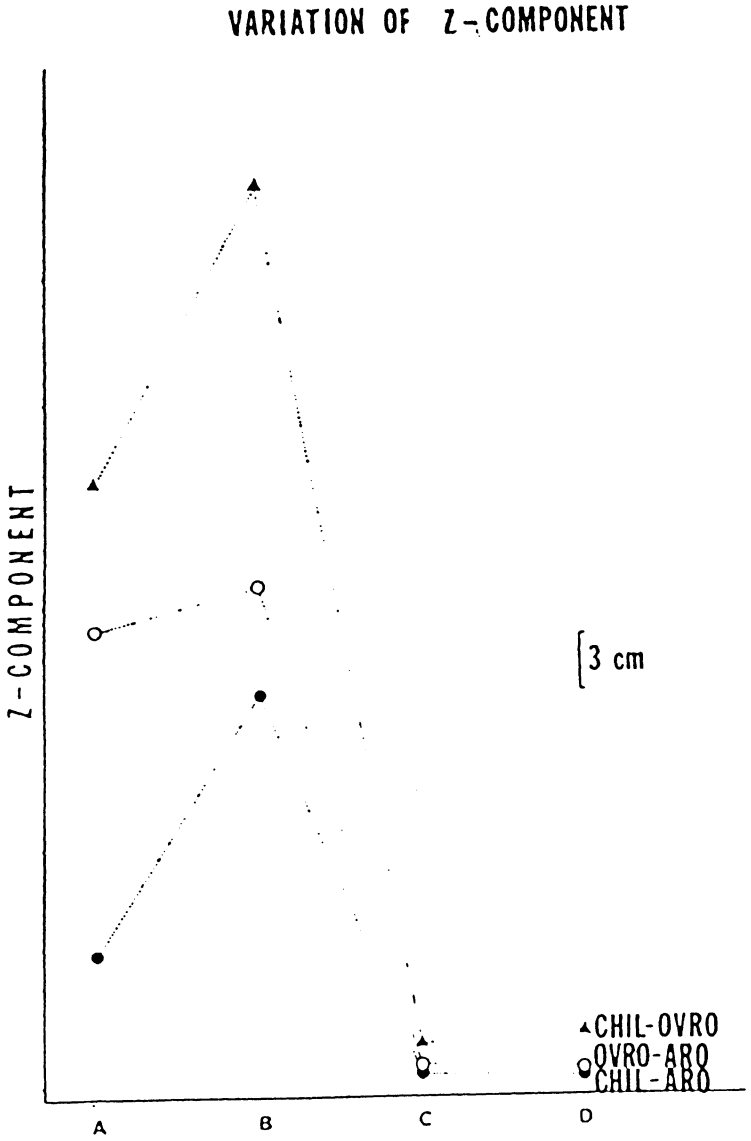

Fig. 5.7. Canadian VLBI Array.

A--No Tidal Correction applied.

B--Body Tide Correction applied (previous model).

C--Body Tide Correction applied (present study).

D--Body Tide and Ocean Loading Corrections applied.

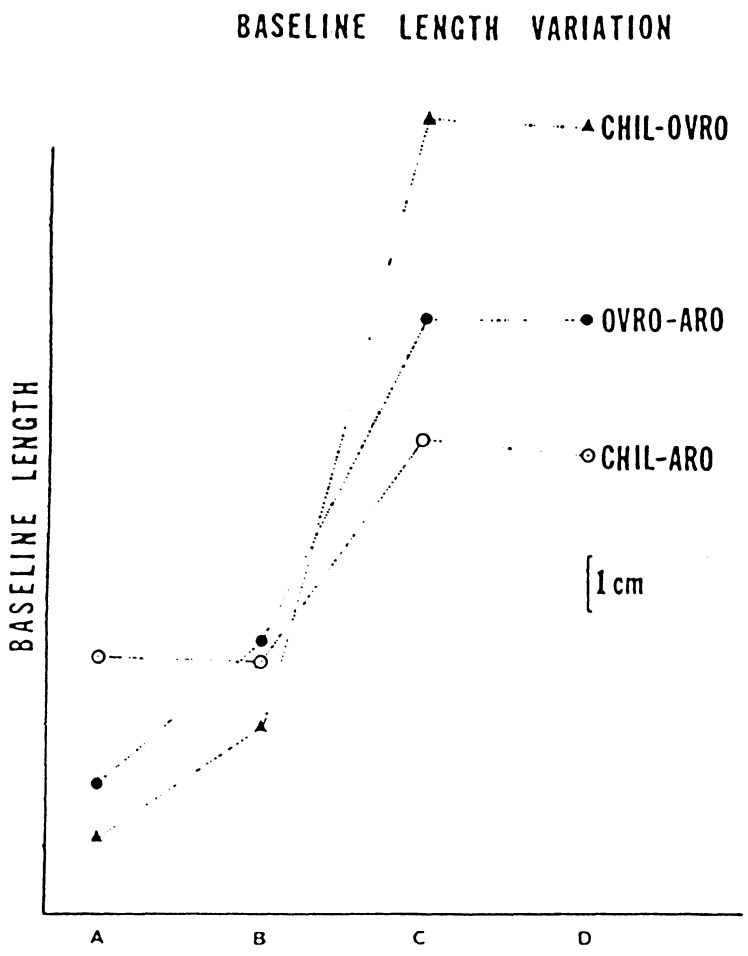

Fig. 5.8. Canadian VLBI Array.

A--No Tidal Correction applied.

B--Body Tide Correction applied (previous model).

C--Body Tide Correction applied (present study).

D--Body Tide and Ocean Loading Corrections applied.

distribution of the group delay residuals remains almost unchanged.

Applying load corrections, no significant change appears in the results. A change in the baseline components, ranging from -8.3 mm to +9 mm and in the baseline lengths from 0.0 mm to -2.5 mm was found. The standard errors for the components as well as for the baseline lengths improved slightly, although the improvement is less than 1 cm.

Polar motion affects only the orientation of the baselines and a maximum difference of 0".010 was found in the declination, from the previous version, which used a constant value for the pole position for the whole observation period.

The computational efficiency of the Canadian VLBI programme (Appendix G) increases significantly. The simplicity of the body tide model developed in this study, increases the computational efficiency by 25% with respect to the previous version. Routine TIDEUP (Fig. G.2, Appendix G) evaluates the deformation of the lithosphere in terms of radial, north-south and east-west components due to body tide and ocean loading. Entry DISP evaluates the body tide deformation. Routine LOAD evaluates the load effect, which is stored in terms of amplitudes and phases. The coordinates of the pole are

evaluated from routine WOBRED. The total computer time for the modified GEOAIM is now used as follows; 83.0% least squares adjustments and other corrections (e.g. precession and nutation); 1.4% body tide corrections; 1.4% ocean loading corrections; and 14.2% polar motion corrections.

The total time (CPU) for the VLBI programme is now 35.27 seconds for the 180 observations. For the previous version it was 39.5 seconds including only body tide corrections.

Results of the effect of the ocean loading using (3.12) and (3.13) on the three stations of the Canadian VLBI array are presented in Table 5.2 (p. 63). Also, co-range and co-tidal charts for the radial displacements for North America are presented in Figures A.1 to A.12 (Appendix A). Co-range maps for north-south and east-west displacements were also produced for North America (Figures A.13 to A.24).

CHAPTER VI

CONCLUSIONS AND RECOMMENDATIONS

The objectives of the work undertaken for this thesis were to develop a mathematical model for the evaluation of the deformation of the terrain due to body tide and ocean loading; to derive an approximation procedure for polar motion; and to update the Canadian VLBI software package (GEOAIM) to account for the above effects.

Green's functions were derived for radial and horizontal displacements due to load as well as for gravity perturbations and tilt. These functions were based on the Green's functions published by Farrell (1972) for the Gutenberg-Bullen A earth model. They were derived under the assumptions that the points of interest are at least 100 km from the coast and that the earth responds elastically under tidal frequencies.

To test the derived Green's functions, gravity perturbations were determined for eight stations from different points of the earth. At these stations, gravity perturbations due to ocean loading have been determined in the past with high accuracy, from actual observations.

The comparisons show very good agreement. A mean absolute difference between the observed and predicted effects for inland locations of 0.32 μGal with an rms scatter of 0.19 μGal was obtained.

The Green's functions tabulated by Farrell (1972) were interpolated for intermediate values of ψ, using cubic splines. There is some room here for improvements in this procedure. An approximating function for the Green's functions computed by Farrell or even better for the Green's functions derived here (which seem to be smoother) would be computationally more efficient.

The body tide model developed here gives results (in three dimensions) with an accuracy of 1 cm. Its algorithm is simpler than that of Merriam's (1978) and consequently more efficient, since it reduces the computer processing time of GEOAIM by 25% with respect to the previous version.

Polar motion was determined using data based on the "1979 BIH system" and Lagrangian interpolation of four values separated by five days centered at the time of observation. The software for the interpolation was developed in the M.I.T. Department of Earth and Planetary Sciences and has been modified by the author to fit the Canadian VLBI programme. The data for the pole position are stored on tape. A transfer of these data on disk in a

form of a direct access file would improve the computational efficiency.

The use of the above models with the Canadian VLBI data didn't show any significant change in the results, due to the large standard errors. Another set(s) of good quality data could be used such as, Mk III with a repeatability in the determination of the baseline lengths of a few centimetres.

Ocean tide loading is a rather complicated phenomenon and it has been studied by several investigators. Here, in this study, only a simple view of the mechanism of the phenomenon was given, allowing some simplifying assumptions to be made. The effect becomes even more complicated if one considers points near the coast. The thickness of the lithosphere, local geology as well as uncertainties in the ocean tide models near the coast start playing an important role. Further investigations are needed for the evaluation of the load effect in coastal regions.

With improvements in the VLBI data aquisition system and in the modelling of the load effects a lot can be concluded about the internal constitution of the earth and its response to load.

APPENDIX A

CO-RANGE AND CO-TIDAL CHARTS

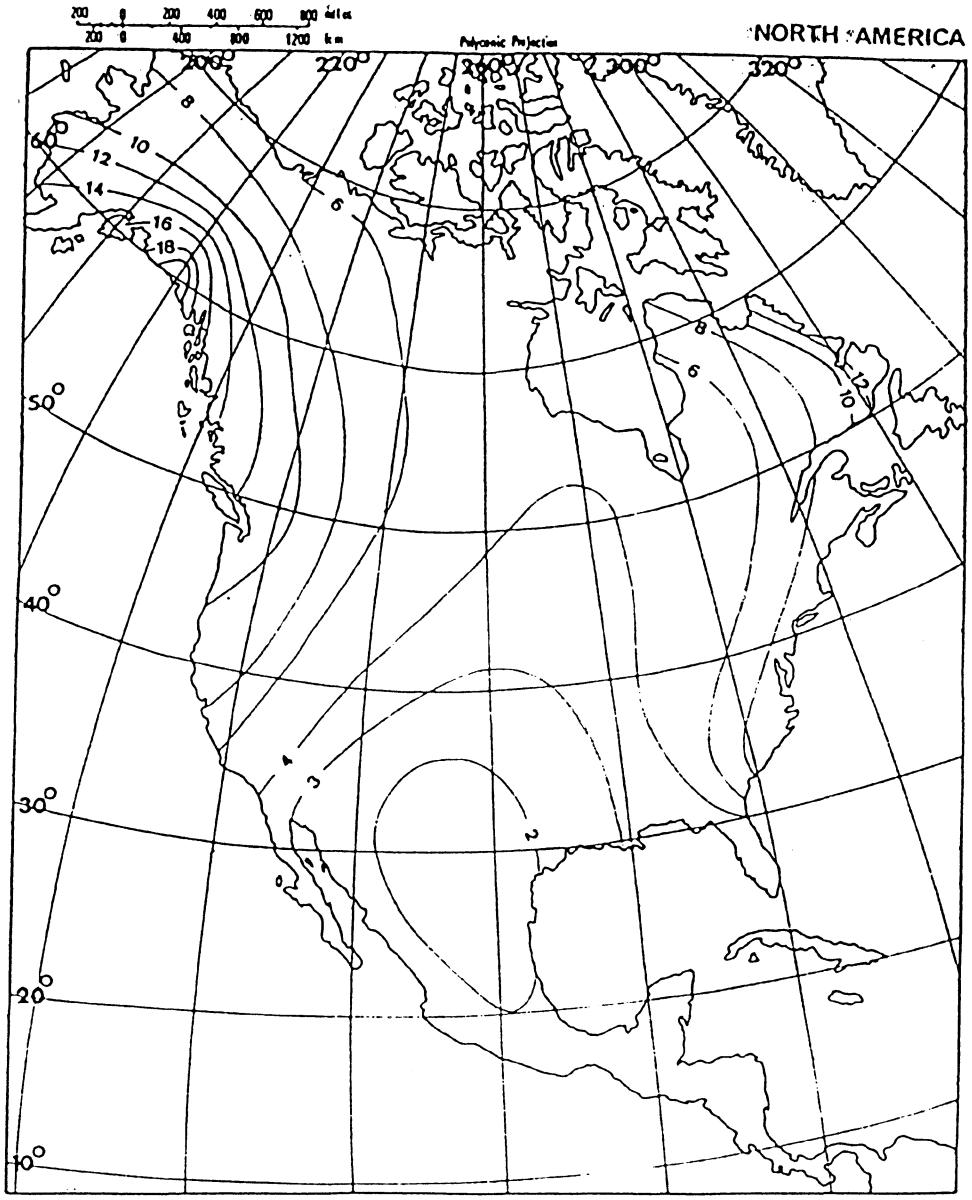

Fig. A.1. M_2 load. Radial displacement in mm.

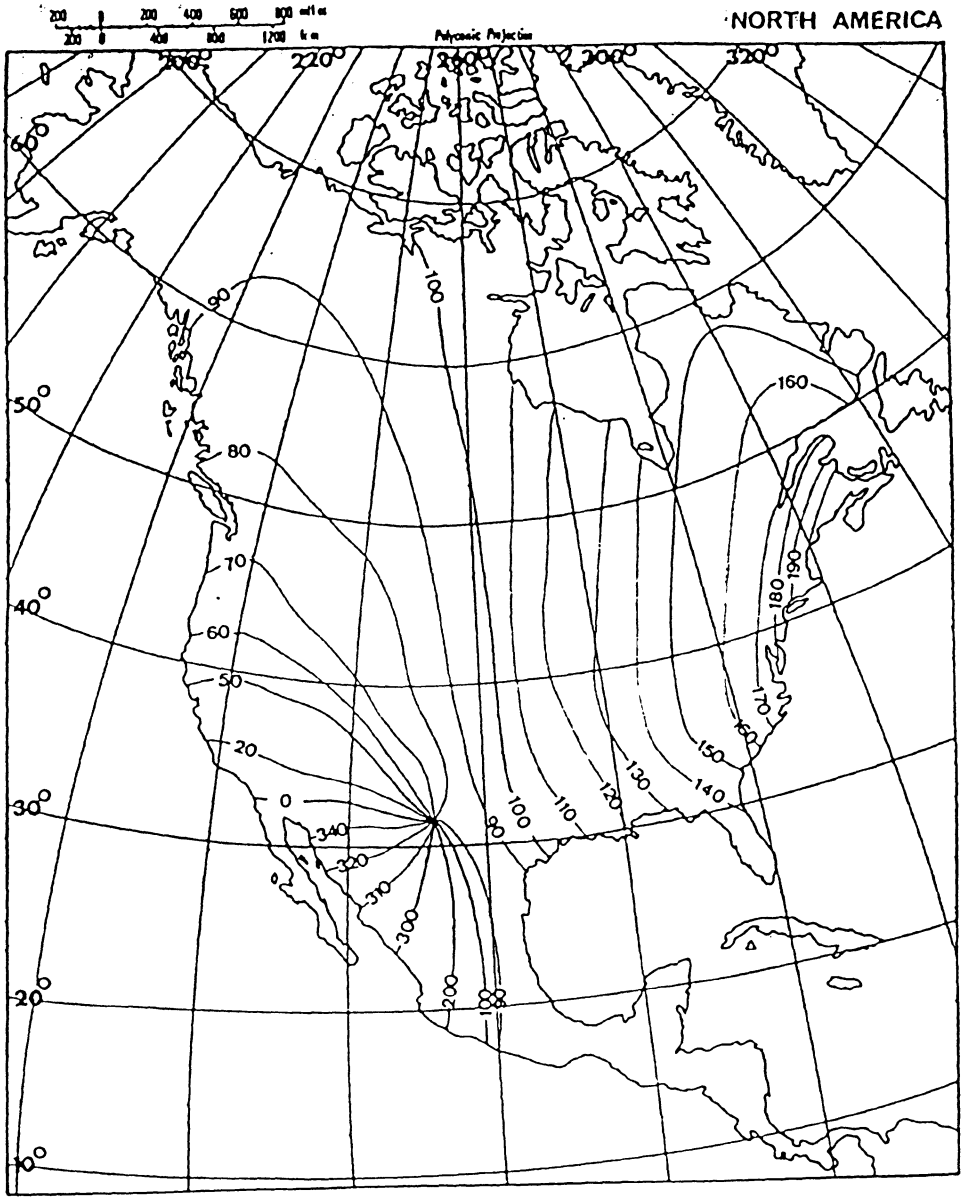

Fig. A.2. M_2 load. Radial displacement Greenwich phases (degrees).

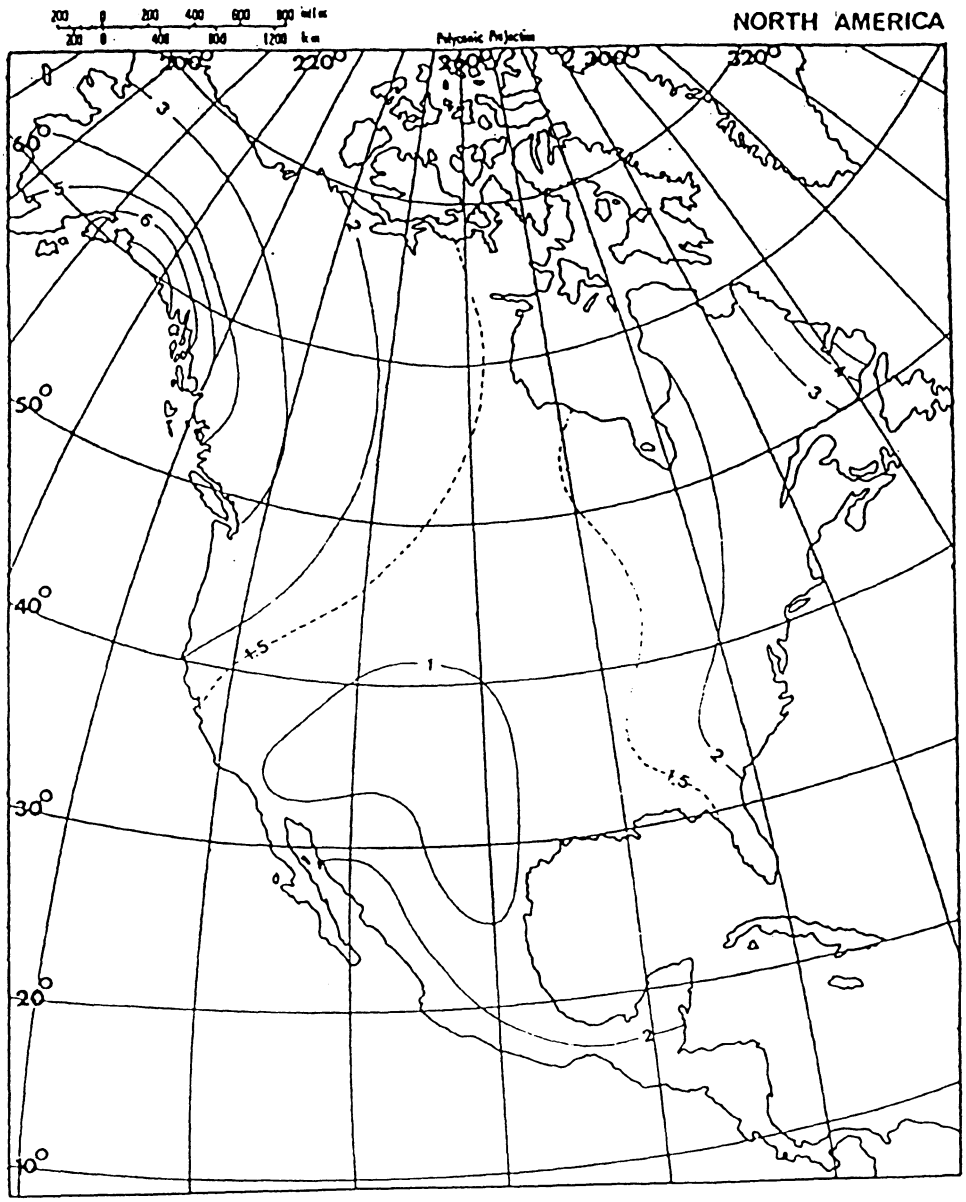

Fig. A.3. S_2 load. Radial displacement in mm.

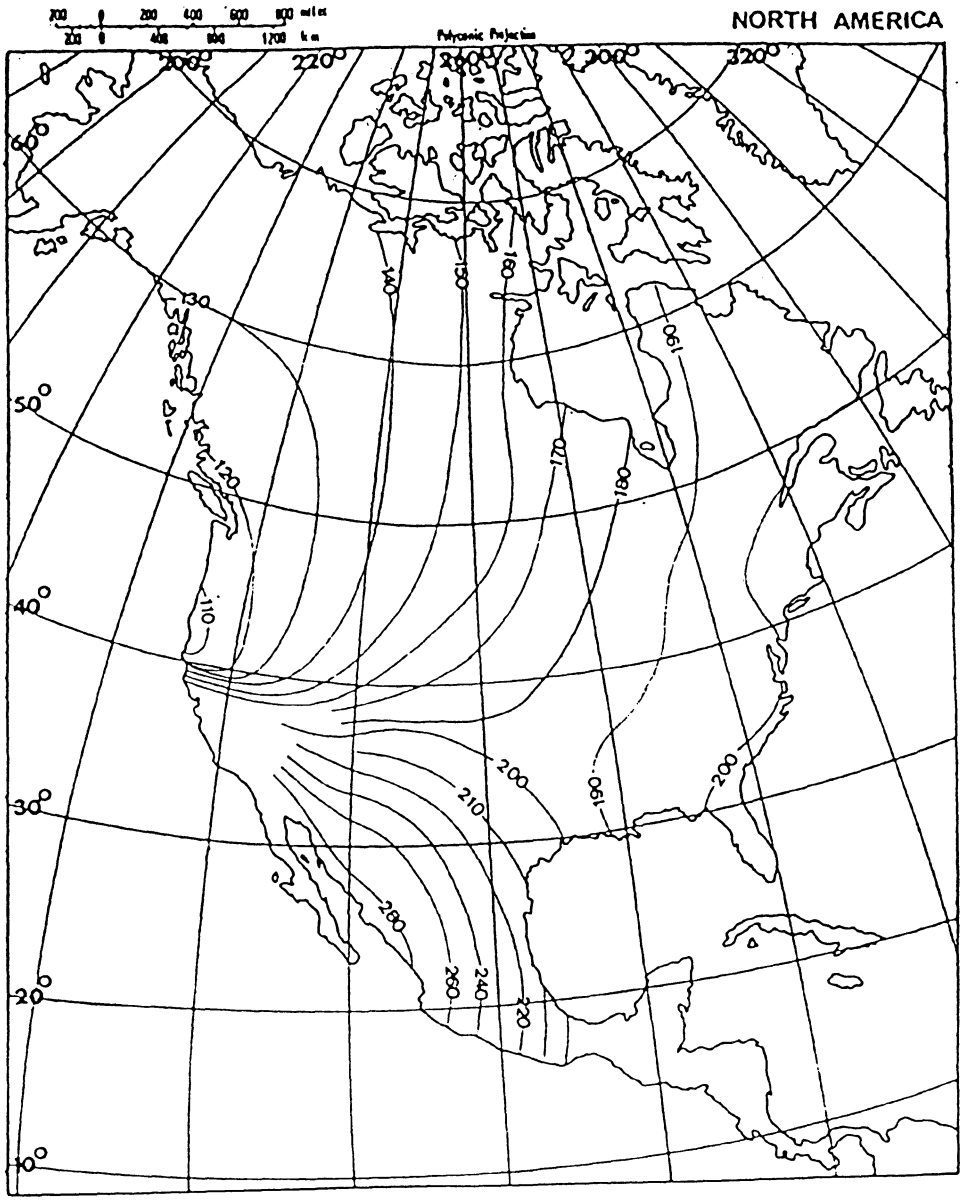

Fig. A.4. S_2 load. Radial displacement Greenwich phases (degrees).

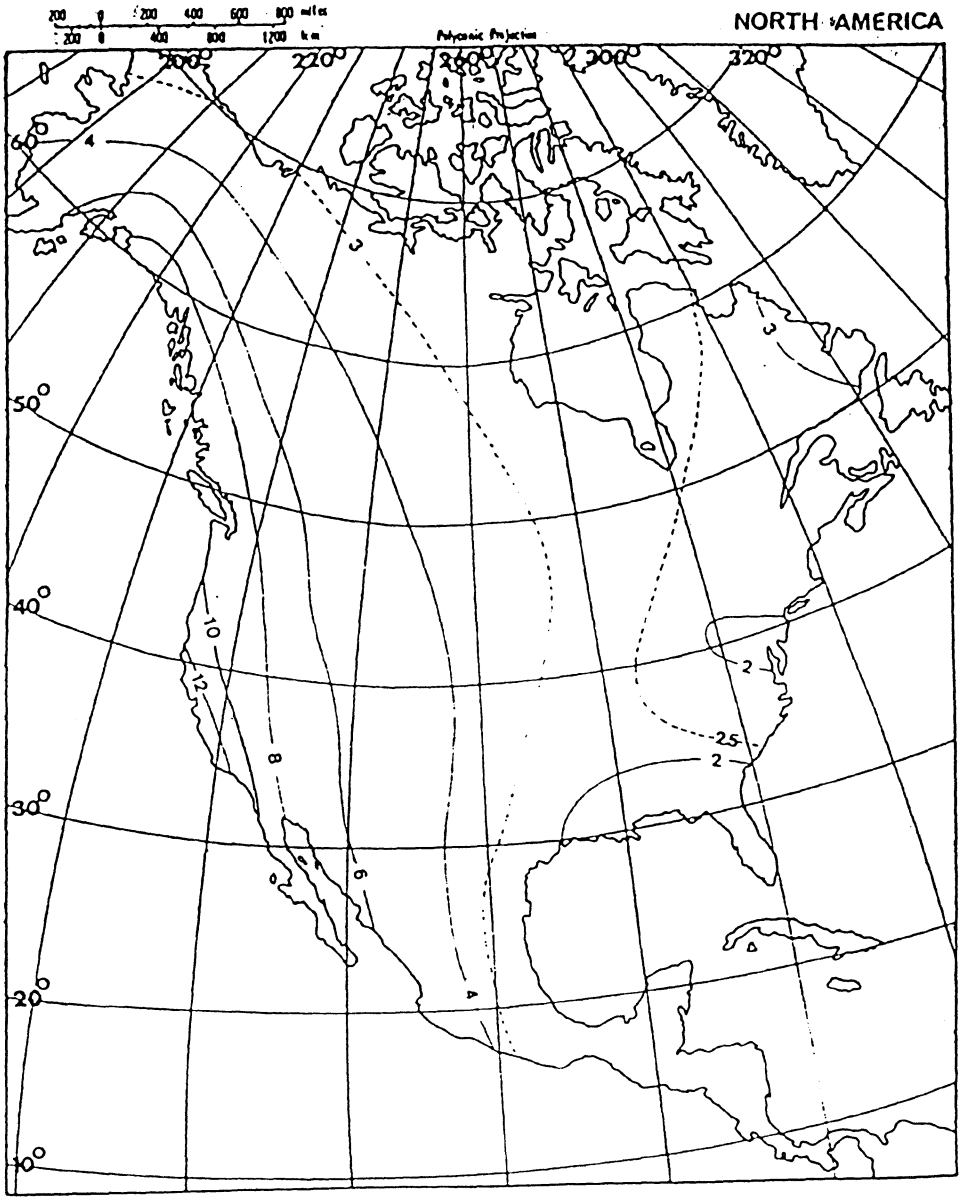

Fig. A.5. K_1 load. Radial displacement in mm.

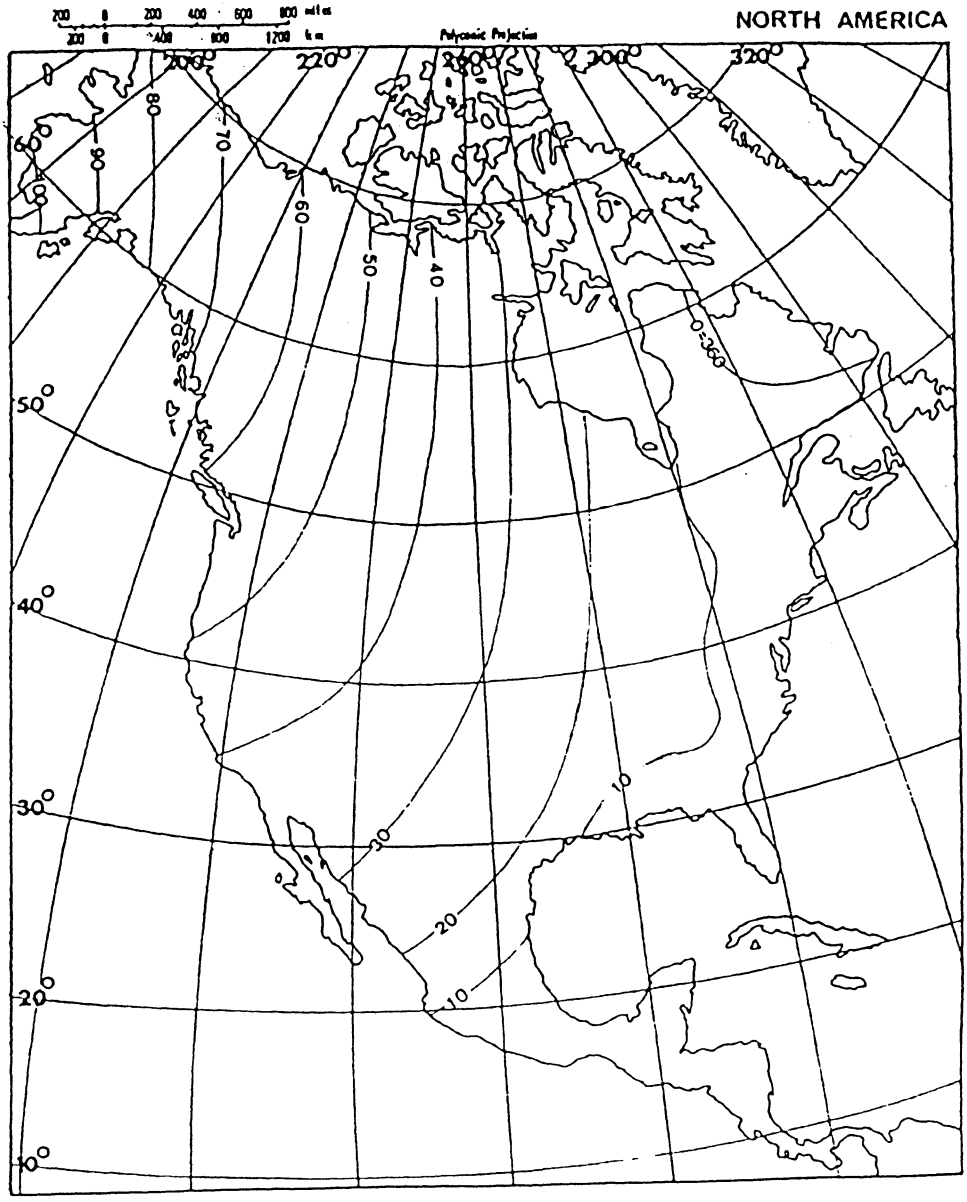

Fig. A.6. K_1 load. Radial displacement Greenwich phases (degrees).

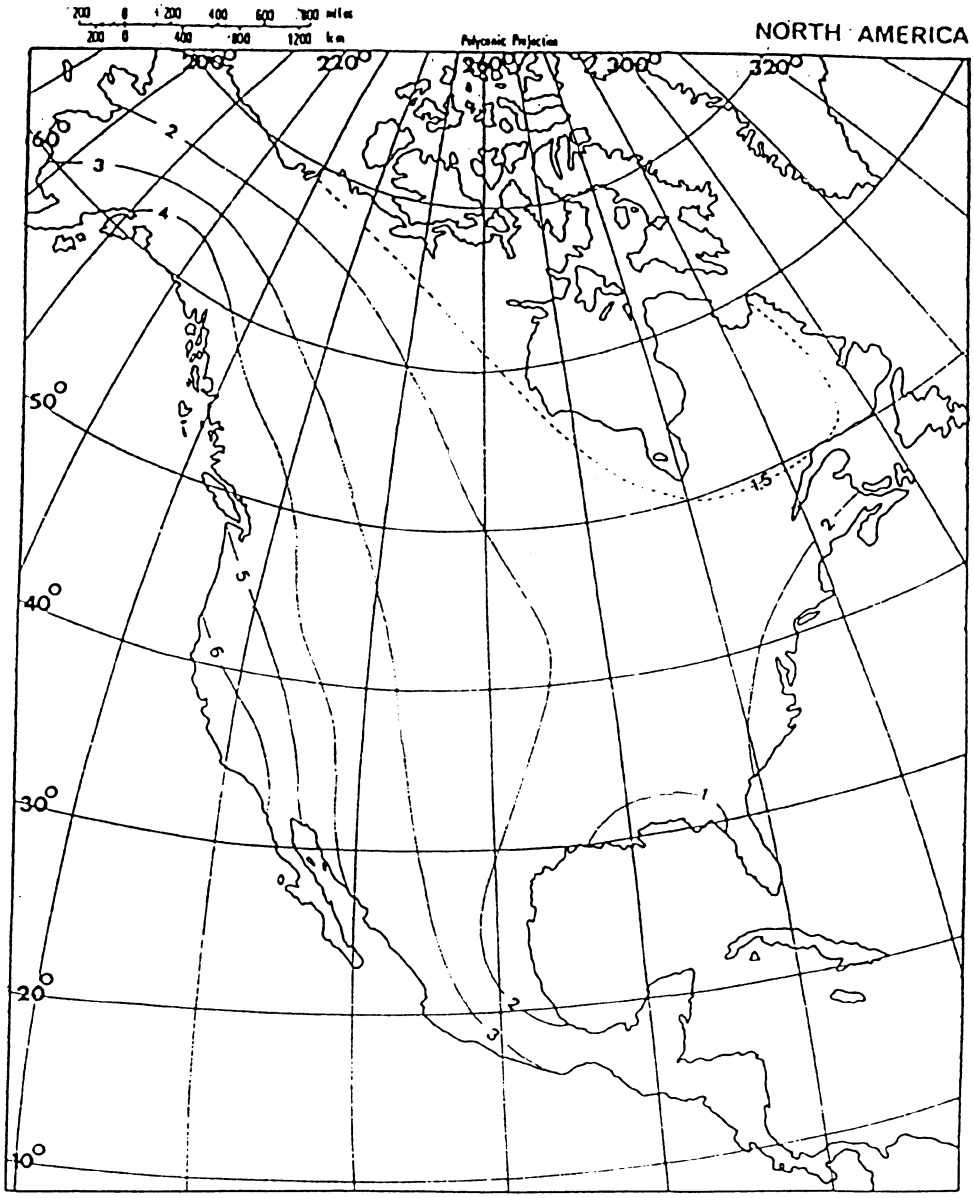

Fig. A.7. O_1 load. Radial displacement in mm.

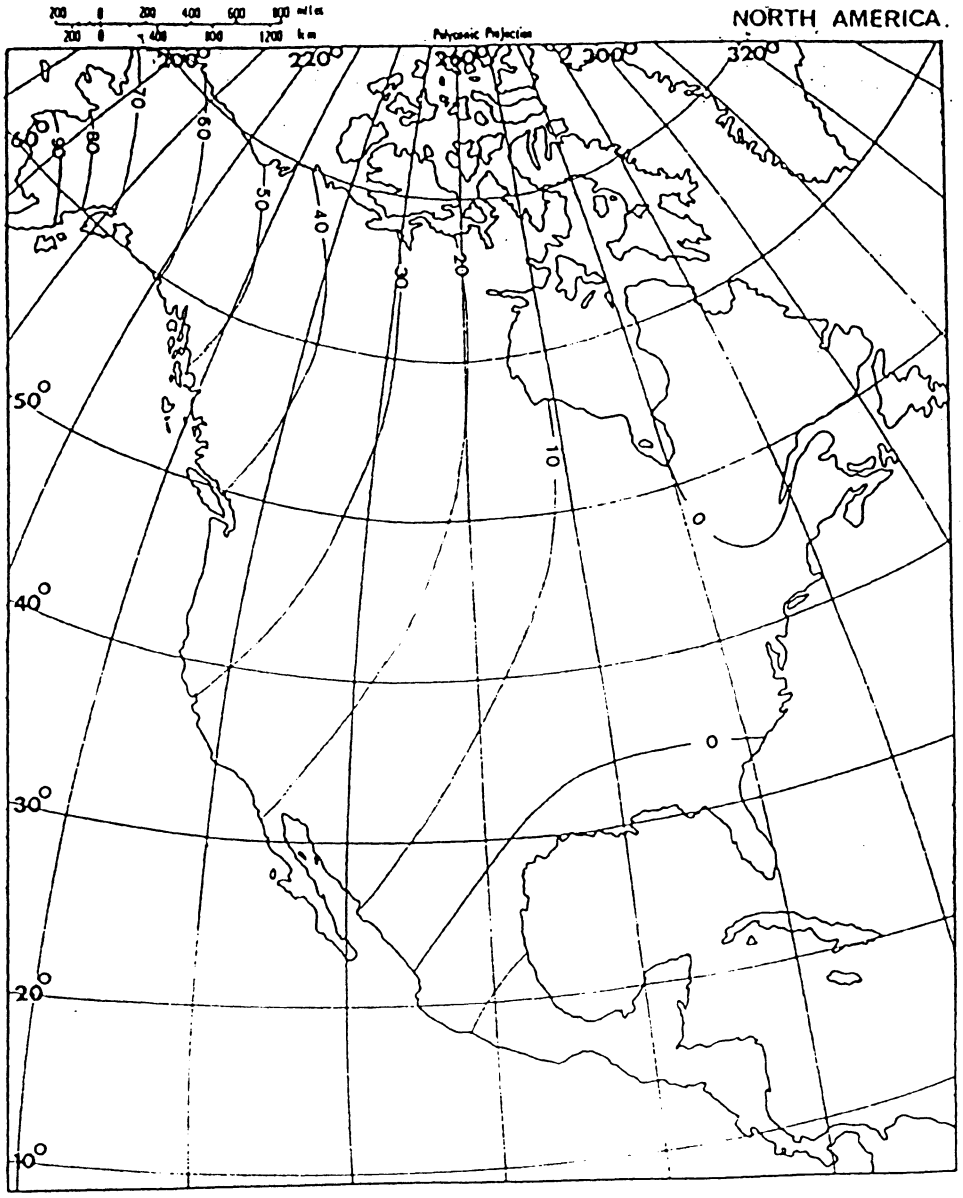

Fig. A.8. O_1 load. Radial displacement Greenwich phases (degrees).

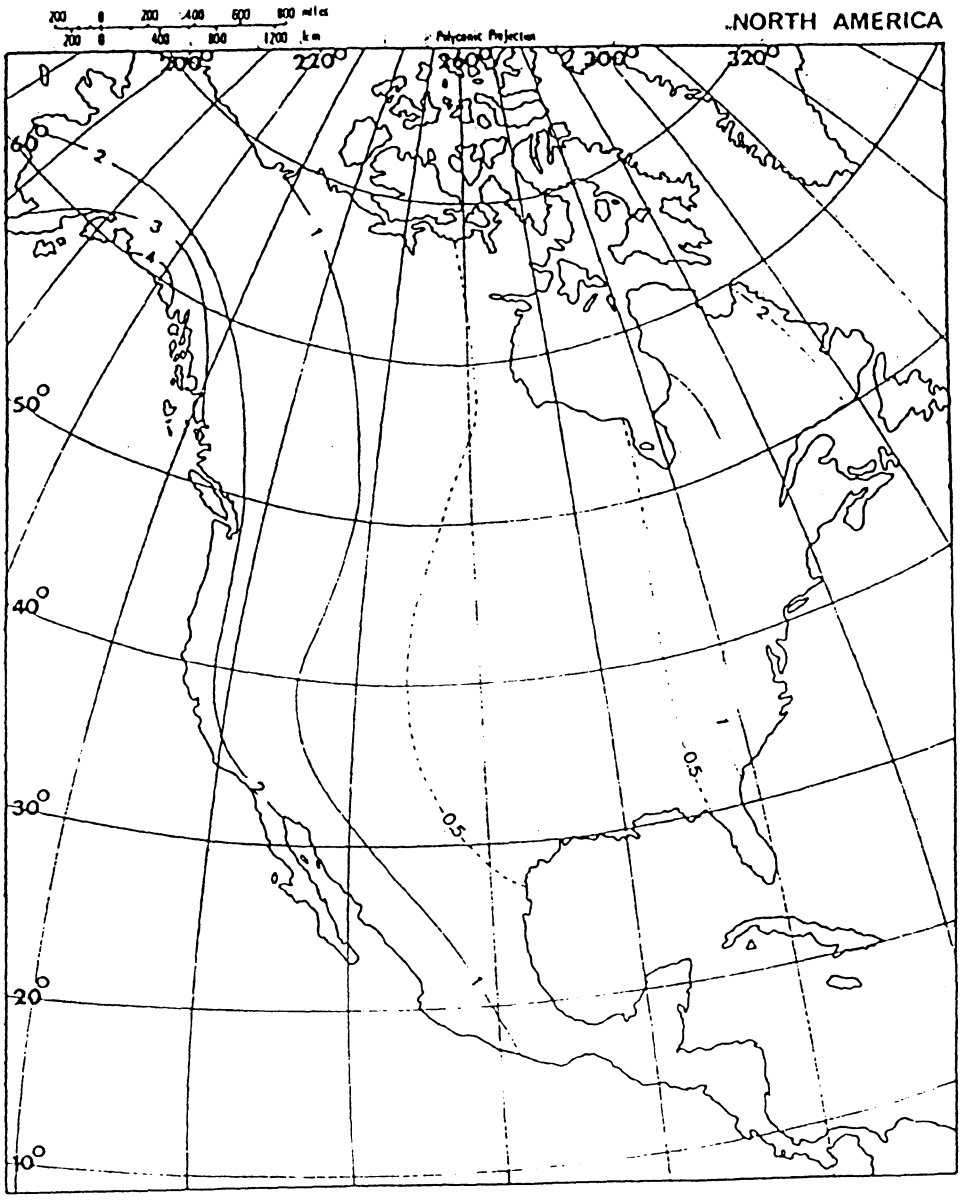

Fig. A.9. N_2 load. Radial displacement in mm.

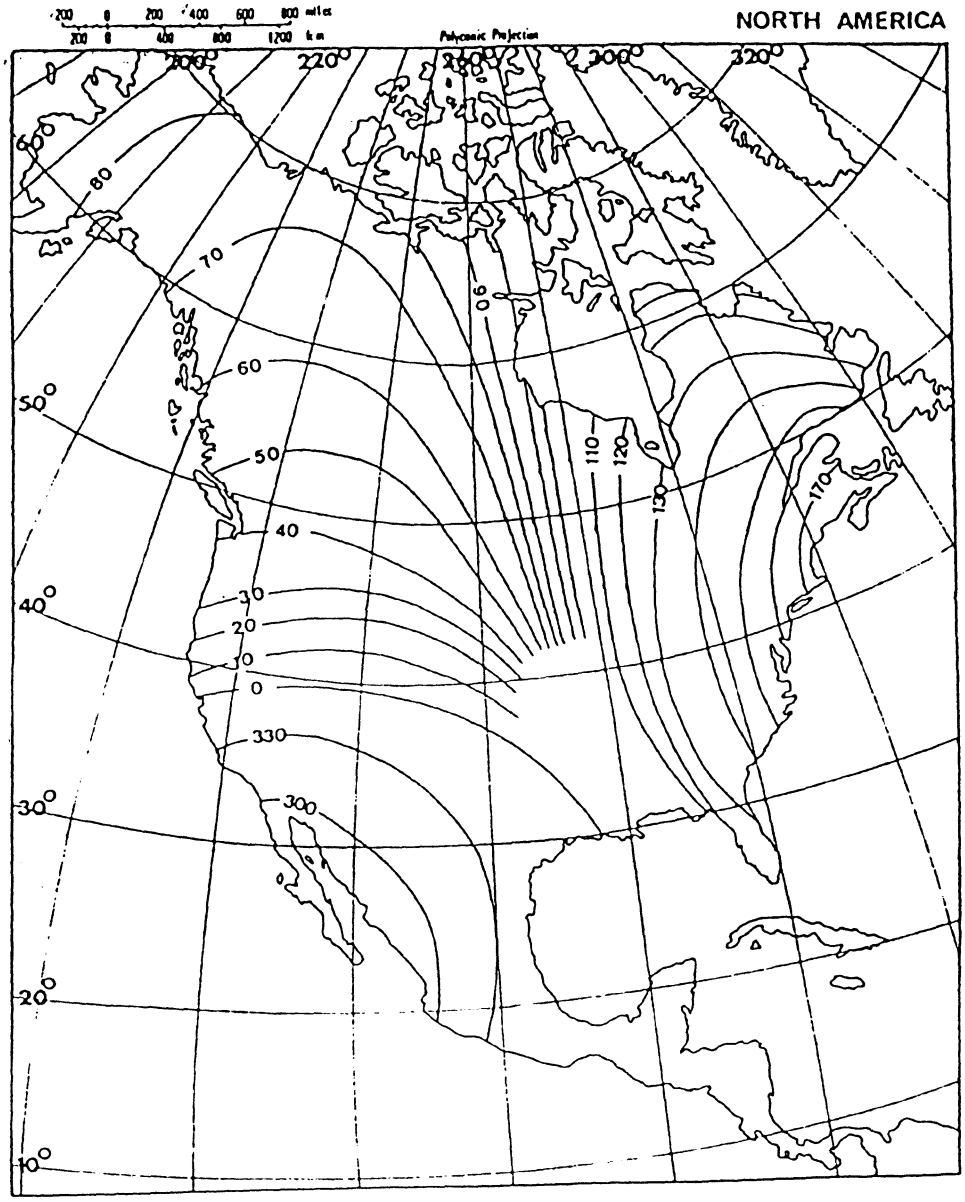

Fig. A.10. N_2 load. Radial displacement Greenwich phases (degrees).

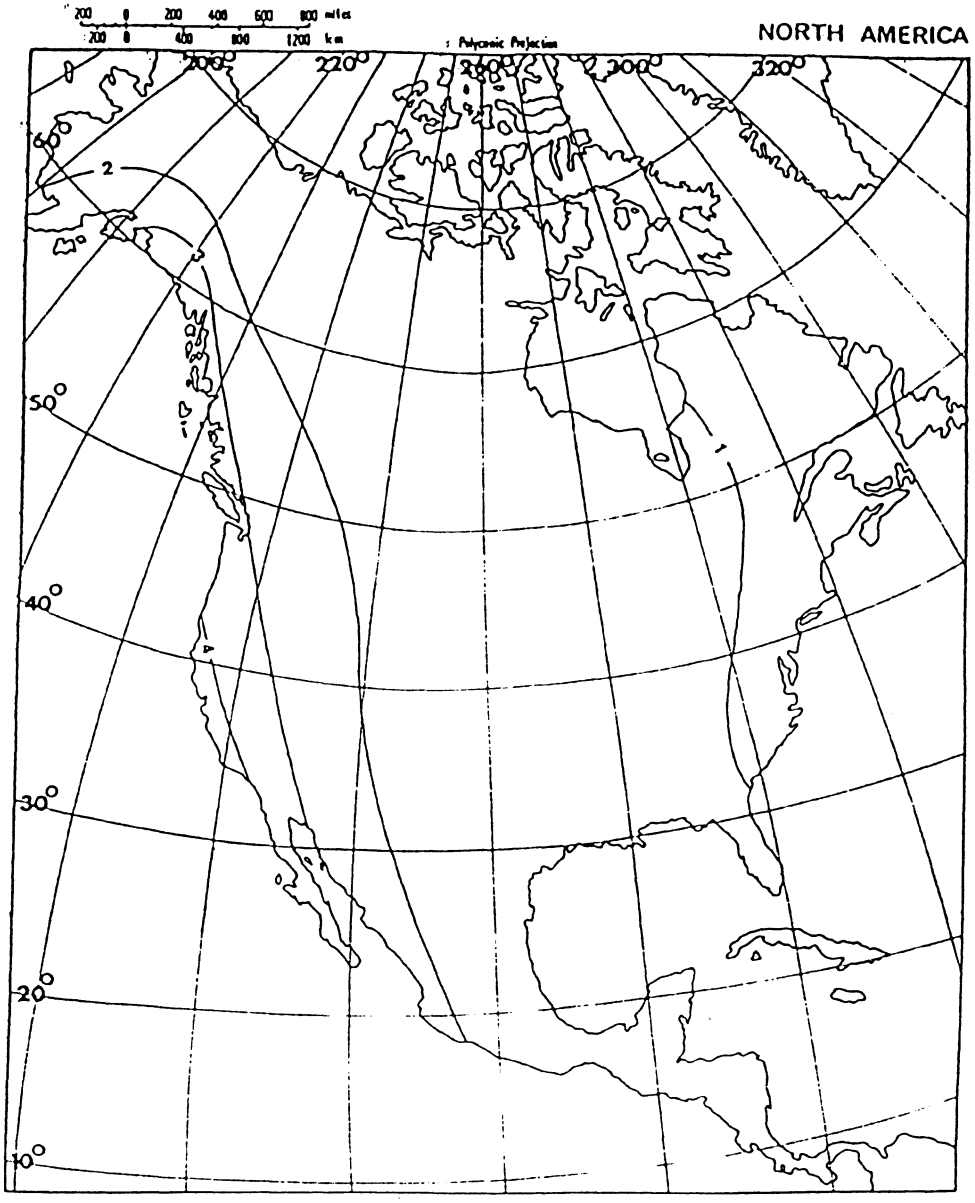

Fig. A.11. P_1 load. Radial displacement in mm.

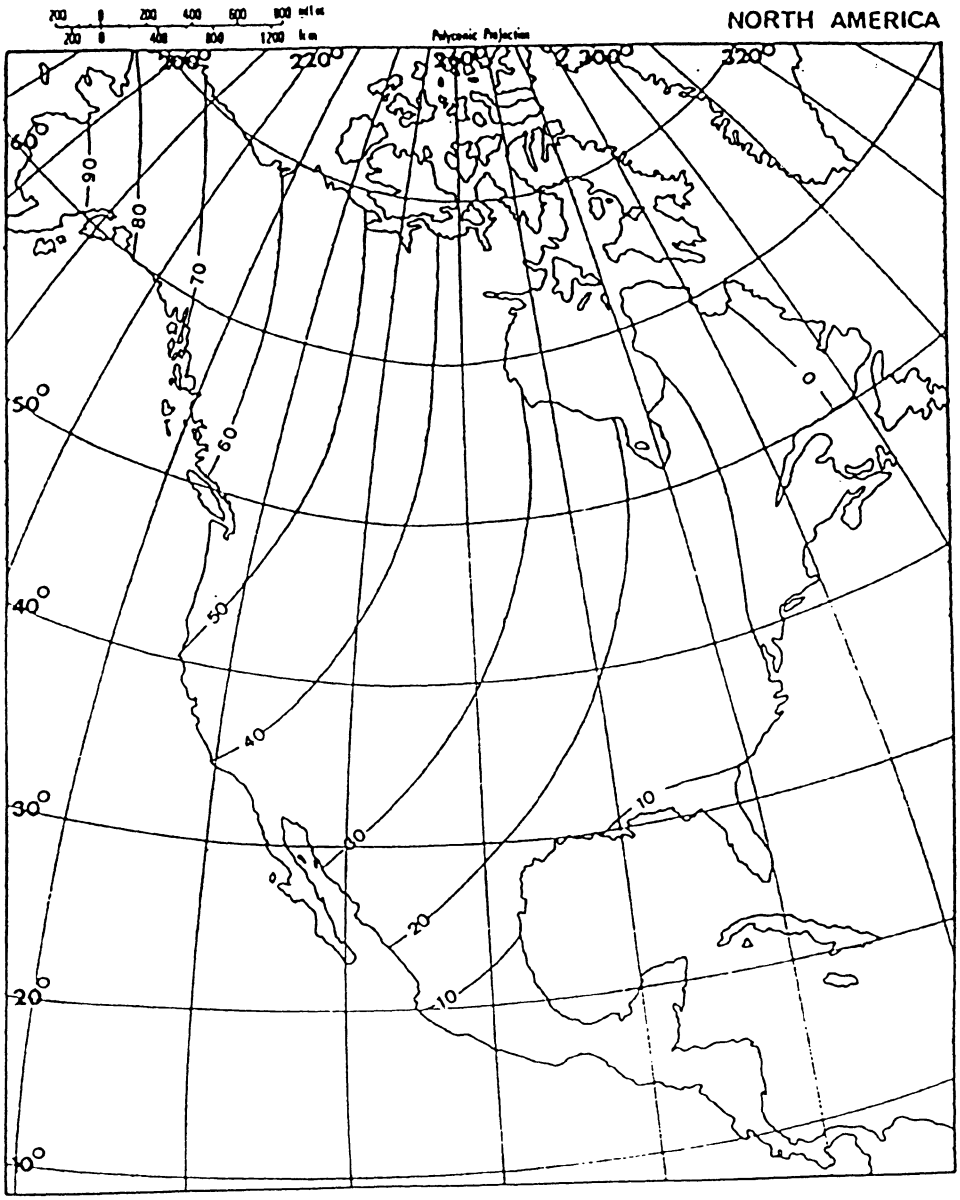

Fig. A.12. P_1 load. Radial displacement Greenwich phases (degrees).

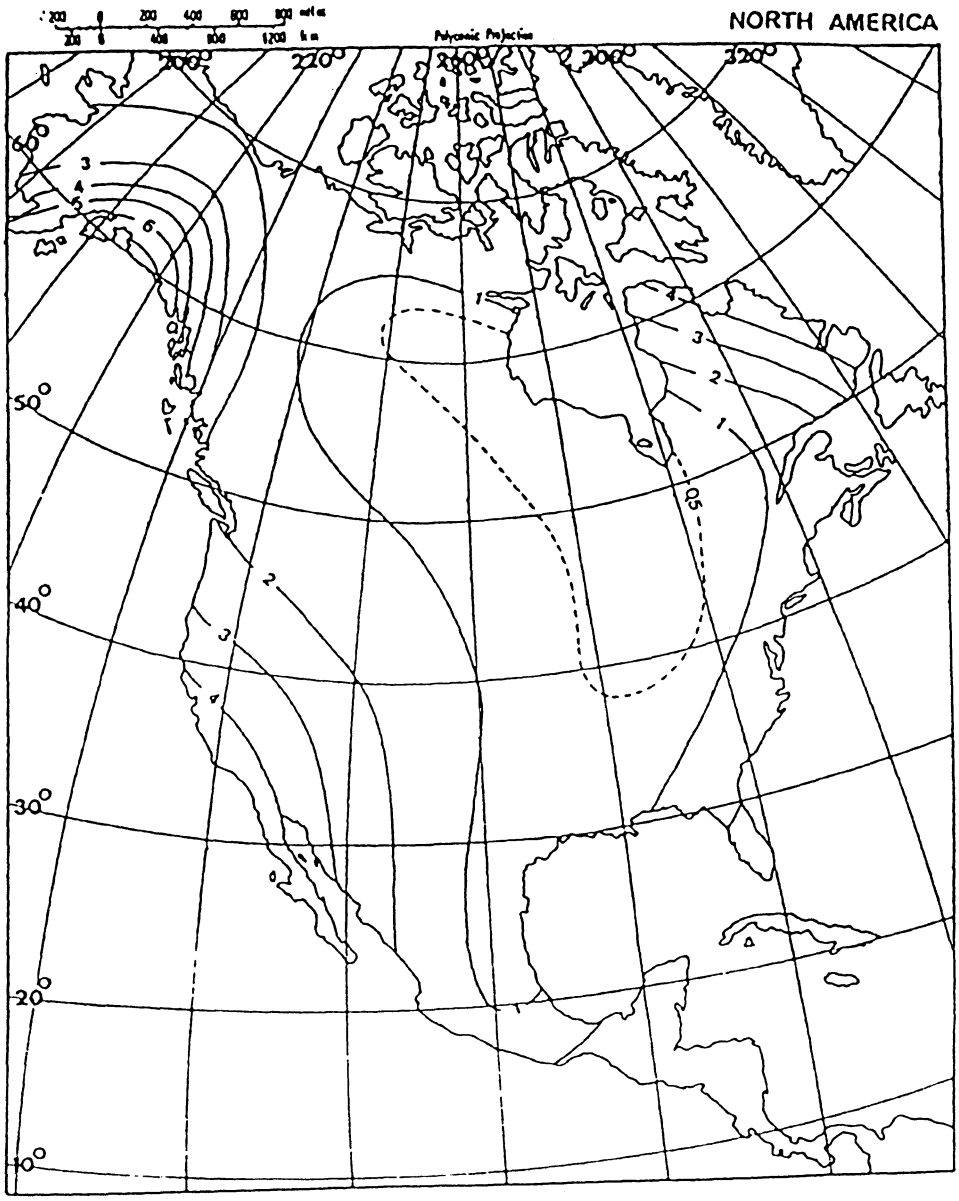

Fig. A.13. M_2 load. N-S displacement in mm.

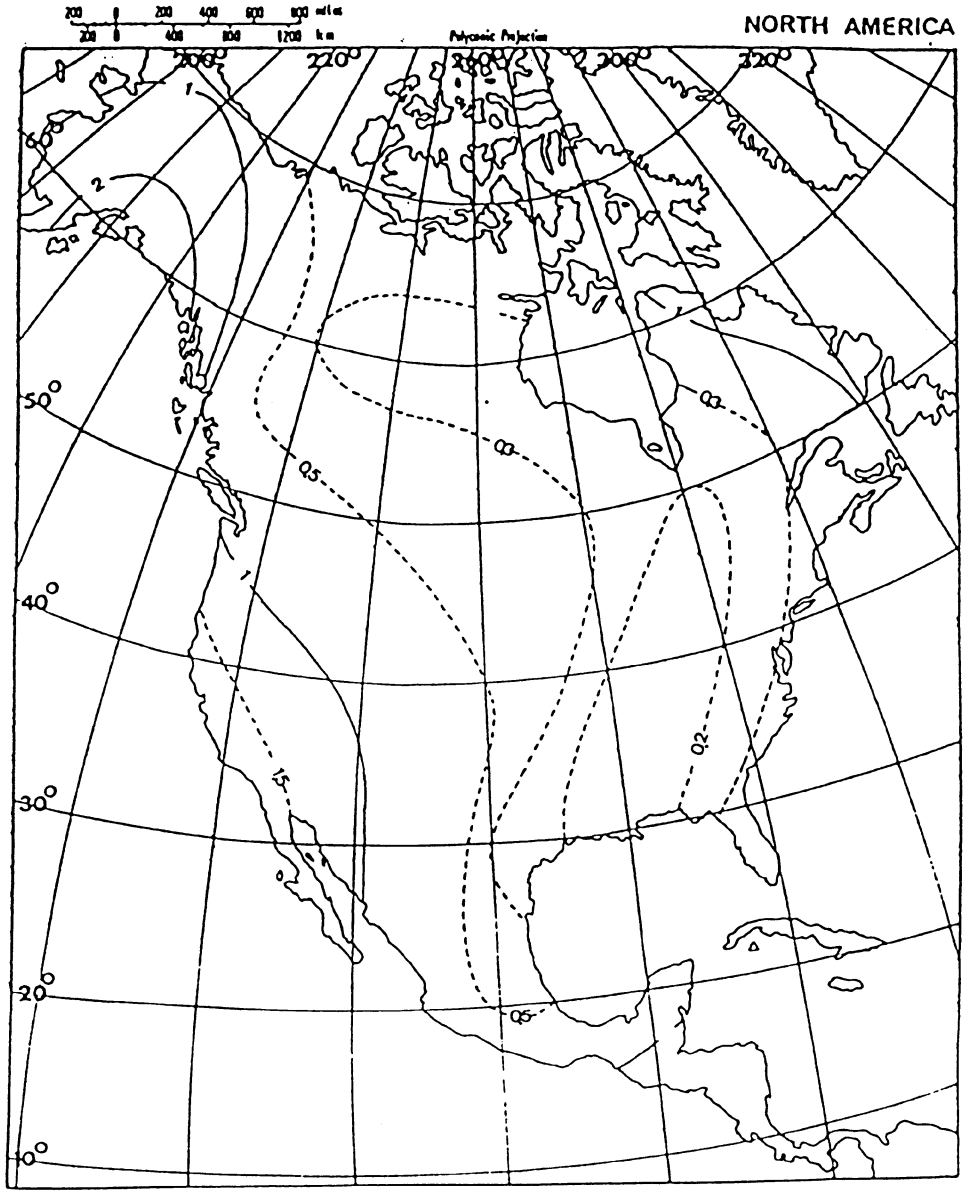

Fig. A.14. S_2 load. N-S displacement in mm.

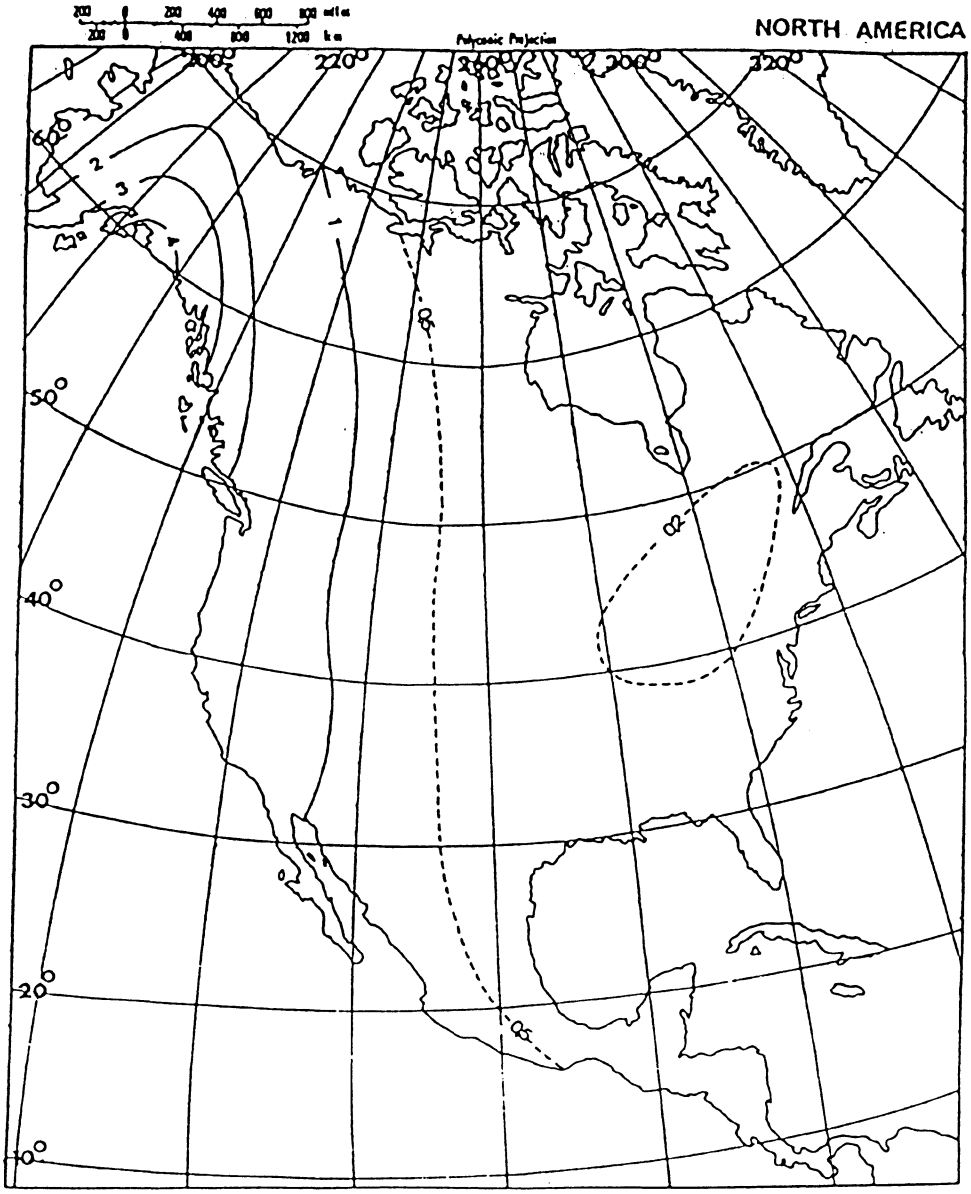

Fig. A.15. K_1 load. N-S displacement in mm.

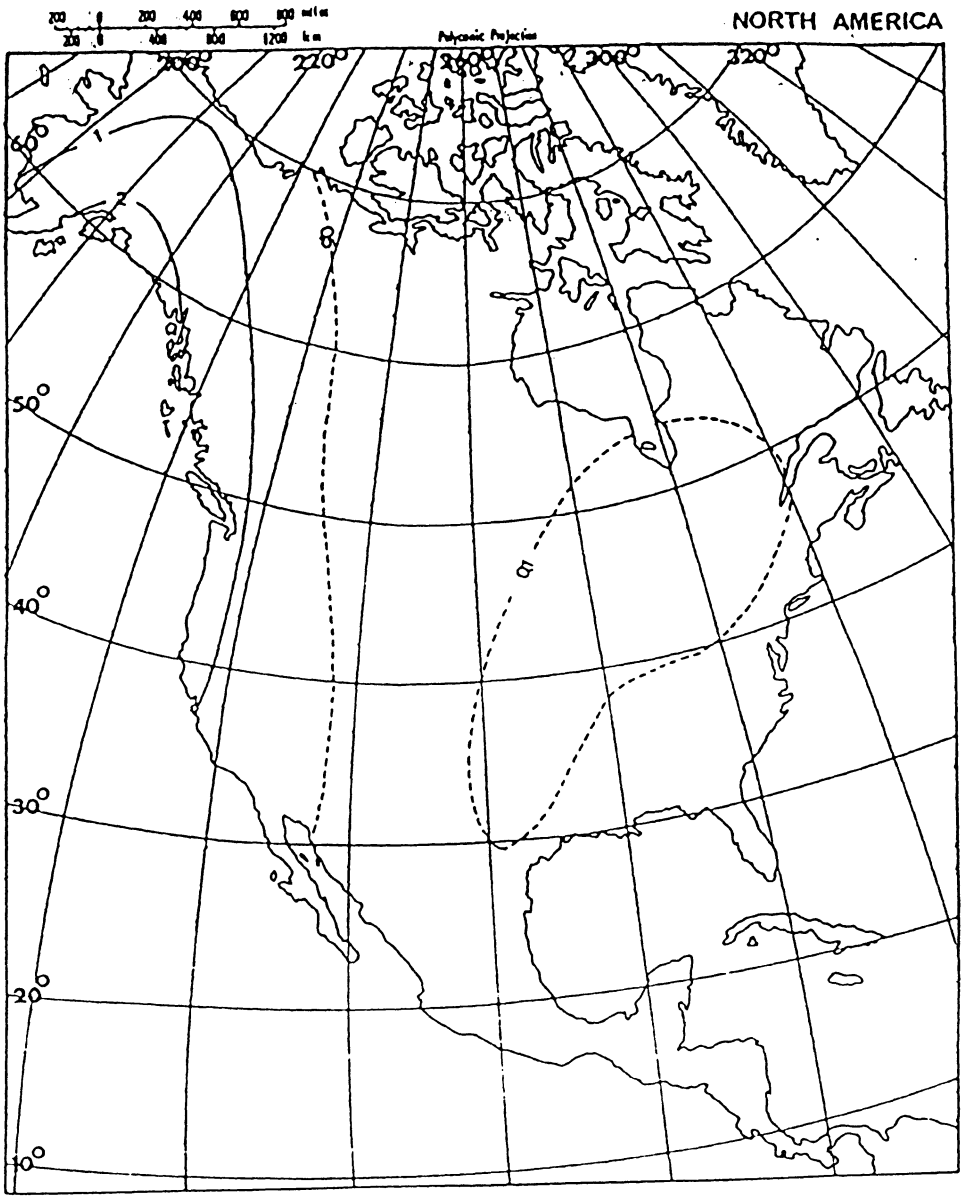

Fig. A.16. O_1 load. N-S displacement in mm.

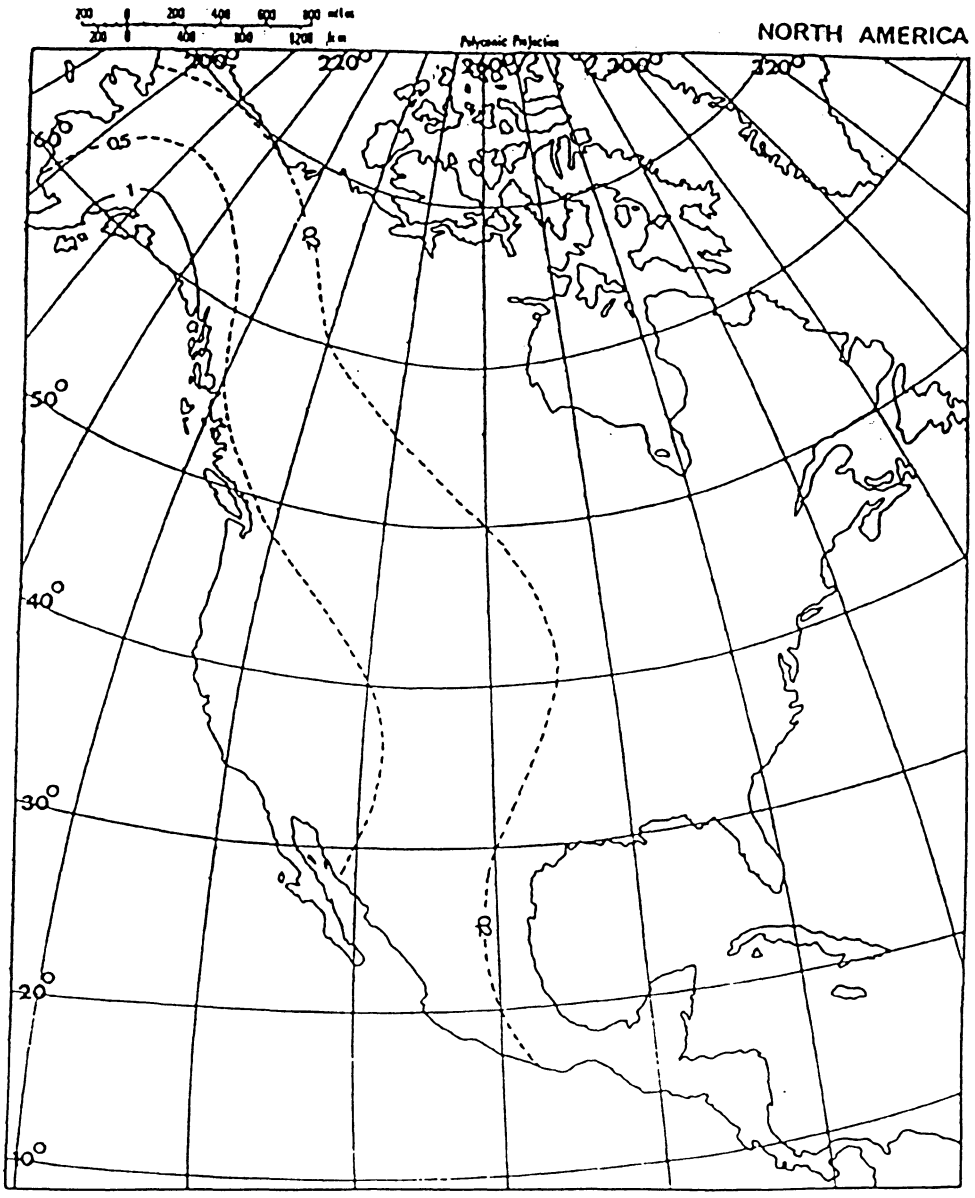

Fig. A.17. N_2 load. N-S displacement in mm.

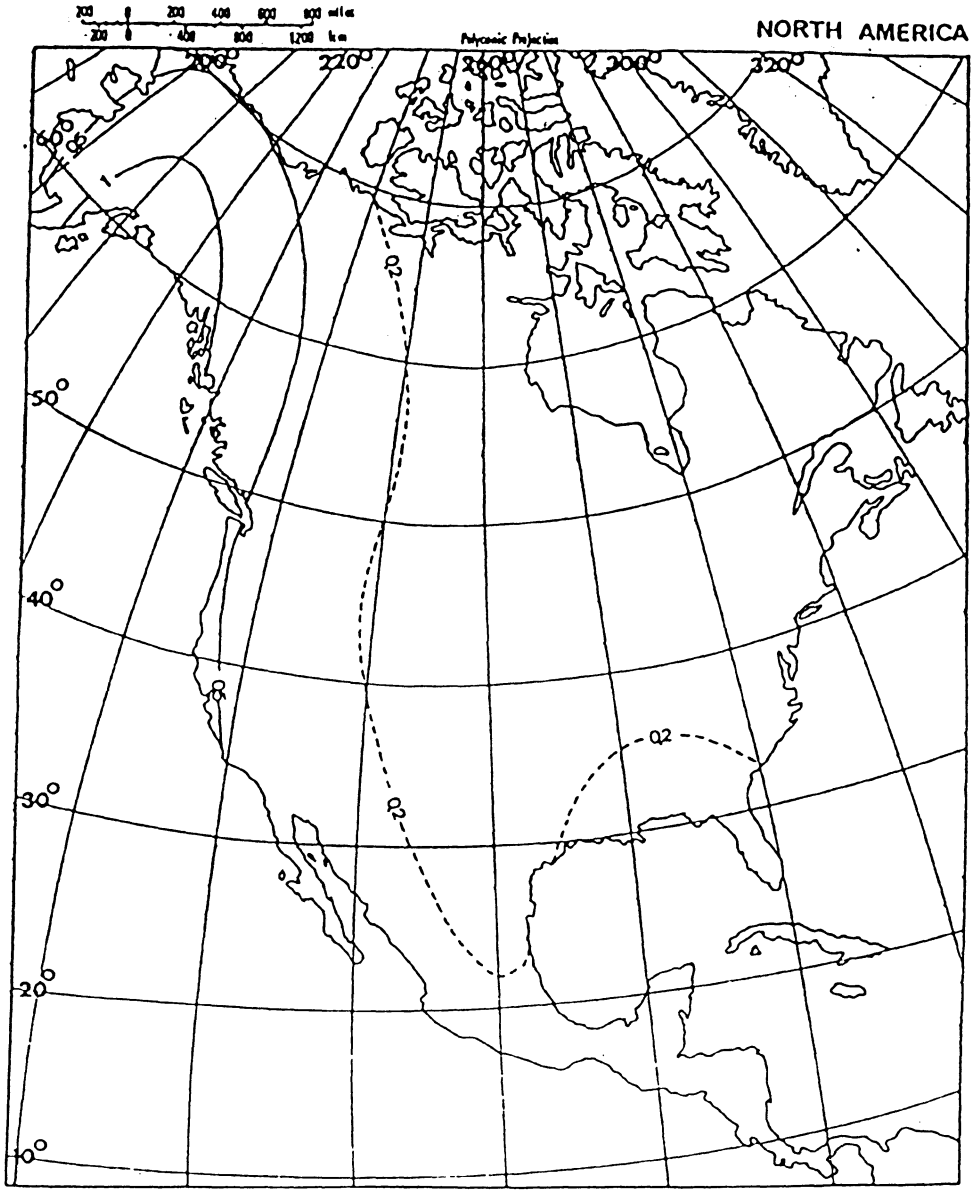

Fig. A.18. P_1 load. N-S displacement in mm.

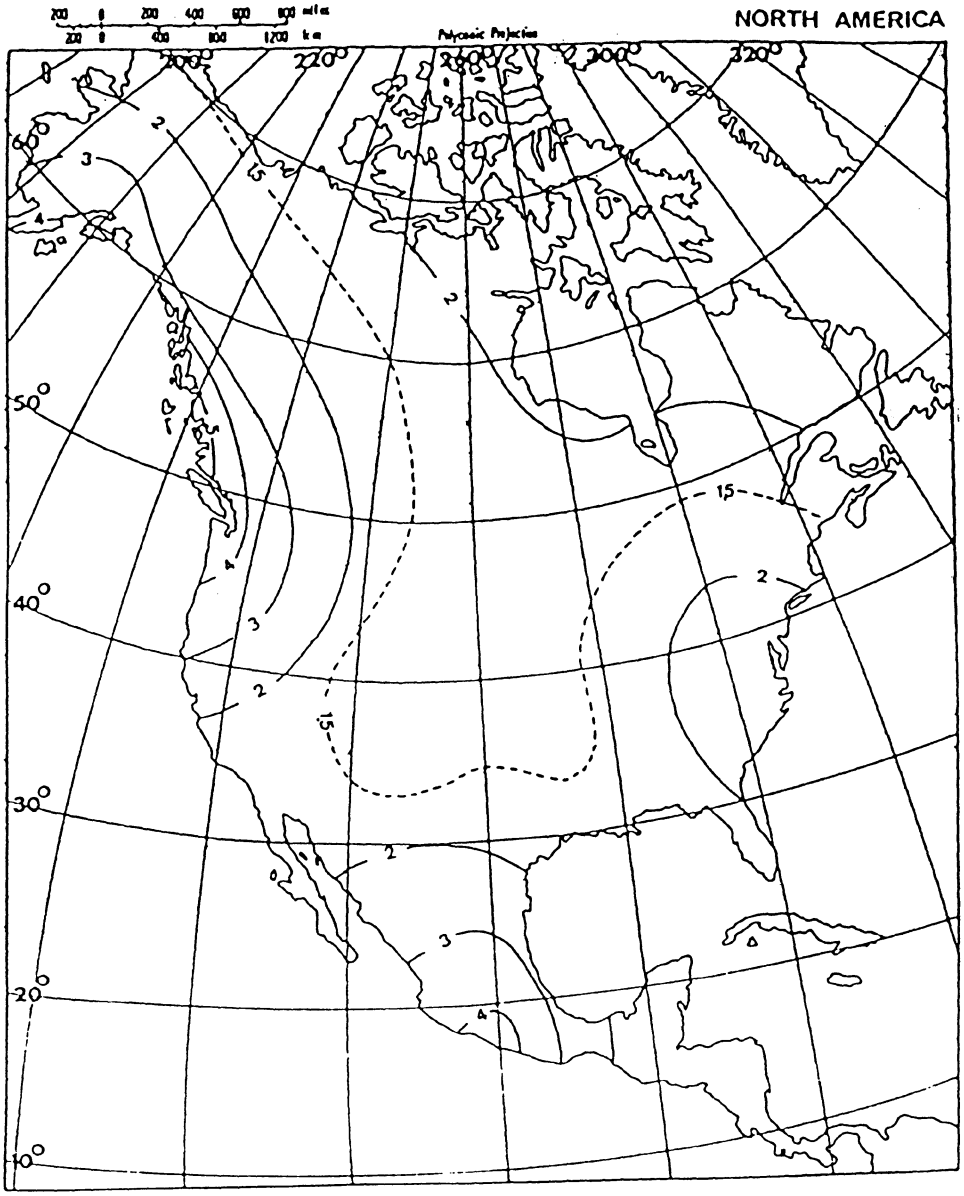

Fig. A.19. M_2 load. E-W displacement in mm.

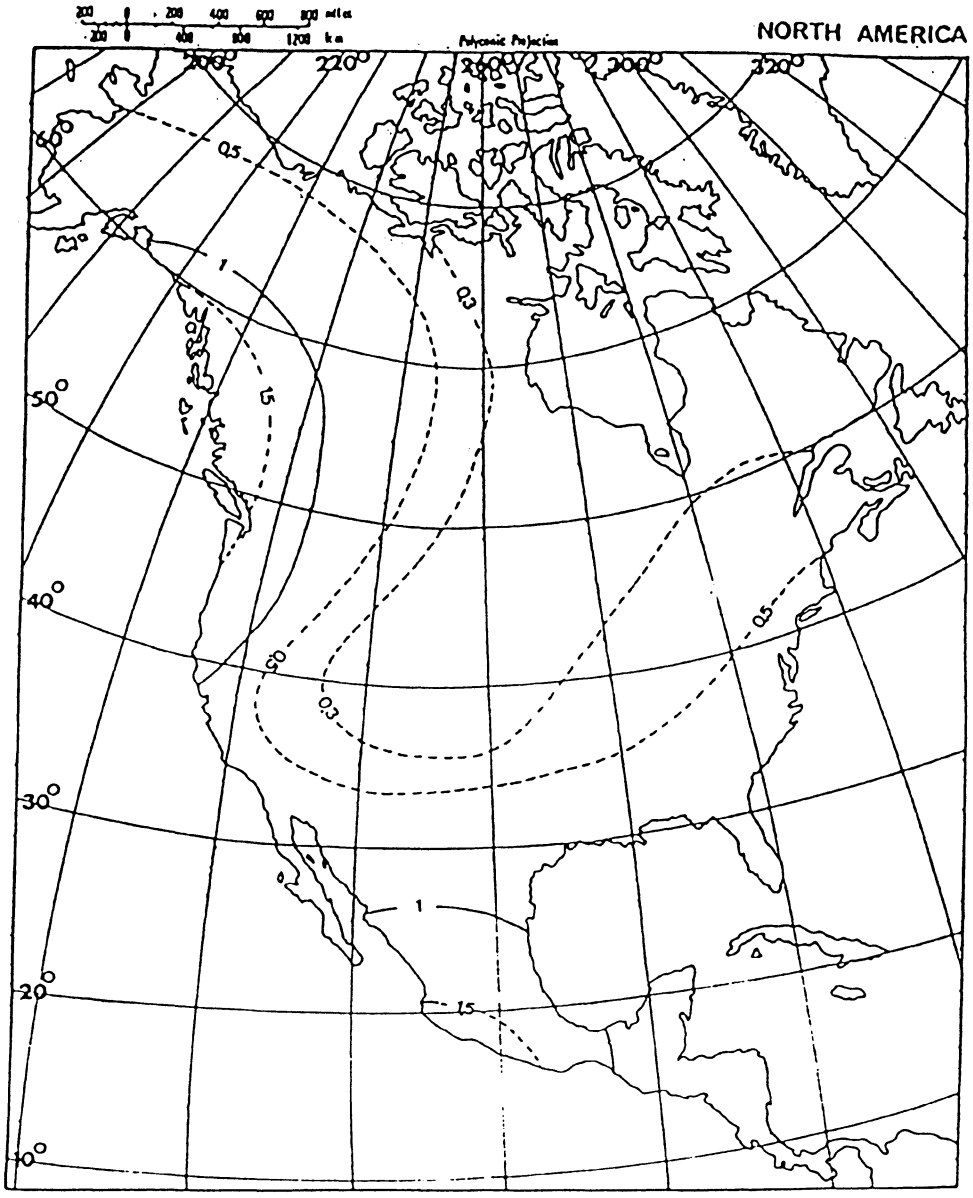

Fig. A.20. S_2 load. E-W displacement in mm.

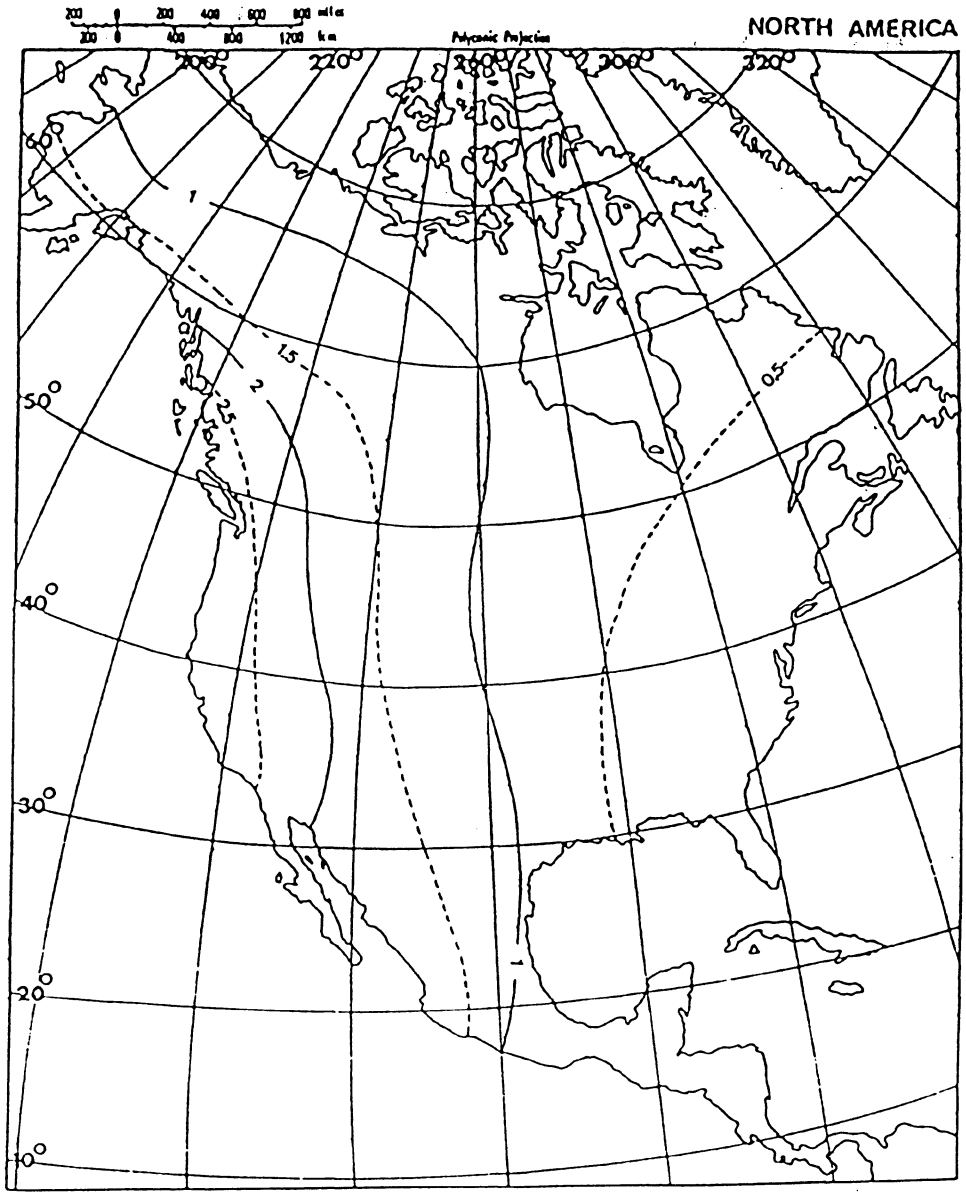

Fig. A.21. K_1 load. E-W displacement in mm.

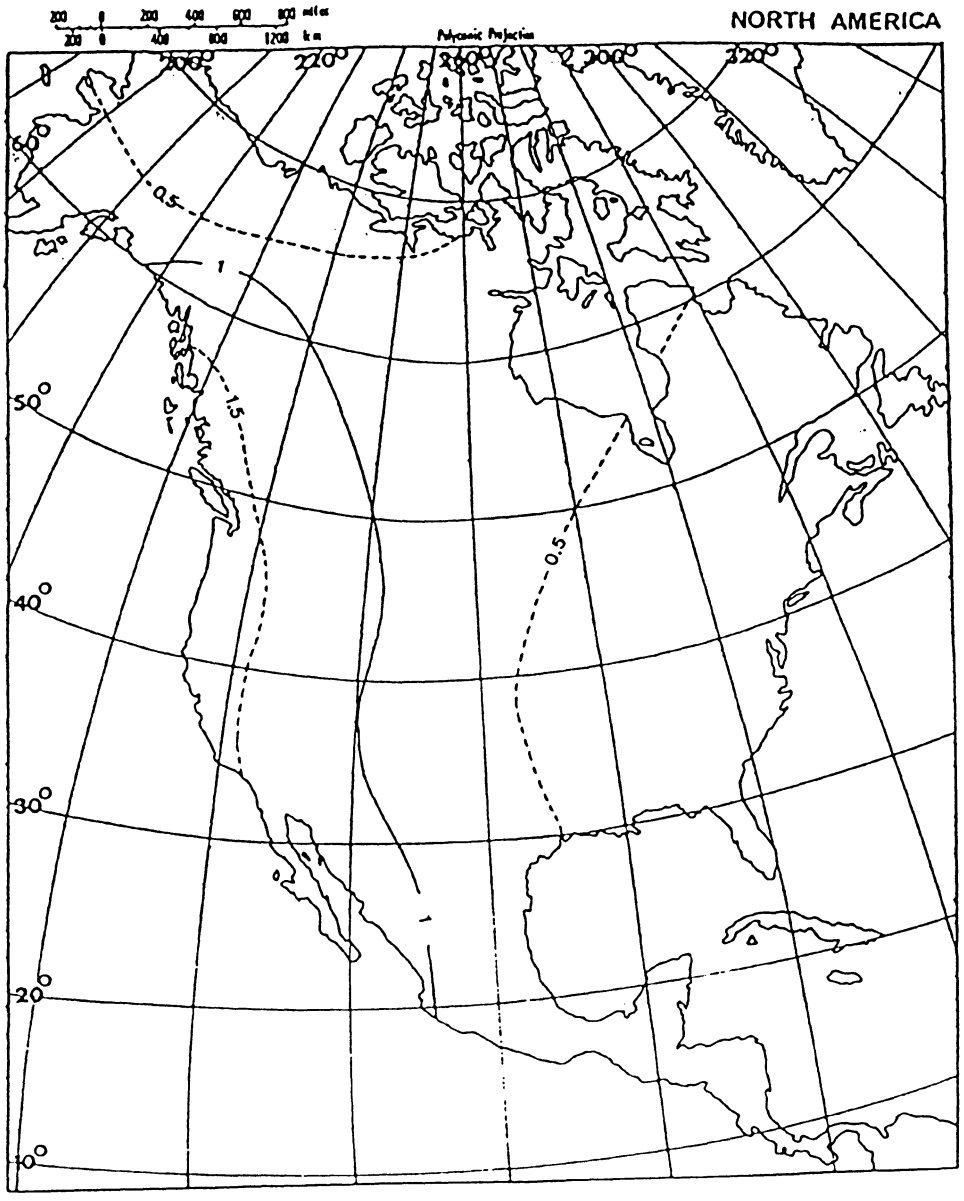

Fig. A.22. O_1 load. E-W displacement in mm.

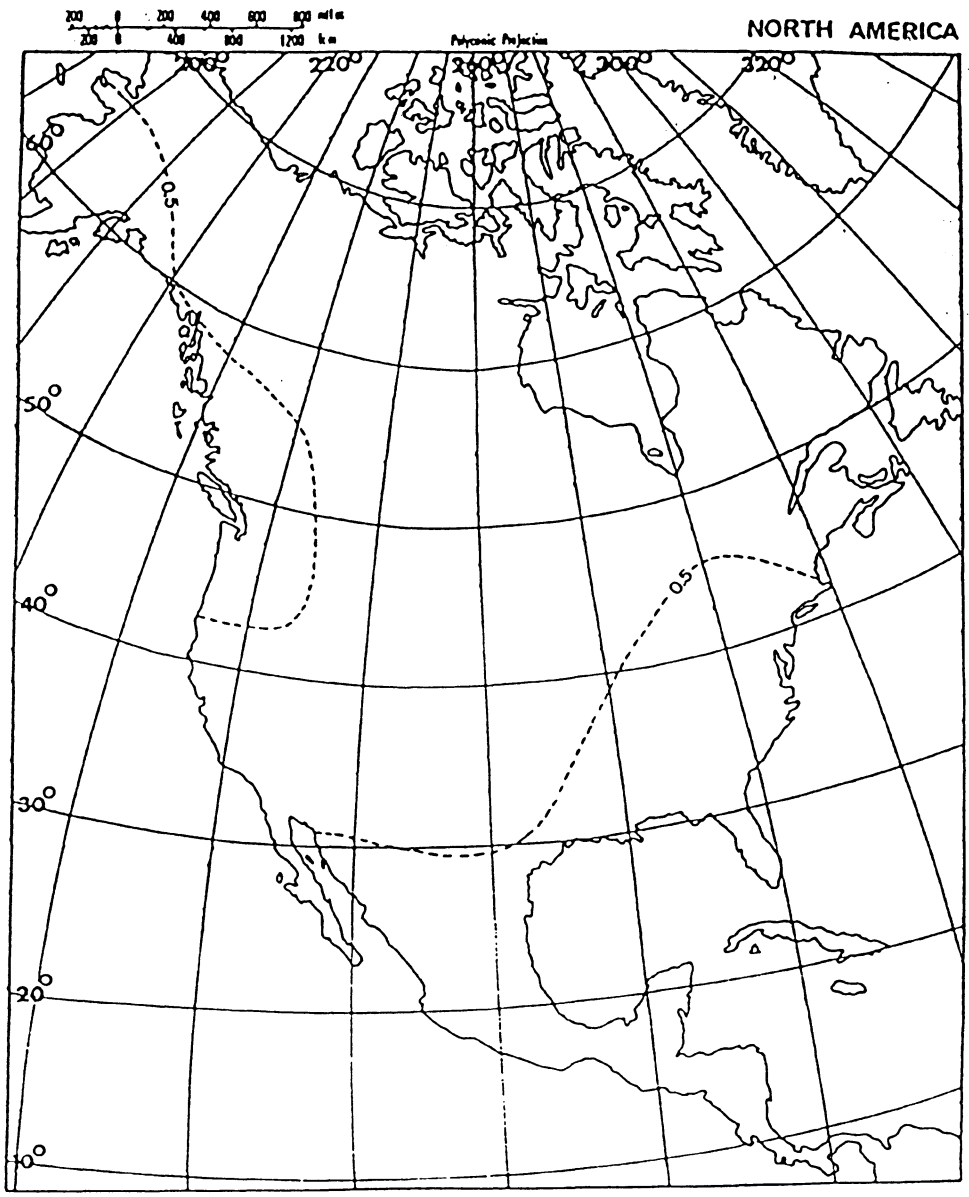

Fig. A.23. N_2 load. E-W displacement in mm.

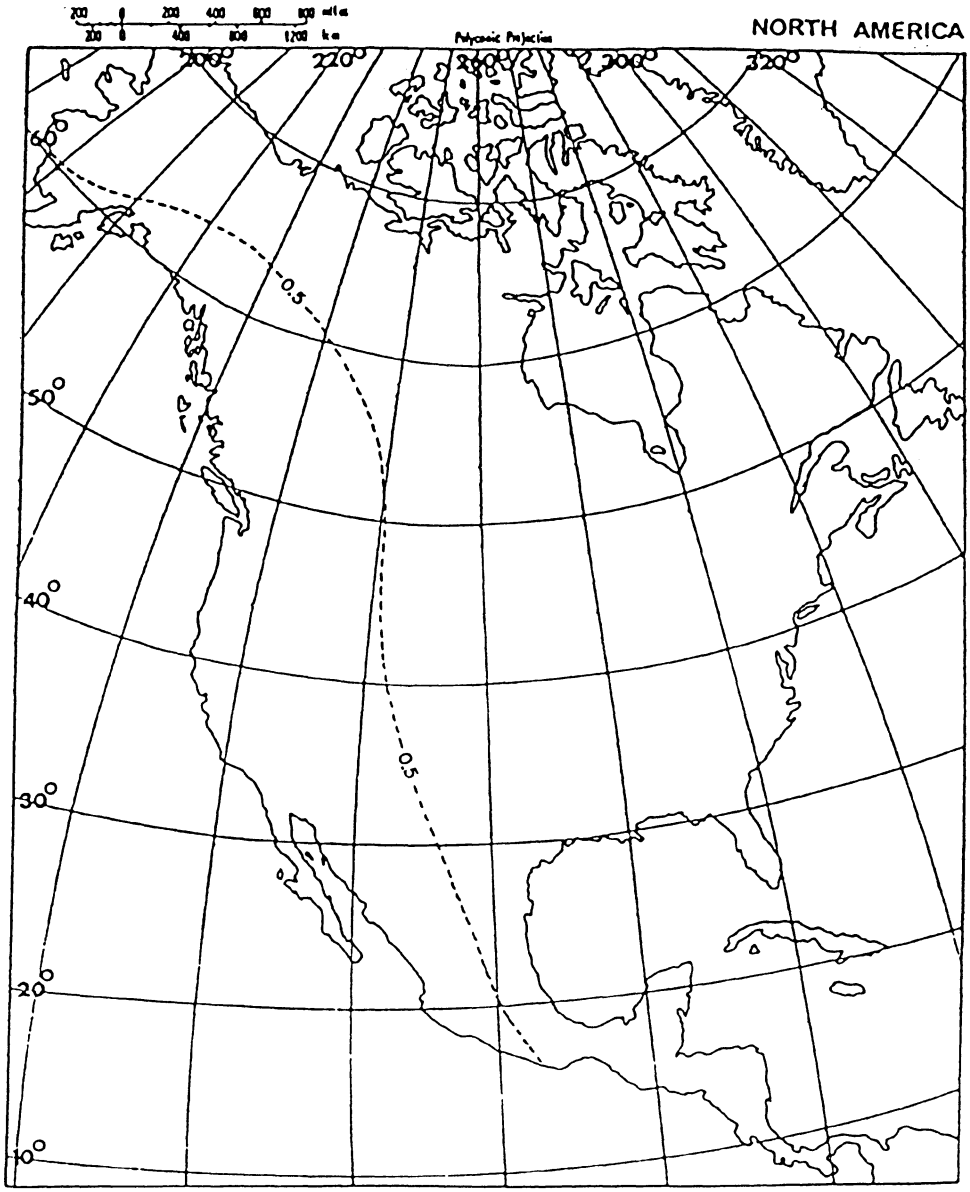

Fig. A.24. P_1 load. E-W displacement in mm.

APPENDIX B

RELATIVE TILT OF THE TERRAIN AND OTHER EFFECTS DUE TO OCEAN TIDE LOADING

B.1. Relative Tilt of the Terrain.

The relative tilt of the terrain (observed by terrestrial means) is

$$\theta_n^R = (1+k_n'-h_n')g^{-1}\frac{\partial W_n^L}{\partial \psi} . \qquad (B.1)$$

Combining (B.1) and (2.9) yields

$$\theta^R = \frac{G\sigma_w}{R\bar{g}} \iint_{\text{oceans}} \zeta \sum_{n=0}^{\infty} (1+k_n'-h_n') \frac{\partial P_n(\cos\psi)}{\partial \psi} dS . \qquad (B.2)$$

Farrell (1972) gives for tilt (ibid. Eq. 47):

$$t(\psi) = -\frac{1}{M_e}\sum_{n=0}^{\infty}(1+k_n'-h_n')\frac{\partial P_n(\cos\psi)}{\partial \psi} . \qquad (B.3)$$

He also tabulates (ibid. Table A3) the following:

$$\tilde{t}(\psi) = t^E(\psi)\ 10^{12}\ (R\psi)^2 , \qquad (B.4)$$

where $t^E(\psi)$ is the "elastic" tilt and is given by

$$t^E(\psi) = t(\psi) - t^N(\psi) . \qquad (B.5)$$

Here, $t^N(\psi)$ is the Newtonian tilt given by

$$t^N(\psi) = \frac{\cos(\psi/2)}{4M_e \sin^2(\psi/2)} . \qquad (B.6)$$

Following the same procedure as in the derivation of the

gravity kernel one obtains for tilt

$$K^{\theta^R} = \frac{G\sigma_w}{R\bar{g}} \left\{ \frac{M_e}{10^{12} R^2} \frac{\tilde{t}(\psi)}{\psi^2} + \frac{\cos(\psi/2)}{4 \sin^2(\psi/2)} \right\} \qquad (B.7)$$

where $\tilde{t}(\psi)$ corresponds to Farrell's tabulated values. K^{θ^R} is plotted in Fig. B.1. The above formula refers to tilt in the direction of the load. Similar to the horizontal displacement, (3.13) must be used to express tilt in north-south and east-west components. Tilt is considered positive towards load.

B.2. Other Effects.

There are also some other effects of interest arising from the load phenomena. Only a list (Vaníček, 1978) is given here for completeness, since they do not affect significantly VLBI observations.

a. Vertical movement of the equipotential surface with respect to the geocentre (variation in the geoid)

$$u^G = \sum_{n=0}^{\infty} (1+k'_n) \frac{W_n^L}{g} \quad . \qquad (B.8)$$

b. Relative movement of the terrain with respect to the equipotential surface (this is observable by terrestrial means)

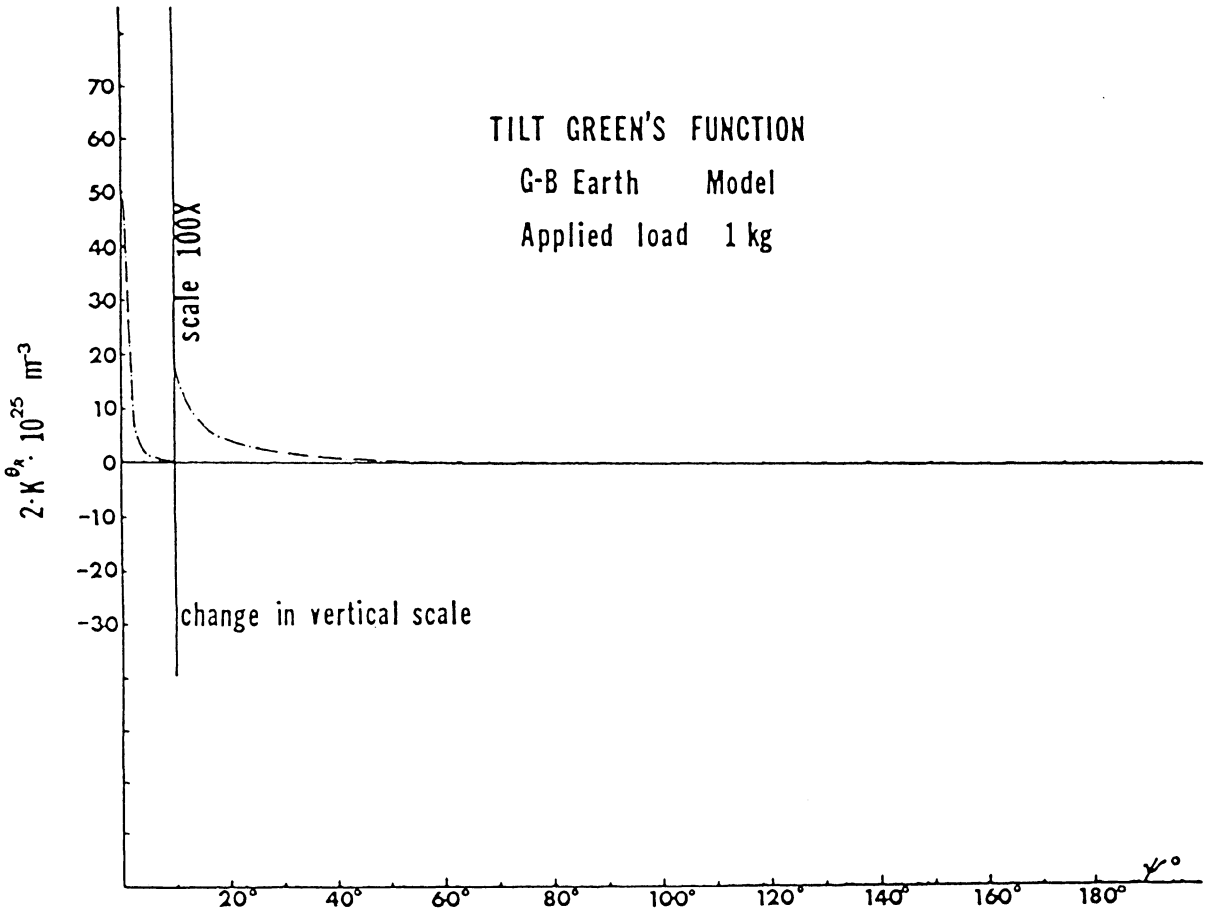
TILT GREEN'S FUNCTION
G-B Earth Model
Applied load 1 kg
scale 100X
change in vertical scale
$2 \cdot K^{\theta_R} \cdot 10^{25}$ m^{-3}
70
60
50
40
30
20
10
0
-10
-20
-30
20°
40°
60°
80°
100°
120°
140°
160°
180°
ψ°

Fig. B.1

$$u^R = \sum_{n=0}^{\infty} (1+h'_n-k'_n) \frac{W_n^L}{g} \quad . \tag{B.9}$$

c. Tilt of the terrain in the direction of ψ with respect to its undisturbed position

$$\theta^D = \sum_{n=0}^{\infty} h'_n \, g^{-1} \frac{\partial W_n^L}{\partial \psi} \quad . \tag{B.10}$$

d. Tilt of the equipotential surface with respect to its undisturbed position (variation in the deflection of the vertical)

$$\theta^G = \sum_{n=0}^{\infty} (1+k'_n) g^{-1} \frac{\partial W_n^L}{\partial \psi} \quad . \tag{B.11}$$

APPENDIX C

EVALUATION OF LOAD RESPONSE DIRECTLY BENEATH THE LOAD

It has been mentioned in Subsection 2.4, the potential of the load is undefined when the distance between the point of interest and the load becomes zero. This happens when one is interested in evaluating the load effects at the bottom of the sea. This singularity must be treated as a special case.

To evaluate the depression of the bottom of the sea due to tidal waters, in close vicinity to the point of interest (e.g. circular area with radius approximately $0^{\circ}.5$), once more the response of the earth to nearly diurnal and semidiurnal frequencies is considered to be elastic. Furthermore, the medium above some starting depth z_o is considered as a uniform half-space. A uniform half-space (elastic, isotropic and homogeneous half-space) can be regarded as a body of revolution whose envelope and lower surface (defined by z_o) are not loaded and tend towards infinity; the upper surface is loaded in the axis of the body by a concentrated load (Fig. C.1). In other words, the deformations coming from the load are present only in the half-space, whereas outside of it they are negligible. The depth z_o of the lower surface of the uniform half-space depends on the rheology of the medium and the wavelength of the deformation (Farrell,

UNIFORM HALF-SPACE

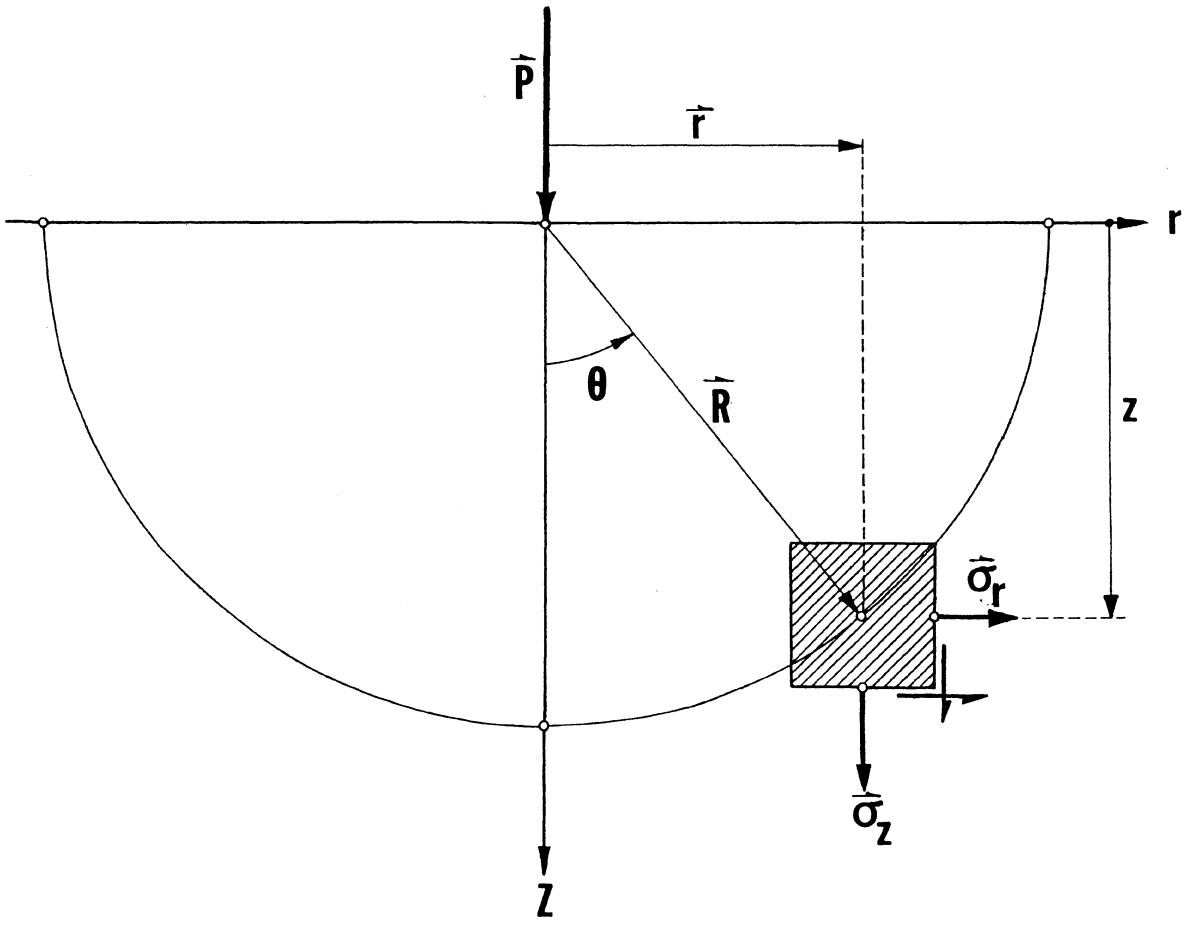

Fig. C.1

1972).

For the determination of strains and stresses in a uniform half-space, the following conditions must be satisfied (Suklje, 1969):

a) At infinity ($r \to \infty$) stresses vanish and strains are zero.

b) The shear stresses are zero over all the boundary surface ($z=0$) of the half-space.

c) The normal stresses at this surface are zero also, except at the point of the application of the load.

d) The resultant of stresses acting at the surface of an arbitrary complete segment of the half-space (e.g. at the surface of the hemisphere) has the direction of the z axis and is in equilibrium with the force P.

If R is the radius of the hemisphere and θ is the radial distance of the complete segment from z axis, the following solution for the radial displacement holds (Suklje, 1969)

$$u = \frac{P}{4\pi R} \frac{1}{\Gamma} \{2(1-\nu) + \cos^2\theta\} , \qquad (C.1)$$

where Γ is the shear modulus given by (Nadeau, 1964)

$$\Gamma = \frac{E}{2(1+\nu)} , \qquad (C.2)$$

E and ν are the Young modulus and Poisson's ratio respectively. The Young modulus E is defined as the ratio of a normal force per unit area applied to a body, to its relative longitudinal extension (Nadeau, 1964). Poisson's ratio is defined as the negative ratio of a relative lateral contraction to the relative longitudinal extension.

In order to obtain the radial displacement u_o of an arbitrary point P on the axis of a circular loaded area one has (Fig. C.2)

$$dA = rd\phi dr \ . \tag{C.3}$$

The elementary concentrated load is

$$P = q \cdot dA, \tag{C.4}$$

or

$$P = q \cdot rd\phi dr, \tag{C.5}$$

where q is the load per unit area. Using (C.1) and (C.5) one obtains

$$du = \frac{qrd\phi dr}{4\pi R}\frac{1}{\Gamma}\{2(1-\nu)+\cos^2\theta\} \ . \tag{C.6}$$

Integration of (C.6) with respect to ϕ and r yields

$$u_o = \frac{2aq}{E}\frac{1+\nu}{\sin\alpha}\{2(1-\nu)-(1-2\nu)\cos\alpha-\cos^2\alpha\} \ , \tag{C.7}$$

where a is the radius of the loaded area. In the case of

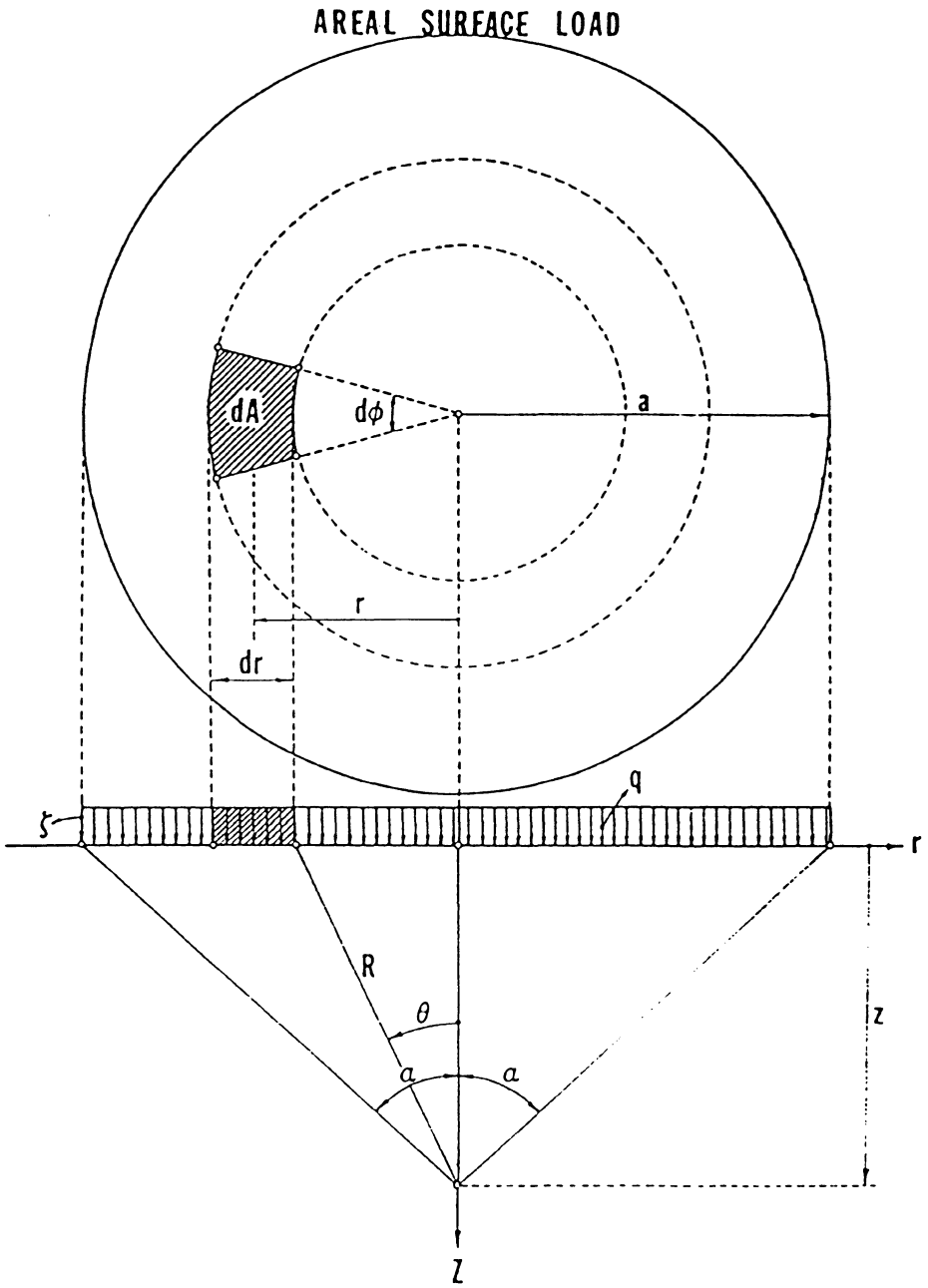

Fig. C.2

the ocean loading, since the water is incompressible, q is transfered at the bottom of the sea unchanged and thus radial displacement is obtained by (C.7), setting $\alpha = 90^{\circ}$:

$$u_o^L = \frac{-4qa}{E}(1-\nu^2) \quad , \tag{C.8}$$

where the minus sign denotes depression. Equation (C.8) can be used to evaluate the load depression coming from an area of radius less than 0°5 and centered over the point of interest.

APPENDIX D

DATA SETS

D.1. Ocean Tide Data Set.

The ocean tide data set maintained at U.N.B. contains data for the six leading tidal constituents (M_2, S_2, K_1, O_1, N_2, P_1), in the form of amplitudes $\xi^i_{m,n}$ (in metres) and Greenwich phases $\delta^i_{m,n}$ (in degrees, 0°-360°) on a 1°x1° spherical grid system. This data was obtained from the NSWC GOTD-1978 tape. The entire data set ($\xi^i_{m,n}$, $\delta^i_{m,n}$) is arranged by tables on disk (SE0002) in the following form:

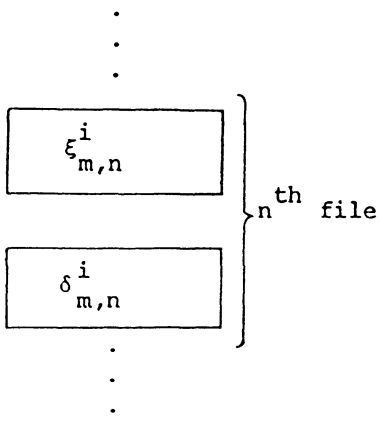

There are 168 such files corresponding to the same constituent i. The number of file corresponds to the co-latitude number n, which takes values from 1 to 168. Each of the above tables consists of 360 values corresponding

to the longitude number m. The tidal constants ($\xi^i_{m,n}$; $\delta^i_{m,n}$) are representatives of the $1^\circ x 1^\circ$ square with geographical centre point (λ_m, θ_n) (Schwiderski and Szeto, 1981), where

$$\lambda_m = (m-0.5) \quad = \text{East longitude} \quad (m = 1, 2, 3, \ldots, 360^\circ),$$

$$\theta_n = (n-0.5) \quad = \text{Co-latitude} \quad (n = 1, 2, 3, \ldots, 168^\circ).$$

For the rest of the constituents, the file number is determined by

$$\text{number of file} = n + (i-1)\cdot 168^\circ \ ,$$

where i is the constituent (i=1,2,3,4,5,6, and i=1 for M_2). On land all tidal constants have been set to

$$\xi^i_{m,n} = 9.9999, \quad \delta^i_{m,n} = 999.9$$

D.2. Polar Motion Data Set.

Polar motion data in "1979 BIH system" are stored on tape PEP583 (1600 bpi, SL), slot 3115 (U.N.B. Computing Centre), file 108 under the name PEPRLL.191.WOBBIH79.DATA.B1. The file contains data for the time period January 1969-April 1981.

APPENDIX E

OCEAN TIDE

The instantaneous partial ocean tide is determined by (Schwiderski, 1978)

$$\zeta_i = \xi_i \cos (\omega_i t + V_i - \delta_i) \ , \qquad (E.1)$$

where the subscript i denotes the constituent, ξ_i , δ_i are the amplitude and the Greenwich phase of the i-th constituent respectively, ω_i is the frequency, t is the Universal Time (UT) of day and V_i the astronomical argument of the i-th constituent at 00 hours UT. The mean astronomical argument is given by Schwiderski (1979, 1981a-1981f) in terms of the mean orbital elements of the moon and the sun. Also, there are tables prepared by the German Hydrographic Institute, which give the astronomical argument for each individual constituent at the beginning of each year, at 00 hours UT for the years 1900 to 2000, incorporating automatically the nodal correction (Godin, 1980). Using these values, t must be the UT elapsed since the beginning of the year.

APPENDIX F

PHASE LAGS

Throughout this study, different definitions for the phases of the load effects were used. Since the phase varies with the time origin chosen for the analysis, it is always a source of confusion. It is expedient to give here the different definitions for the phase.

F.1. Greenwich Phase Lag.

The load effect as any other tidal phenomenon can be written as a superposition of n harmonic terms; e.g. the radial displacement can be written as

$$u'_\ell(t) = \sum_{i=1}^{n} \{a_i \cos(\omega_i t+V_i)+b_i \sin(\omega_i t+V_i)\}, \qquad (F.1)$$

or equivalently

$$u'_\ell(t) = \sum_{i=1}^{n} A_i \cos(\omega_i t+V_i(t_o) - \delta_i) \qquad (F.2)$$

where ω_i is the frequency of the constituent i, t is UT, $V_i(t_o)$ is the astronomic argument of the constituent i at 00 hours UT and δ_i is the Greenwich phase lag. The amplitude of the constituent i i.e. A_i can be determined by

$$A_i = (a_i^2+b_i^2)^{1/2} \qquad (F.3)$$

and the Greenwich phase lag by

$$\delta_i = \arctan \frac{b_i}{a_i} . \qquad (F.4)$$

Note here that (F.4) will give the Greenwich phase lag of the i-th constituent if the effect is expressed by (F.1).

Greenwich phase lag is the phase lag between the instant the component in the tidal force reaches its peak and the instant of maximum contribution of the constituent to the local tide. Physically, it is the delay between the time a force is applied and the time it causes maximum deformation (Godin, 1980). Needless to say the Greenwich phase lag is independent of the time origin.

F.2. Greenwich Phase Lag in Local Time.

In some cases it is expedient to use local time instead of UT for t in (F.1). Thus, one must use the Greenwich phase lag in local time for δ_i. Suppose that one wants to translate the Greenwich phase lag δ_i for a local time zone Z=r, where r is the number of hours local time is behind UT. The Greenwich phase lag in local time is given by

$$\delta_i^r = \delta_i - r\omega_i , \qquad (F.5)$$

where ω_i is the frequency of the constituent i in degrees

per hour.

For stations with east longitude, r is negative.

F.3. Local Phase Lag with Respect to the Theoretical Tide.

Local phase lag with respect to the theoretical tide is defined as the time elapsed since the transit of the moon or the sun over the local meridian, up to the occurrence of maximum deformation.

The local time of the transit of the moon or the sun over the local meridian is determined by the hour angle. When the hour angle is zero, the celestial body is over the local meridian. The local hour angle in local time can be determined as follows:

$$H_{\star}^{\text{Local}} = ST - \Delta T + \lambda - \alpha_{\star} , \qquad (F.6)$$

where; (a) ST is the sidereal time at 00 hours UT; (b) ΔT is the local standard time and is considered positive east of Greenwich; (c) λ is the longitude of the site and is considered positive east of Greenwich; (d) $\alpha_{\star}$ is the right ascension of the celestial body at 00 hours UT and is taken with its sign.

If τ is the local time at which maximum deformation occurs, then the local phase lag with respect to the

theoretical tide can be determined by

$$\beta = H_{*}^{Local} - \tau. \qquad (F.7)$$

If β is positive, the deformation will lead the theoretical tide.

APPENDIX G

SOFTWARE PACKAGES

The programme for the evaluation of the load effects (LOADSDP) is stored on tape (TAPE=TIDE, SLOT=3721, 1600 bpi, NL) as separate subroutines as follows:

FILE 1: SUBROUTINE AMPHA.

FILE 2: SUBROUTINE AREA.

FILE 3: SUBROUTINE AZMTH.

FILE 4: SUBROUTINE KERNEL.

FILE 5: SUBROUTINE PSIO.

FILE 6: REAL FUNCTION SEVALS.

FILE 7: SUBROUTINE LOAD.

FILE 8: SUBROUTINE TIDE.

Three of the subroutines of GEOAIM which have been changed in this study are also stored on the same tape as follows:

FILE 9: SUBROUTINE FF$DLY.

FILE 10: SUBROUTINE RDWRT.

FILE 11: SUBROUTINE WOBRED.

The rest of the subroutines of GEOAIM are stored on another tape (TAPE=YORK01, SLOT=3441, 1600 bpi, NL).

PROGRAM LOADSDP
FLOWCHART
(U.N.B. MAY '82)

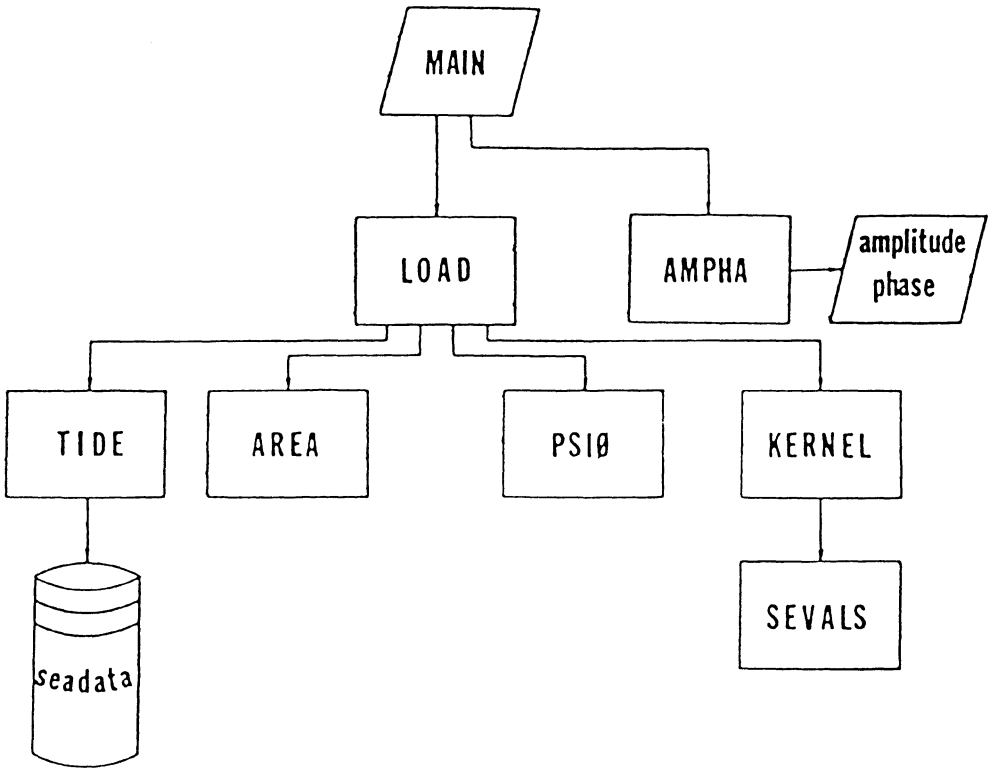

Fig. G.1

CANADIAN FRINGE FREQUENCY AND DELAY ANALYSIS PROGRAM

LEAST SQUARES ADJUSTMENT (U.N.B. MAY 1982)

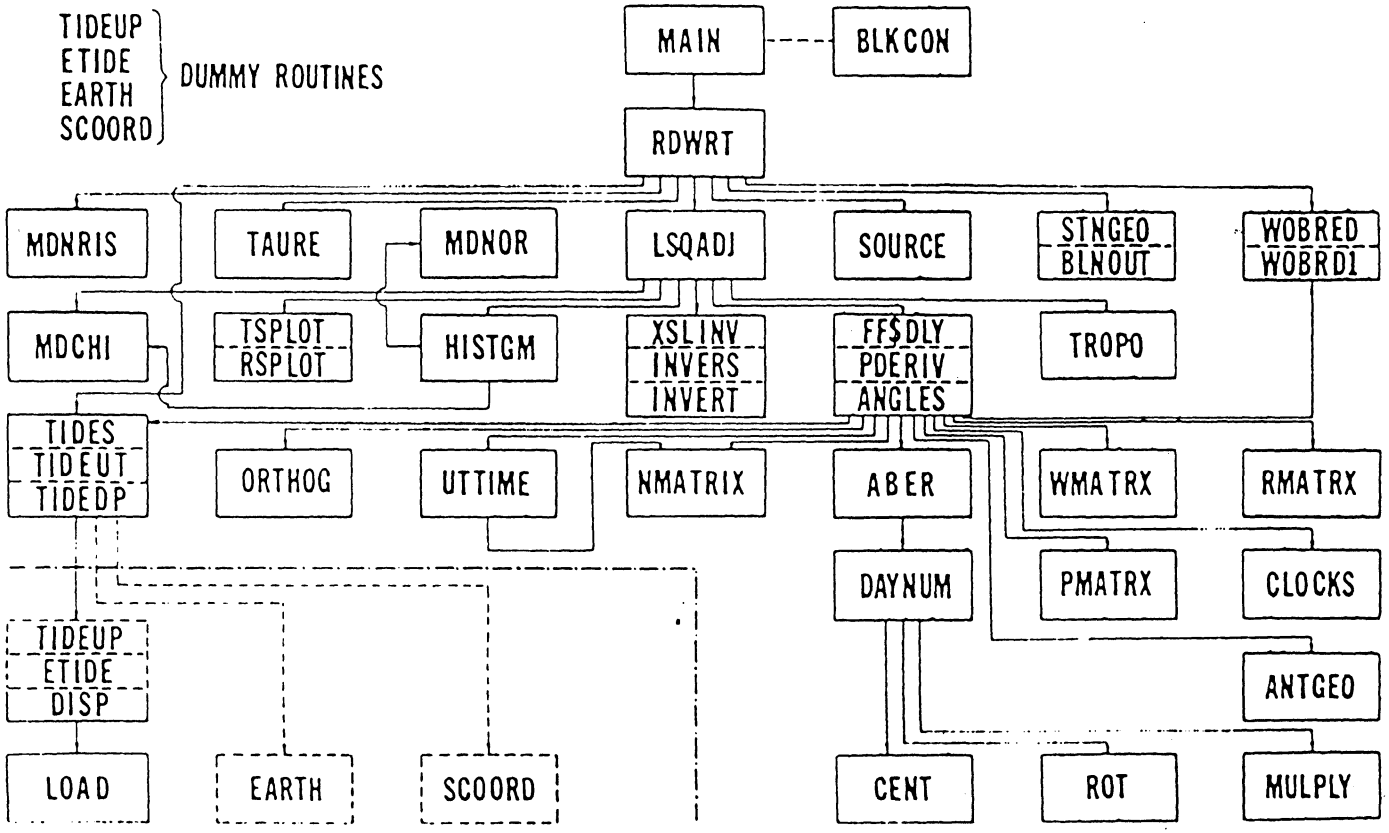

Fig. G.2

```
C-----------------------------------------------------------------------
C
C                    ------------------------------------
C                    |  P R O G R A M M E   L O A D S D P  |
C                    ------------------------------------
C
C     THIS PROGRAM EVALUATES THE RADIAL AND LATERAL DISPLACEMENTS OF THE
C     TERRAIN DUE OCEAN TIDE LOADING.
C
C     COMPUTATIONAL ALGORITHM : CONVOLUTION OF APPROPRIATE GREEN'S
C                               FUNCTIONS WITH KNOWN OCEAN TIDE MODEL.
C
C     OCEAN TIDE MODEL        : NAVAL SURFACE WEAPONS CENTRE'S
C                               HYDRODYNAMICALLY INTERPOLATED MODEL
C                               (SCHWIDERSKI, 1978).
C
C     CONSTITUENTS IN USE     : M2, S2, K1, O1, N2, P1.
C
C     INPUT DATA
C     ==========
C
C     1. COLAT  = CO-LATITUDE OF THE POINT OF INTEREST IN (D MIN SEC).
C     2. ELONG  = EAST LONGITUDE OF THE POINT OF INTEREST IN (D MIN SEC)
C     3. STN    = NAME OF THE STATION (MAXIMUM 40 CHARACTERS).
C
C     OUTPUT
C     ======
C
C     AMPLITUDES (CM) AND GREENWICH PHASE LAGS (DEGREES) FOR EACH OF THE
C     CONSTITUENTS.
C
C     EXTERNALS
C     =========
C
C     1. SUBROUTINE LOAD.
C     2. SUBROUTINE AMPHA.
C
C     REFERENCES
C     ==========
C
C     FARRELL, W.E. (1972): DEFORMATION OF THE EARTH UNDER SURFACE MASS
C                   LOADS, REVIEWS OF GEOPHYSICS AND SPACE PHYSICS,
C                   VOL. 10, NO 3, PP.761-797.
C
C     PAGIATAKIS, S.D. (1982): OCEAN TIDE LOADING, BODY TIDE AND POLAR
C                   MOTION EFFECTS ON VERY LONG BASELINE INTERFEROMETRY,
C                   M.SC. THESIS, DEPT. OF SURVEYING ENGINEERING,
C                   UNIVERSITY OF N. BRUNSWICK, FREDERICTON, N.B.
```

```
C
C     SCHWIDERSKI, E.W. (1978): GLOBAL OCEAN TIDES, PART I: A DETAILED
C                    HYDRODYNAMICAL INTERPOLATION MODEL, NSWC/DL TR-3866,
C                    NAVAL SURFACE WEAPONS CENTRE, DAHLGREN, VA.
C
C     DEVELOPED BY SPIROS D. PAGIATAKIS, DEPT. OF SURVEYING ENGINEERING,
C     UNIVERSITY OF NEW BRUNSWICK, SEPT. 1981 - MAY 1982.
C
C-----------------------------------------------------------------------
ISN 0002       IMPLICIT REAL *8 (A-H,O-Z)
ISN 0003       REAL *8 LLAT,LLON,NORTH,LOADUP
ISN 0004       DIMENSION C(6),NORTH(2,6),WEST(2,6),UPLIFT(2,6)
ISN 0005       READ (5,1000) K1,K2,AK,L1,L2,AL,STN1,STN2,STN3,STN4,STN5
ISN 0006       READ (5,1001) (C(I),I=1,6)
ISN 0007       WRITE (6,1002) STN1,STN2,STN3,STN4,STN5,K1,K2,AK,L1,L2,AL
ISN 0008       D=3.14159265358979300/180.D0
ISN 0009       COLAT=((((AK/60)+K2)/60)+K1)*D
ISN 0010       ELONG=((((AL/60)+L2)/60)+L1)*D
ISN 0011       DO 30 II=1,6
ISN 0012       J=1
ISN 0013       AII=66.625D0
ISN 0014    10 CALL LOAD (COLAT,ELONG,AII,LOADUP,LLAT,LLON,II)
ISN 0015       UPLIFT(J,II)=LOADUP
ISN 0016       NORTH(J,II)=LLAT
ISN 0017       WEST(J,II)=LLON
ISN 0018       AII=AII+0.041666666666666666666667D0
ISN 0019       J=J+1
ISN 0020       IF (J.GT.2) GO TO 20
ISN 0022       GO TO 10
ISN 0023    20 CALL AMPHA (UPLIFT,C,II,AMP,GPL)
ISN 0024       WRITE (6,1003) C(II),AMP,GPL
ISN 0025       CALL AMPHA (NORTH,C,II,AMP,GPL)
ISN 0026       WRITE (6,1004) AMP,GPL
ISN 0027       CALL AMPHA (WEST,C,II,AMP,GPL)
ISN 0028       WRITE (6,1005) AMP,GPL
ISN 0029    30 CONTINUE
ISN 0030  1000 FORMAT (I3,1X,I2,1X,F6.3,3X,I3,1X,I2,1X,F6.3,3X,5A8)
ISN 0031  1001 FORMAT (6(A2))
ISN 0032  1002 FORMAT ('1',//////,26X,
          * 'OCEAN  TIDE  LOADING   DEFORMATIONS   OF   THE   LITHOSPHERE',
          * /,26X,60(1H=),///,30X,'STATION NAME   =',1X,5A8,/,30X,
          *'CO-LATITUDE     =',1X,I3,1X,I2,1X,F6.3,2X,'(D MIN SEC)',/,30X,
          * 'EAST LONGITUDE =',1X,I3,1X,I2,1X,F6.3,2X,'(D MIN SEC)',////,17X,
          *'CONSTITUENT          RADIAL DISP. (CM)       N-S DISP. (CM)
          *E-W DISP. (CM)',
          *//,39X,'(OUTWARDS +)              (NORTH +)                    (WEST +)',//
          *//,39X,'AMP.    PHASE          AMP.    PHASE              AMP.    PHASE',
          */ ,39X,'====    =====          ====    =====              ====    =====')
```

```
ISN 0033        1003 FORMAT (21X,A2,16X,F4.2,3X,F5.1)
ISN 0034        1004 FORMAT ('+',59X,F4.2,3X,F5.1)
ISN 0035        1005 FORMAT ('+',82X,F4.2,3X,F5.1)
ISN 0036             STOP
ISN 0037             END
```

```
ISN 0002            SUBROUTINE AMPHA (DEFORM,C,II,AMP,GPL)
                C-----------------------------------------------------------------
                C
                C     SUBROUTINE AMPHA COMPUTES THE AMPLITUDE AND GREENWICH PHASE LAG OF
                C     THE LOADING CONSTITUENTS.
                C
                C     CALLED FROM: MAIN
                C
                C     INPUT
                C     =====
                C
                C     1. DEFORM = THE DEFORMATION (UPLIFT, N-S OR E-W) OF THE TERRAIN
                C                 IN CM CORRESPONDING TO THE DAY MARCH 7, 1976, 15.00
                C                 AND 16.00 HOURS U.T.
                C     2. C      = ARRAY OF THE CONSTITUENTS IN ALPHANUMERIC CHARACTERS.
                C     3. II     = THE CONSTITUENT NUMBER.
                C
                C     OUTPUT
                C     ======
                C
                C     1. AMP = AMPLITUDE OF THE DEFORMATION IN CENTIMETRES.
                C     2. GPL = GREENWICH PHASE LAG OF THE DEFORMATION IN DEGREES.
                C
                C     WRITTEN BY SPIROS D. PAGIATAKIS, MARCH, 1982
                C
                C-----------------------------------------------------------------
ISN 0003            IMPLICIT REAL *8 (A-H,O-Z)
ISN 0004            INTEGER II
ISN 0005            DIMENSION DEFORM(2,6),A(2,6),B(2,6),X(2,6),Y(2,6),C(6)
ISN 0006            A(1,1)=0.369459644D0
ISN 0007            A(1,2)=0.001745328D0
ISN 0008            A(1,3)=0.598594901D0
ISN 0009            A(1,4)=0.946731146D0
ISN 0010            A(1,5)=0.493512794D0
ISN 0011            A(1,6)=-0.865419742D0
ISN 0012            A(2,1)=0.773468642D0
ISN 0013            A(2,2)=-0.498487739D0
ISN 0014            A(2,3)=0.785969130D0
ISN 0015            A(2,4)=0.996430663D0
ISN 0016            A(2,5)=0.019755842D0
ISN 0017            A(2,6)=-0.965425329D0
ISN 0018            B(1,1)=-0.929246776D0
ISN 0019            B(1,2)=0.999984769D0
ISN 0020            B(1,3)=-0.801051898D0
ISN 0021            B(1,4)=-0.322025056D0
ISN 0022            B(1,5)=0.869738536D0
ISN 0023            B(1,6)=0.501047571D0
```

```
ISN 0024            B(2,1)=-0.633834567800
ISN 0025            B(2,2)=0.866896749100
ISN 0026            B(2,3)=-0.618265741D0
ISN 0027            B(2,4)=-0.084415244500
ISN 0028            B(2,5)=0.999804834300
ISN 0029            B(2,6)=0.260679751400
C-----------------------------------------------------------------------
C
C     COMPUTE THE COEFFICIENTS AA AND BB OF THE TRIGONOMETRIC EXPRESSION
C
C                              AA*COS(W*T+V)+BB*SIN(W*T+V),
C
C     FOR THE CONSTITUENT II, WHERE W IS IT'S FREQUENCY, T IS THE U.T.
C     OF THE DAY AND V IS THE ASTRONOMIC ARGUMENT OF THE CONSTITUENT AT
C     00 HOURS U.T. OF THE DAY.
C
ISN 0030            D=A(1,II)*B(2,II)-A(2,II)*B(1,II)
ISN 0031            DX=DEFORM(1,II)*B(2,II)-B(1,II)*DEFORM(2,II)
ISN 0032            DY=A(1,II)*DEFORM(2,II)-DEFORM(1,II)*A(2,II)
ISN 0033            AA=DX/D
ISN 0034            BB=DY/D
C-----------------------------------------------------------------------
C
C     COMPUTE THE AMPLITUDE AND THE PHASE OF THE CONSTITUENT II USING
C     THE FORMULAE:
C                              AMP=SQRT(AA**2+BB**2),
C                                GPH=ARCTAN(BB/AA).
C
ISN 0035            AMP=DSQRT(AA**2+BB**2)
ISN 0036            A0=DABS(AA)
ISN 0037            B0=DABS(BB)
ISN 0038            ARC=DATAN(B0/A0)*57.295779513100
ISN 0039            IF (BB.LT.0) GO TO 20
ISN 0041            IF (AA.LT.0) GO TO 10
ISN 0043            GPL=ARC
ISN 0044            GO TO 40
ISN 0045         10 GPL=180.D0-ARC
ISN 0046            GO TO 40
ISN 0047         20 IF (AA.GT.0) GO TO 30
ISN 0049            GPL=180.D0+ARC
ISN 0050            GO TO 40
ISN 0051         30 GPL=360.D0-ARC
ISN 0052         40 RETURN
ISN 0053            END
```

```
ISN 0002            SUBROUTINE AREA (CLAT,DZ1)
                   C-----------------------------------------------------------------------
                   C
                   C     SUBROUTINE AREA DETERMINES THE AREA OF A MESH CELL OF 1X1 DEGREES
                   C     WITH CENTRE AT THE POINT (CLAT,LONG) IN SQUARE METRES.
                   C
                   C     CALLED FROM: LOAD.
                   C
                   C     INPUT
                   C     =====
                   C
                   C     CLAT = CO-LATITUDE OF THE CENTRE OF THE MESH CELL.
                   C
                   C     OUTPUT
                   C     ======
                   C
                   C     DZ1 = AREA OF THE MESH CELL IN SQUARE METRES.
                   C
                   C     WRITTEN BY SPIROS D. PAGIATAKIS, DECEMBER 1981.
                   C
                   C-----------------------------------------------------------------------
ISN 0003            REAL *8 D0,PI,A,A1,A2,A3,BB,E,DZ1,CLAT,N
ISN 0004            A=6378160.0D0
ISN 0005            E=0.006694605D0
ISN 0006            IF (CLAT.LT.90.) N=DABS(90.5D0-CLAT)
ISN 0008            IF (CLAT.GT.90.) N=DABS(89.5D0-CLAT)
ISN 0010            PI=3.14159265358979D0
ISN 0011            D0=PI/180.D0
ISN 0012            A1=DSQRT(1.0D0-E**2)
ISN 0013            A2=DSIN(D0*(N-0.5D0))
ISN 0014            A3=1.0D0-(E**2)*(A2**2)
ISN 0015            BB=A*A1/A3
ISN 0016            DZ1=2*PI*(BB**2)*(DSIN(D0*N)-DSIN(D0*(N-1)))/360.000
ISN 0017            RETURN
ISN 0018            END
```

```
ISN 0002            SUBROUTINE AZMTH (LATA,LONA,LAT,LON,PSI,AZ)
                   C-----------------------------------------------------------------
                   C
                   C     SUBROUTINE AZMTH COMPUTES THE AZIMUTH OF THE LINE CONNECTING THE
                   C     POINT OF INTEREST AND THE POINT OF LOAD.
                   C
                   C     CALLED FROM: LOAD.
                   C
                   C
                   C     INPUT
                   C     =====
                   C
                   C     LATA = CO-LATITUDE OF THE POINT OF INTEREST IN DEGREES.
                   C     LONA = EAST LONGITUDE OF THE POINT OF INTEREST IN DEGREES.
                   C     LAT  = CO-LATITUDE OF THE POINT OF LOAD IN DEGREES.
                   C     LON  = EAST LONGITUDE OF THE POINT OF LOAD IN DEGREES.
                   C     PSI  = GEOCENTRIC ANGLE BETWEEN THE POINT OF INTEREST AND THE
                   C            POINT OF LOAD, IN DEGREES.
                   C
                   C     OUTPUT
                   C     ======
                   C
                   C     AZ   = AZIMUTH OF THE LINE CONNECTING THE POINT OF INTEREST AND
                   C            THE POINT OF LOAD IN DEGREES.
                   C
                   C     WRITTEN BY: SPIROS D. PAGIATAKIS, MARCH 1982.
                   C
                   C-----------------------------------------------------------------
ISN 0003            REAL *8 LATA,LONA,LAT,LON,LONA0,LON0,A1,A2,D0,A,AZ
ISN 0004            REAL *4 PSI
ISN 0005            D0=3.14159265358979300/180.D0
ISN 0006            IF (LONA.LE.180) LONA0=LONA
ISN 0008            IF (LONA.GT.180) LONA0=180-LONA
ISN 0010            IF (LON.LE.180) LON0=LON
ISN 0012            IF (LON.GT.180) LON0=180-LON
ISN 0014            A1=DCOS(LAT*D0)-DCOS(PSI*D0)*DCOS(LATA*D0)
ISN 0015            A2=DSIN(PSI*D0)*DSIN(LATA*D0)
ISN 0016            A=A1/A2
ISN 0017            IF (A.GE.1) A=1.D0
ISN 0019            IF (A.LE.-1) A=-1.D0
ISN 0021            AZ=DARCOS(A)
ISN 0022            IF (LON0.GT.LONA0) AZ=AZ/D0
ISN 0024            IF (LON0.LE.LONA0) AZ=360-AZ/D0
ISN 0026            RETURN
ISN 0027            END
```

```
ISN 0002              SUBROUTINE KERNEL (KER,RKER,PSI)
                    C-----------------------------------------------------------------
                    C
                    C     SUBROUTINE KERNEL EVALUATES THE INTEGRATION KERNEL FOR A CERTAIN
                    C     GEOCENTRIC ANGLE PSI. USING CUBIC SPLINE INTERPOLATION.
                    C
                    C     CALLED FROM: LOAD.
                    C
                    C     INPUT
                    C     =====
                    C
                    C     PSI = GEOCENTRIC ANGLE  BETWEEN THE POINT OF INTEREST AND THE
                    C           POINT OF LOAD.
                    C
                    C     OUTPUT
                    C     ======
                    C
                    C     RKER = RADIAL DISPLACEMENT INTEGRATION KERNEL.
                    C     KER  = LATERAL DISPLACEMENT INTEGRATION KERNEL.
                    C
                    C     EXTERNALS
                    C     =========
                    C
                    C     REAL FUNCTION SEVALS EVALUATES THE KERNELS COMPUTED BY FARRELL
                    C     (1972) FROM THE COEFFICIENTS OF A CUBIC POLYNOMIAL.
                    C
                    C     VARIABLES
                    C     =========
                    C
                    C     G        = GRAVITATIONAL CONSTANT IN CM3/GR SEC2.
                    C     ME       = MASS OF THE EARTH IN KG.
                    C     R        = RADIUS OF THE EARTH IN METRES.
                    C     GR       = REFERENCE GRAVITY IN METRES/SEC2.
                    C     X        = ABSCISSA VALUE CORRESPONDING TO ANGLE PSI.
                    C     B,C,D,Y  = COEFFICIENTS OF THE CUBIC SPLINE.
                    C
                    C     WRITTEN BY SPIROS D. PAGIATAKIS NOVEMBER 1981.
                    C
                    C-----------------------------------------------------------------
ISN 0003              REAL *8 CI,G,ME,GR,R,PSIO,S2,S3,KER,RKER,S31
ISN 0004              REAL *4 PSI,X(50),B1(50),C1(50),D1(50),Y1(50),S1,S11,
                     *        B(50),C(50),D(50),Y(50)
ISN 0005              INTEGER N
ISN 0006              N=50
ISN 0007              CI=3.14159265358979D0/180.0D0
ISN 0008              G=6.672D-8
ISN 0009              ME=5.974D24
ISN 0010              R=6.371D6
ISN 0011              GR=9.81D0
```

```
ISN 0012          PSIO=DBLE(PSI)
ISN 0013          DATA X/0.0001,0.001,0.01,0.02,0.03,0.04,0.06,0.08,0.1,0.16,0.2,
                 *0.25,0.3,0.4,0.5,0.6,0.8,1.0,1.2,1.6,2.0,2.5,3.0,4.0,5.,6.,7.,8.,
                 *9.,10.,12.,16.,20.,25.,30.,40.,50.,60.,70.,80.,90.,100.,110.,120.,
                 *130.,140.,150.,160.,170.,180./
ISN 0014          DATA B/88.68365,89.09149,89.87742,88.52584,87.0204,85.39413,
                 *81.59371,75.73112,69.98127,50.45112,39.00871,27.87202,19.90376,
                 *10.53396,6.060144,4.225441,3.327042,3.466377,3.50744,3.222597,
                 *2.74966,2.210661,1.751688,1.106537,0.7101553,0.4658393,0.3214873,
                 *0.2312117,0.1756652,0.1431246,0.109921,0.9297513E-1,0.9792816E-1,
                 *0.1089537,0.119657,0.1231491,0.1011455,0.626682E-1,0.1868154E-1,
                 *-0.2309424E-1,-0.5830476E-1,-0.8478686E-1,-0.1029475,-0.1130224,
                 *-0.1157619,-0.1118291,-0.1014214,-0.8518505E-1,-0.6333833E-1,0.0/
ISN 0015          DATA C/237.749,215.4141,-128.0876,-7.070815,-143.4733,-19.15434,
                 *-170.8666,-122.2634,-165.228,-160.2745,-125.7859,-96.94793,
                 *-62.41717,-31.28083,-13.45739,-4.889625,0.3976281,0.2990446,
                 *-0.9373021E-1,
                 *-0.6183763,-0.563968,-0.5140285,-0.4039167,-0.2412346,
                 *-0.1551482,-0.8916753E-1,-0.551844E-1,-0.3509115E-1,-0.2045537E-1,
                 *-0.1208516E-1,
                 *-0.451669E-2,0.2802172E-3,0.9580501E-3,0.1247051E-2,
                 * 0.8936205E-3,-0.5444141E-3,-0.1655951E-2,-0.219178E-2,
                 *-0.2206885E-2,-0.1970693E-2,-0.1550356E-2,-0.1097854E-2,
                 *-0.7182224E-3,-0.2892659E-3,0.1531781E-4,0.3779658E-3,
                 * 0.662805E-3,0.9608315E-3,0.1223836E-2,0.0/
ISN 0016          DATA D/-8272.195,-12722.28,4033.895,-4546.75,4143.964,-2528.536,
                 *810.0529,-716.0742,27.51896,287.406,192.253,230.205,103.7877,
                 *59.41151,28.5592,8.812088,-0.1643058,-0.6546252,-0.4372043,
                 *0.4534025E-1,0.33293E-1,0.7340788E-1,0.5422735E-1,0.2869545E-1,
                 *0.2199357E-1,0.113272E-1,0.6697751E-2,0.4878591E-2,0.27900071E-2,
                 *0.1261411E-2,0.3997422E-3,0.5648605E-4,0.19266677E-3,-0.2356208E-4
                 *,-0.4793447E-4,-0.37051121E-4,-0.1786096E-4,-0.5035195E-6,
                 *0.7873098E-5,0.1401121E-4,0.1508339E-4,0.126544E-4,0.1429854E-4,
                 *0.1015279E-4,0.1208827E-4,0.9494632E-5,0.9934215E-5,0.8766841E-5,
                 *0.9000277E-5,0.0/
ISN 0017          DATA Y/-33.63999,-33.55999,-32.75,-31.86,-30.97999,-30.11999,
                 *-28.44,-26.86999,-25.41,-21.8,-20.02,-18.368,-17.17999,-15.71,
                 *-14.90999,-14.40999,-13.68999,-13.01,-12.31,-10.94999,-9.756999,
                 *-8.519,-7.532999,-6.130999,-5.237,-4.659999,-4.272,-3.998999,
                 *-3.798,-3.64,-3.392,-2.998999,-2.619,-2.102999,-1.529999,
                 *-0.2919999,0.8479999,1.675999,2.083,2.057,1.642999,0.92,
                 *-0.2499999E-1,-1.112,-2.260999,-3.404999,-4.475999,-5.413999,
                 *-6.161,0.0/
```

```
ISN 0018          DATAB1/-0.1089914,0.1084709,2.036993,3.982547,6.032793,7.886245,
                 *11.11684,13.64647,15.29719,16.78269,15.30119,12.57496,9.758868,
                 *5.396829,2.673806,1.157958,0.1846549,0.3984202,0.7566754,
                 *1.1881,1.24091,1.120029,0.9569666,0.6581335,0.4454995,0.295867,
                 *0.1950311,0.1300093,0.8293056E-1,0.5426794E-1,0.2753351E-1,
                 *0.1201266E-1,0.1291584E-1,0.1720066E-1,0.2328102E-1,0.3261248E-1,
                 *0.3196917E-1,0.1951079E-1,0.687588E-3,-0.1746118E-1,-0.3044285E-1,
                 *-0.3596739E-1,-0.3328746E-1,-0.2378264E-1,-0.9282138E-2,
                 *0.8111041E-2,0.266381E-1,0.4463656E-1,0.597156E-1,0.0/
ISN 0019          DATAC1/121.6815,119.9417,94.33859,100.2166,104.8079,80.53706,
                 *80.99313,45.48814,37.04786,-12.28934,-24.74835,-29.77619,
                 *-26.54576,-17.07464,-10.15557 ,-5.002902,0.1363839,0.9324422,
                 *0.8588358,0.219727,-0.8770143E-1,-0.1540607,-0.1720664,-0.1267665,
                 *-0.858674E-1,-0.6376487E-1,-0.3707101E-1,-0.2795077E-1,-0.19128E-1
                 *,-0.9534657E-2,-0.3832558E-2,-0.4765622E-4,0.273453E-3,
                 *0.5835094E-3,0.6325603E-3,0.3005855E-3,-0.3649157E-3,-0.8809212E-3
                 *,-0.1001399E-2,-0.8134776E-3,-0.4846886E-3,-0.6776554E-4,
                 *0.3357585E-3,0.6147238E-3,0.8353258E-3,0.903991E-3,0.9487154E-3,
                 *0.8511305E-3,0.6567731E-3,0.0/
ISN 0020          DATAD1/-644.3786,-948.2658,195.935,153.0425,-809.0285,7.601165,
                 *-591.75,-140.6709,-274.0954,-103.8252,-33.51892,21.53625,
                 *31.5704,23.06358,17.17555,8.565473,1.326763,-0.1226774,
                 *-0.5325897,-0.2561906,-0.4423953E-1,-0.120038E-1,0.1509996E-1,
                 *0.1363305E-1,0.7367499E-2,0.8897967E-2,0.3040079E-2,0.2940922E-2,
                 *0.3197782E-2,0.9503499E-3,0.3154084E-3,0.2675912E-4,0.2067041E-4,
                 *0.3270068E-5,-0.1106583E-4,-0.2218337E-4,-0.1720017E-4,
                 *-0.4015932E-5,0.6264051E-5,0.1095962E-4,0.1389744E-4,0.134508E-4,
                 *0.929885E-5,0.7353391E-5,0.2288841E-5,0.1490814E-5,
                 *-0.3252829E-5,-0.6478581E-5,-0.5833412E-5,0.0/
ISN 0021          DATAY1/-11.25,-11.25,-11.23999,-11.21,-11.15999,-11.09,-10.89999,
                 *-10.64999,-10.35999,-9.368,-8.722999,-8.024,-7.467,-6.725,-6.333,
                 *-6.149999,-6.05,-5.996999,-5.880999,-5.475,-4.980999,-4.387999,
                 *-3.868,-3.067999,-2.522999,-2.156,-1.914999,-1.753999,-1.649,
                 *-1.581999,-1.503999,-1.435,-1.385999,-1.312,-1.211,-0.9259999,
                 *-0.592,-0.3259999,-0.2229999,-0.31,-0.555,-0.8939999,-1.246999,
                 *-1.536999,-1.706,-1.713,-1.539999,-1.182,-0.657,0.0/
ISN 0022          S11=SEVALS(N,PSI,X,Y,B,C,D)/(PSI*CI)
ISN 0023          S31=(ME/(R**2))*1.D-12*DBLE(S11)+0.27D0
ISN 0024          S1=SEVALS(N,PSI,X,Y1,B1,C1,D1)/(PSI*CI)
ISN 0025          S2=-(G*1.027D0)/(R*GR*1.D4)
ISN 0026          S3=(ME/R**2)*1.D-12*DBLE(S1)
ISN 0027          KER=S2*S3
ISN 0028          RKER=S31*G*1.027D0/(R*1.D4*GR)
ISN 0029          RETURN
ISN 0030          END
```

```
ISN 0002            SUBROUTINE LOAD (COLAT,ELONG,AII,LOADUP,LLAT,LLON,II)
C-----------------------------------------------------------------------
C
C     SUBROUTINE LOAD COMPUTES THE RADIAL AND LATERAL (N-S, E-W)
C     DISPLACEMENTS OF THE EARTH'S CRUST DUE TO OCEAN TIDE LOADING.
C
C     CALLED FROM: MAIN.
C
C     INPUT
C     =====
C
C     1. COLAT   = COLATITUDE OF THE POINT OF INTEREST IN RADIANS.
C     2. ELONG   = EAST LONGITUDE OF THE POINT OF INTEREST IN DEGREES.
C     3. AII     = MODIFIED JULIAN DAYS ELAPSED SINCE THE BEGINNING
C                  OF THE YEAR.
C     4. II      = CONSTITUENT NUMBER.
C
C     OUTPUT
C     ======
C
C     1. LOADUP = RADIAL DISPLACEMENT OF THE EARTH'S CRUST IN CM
C                 (POSITIVE UPWARDS).
C     2. LLAT   = NORTH-SOUTH DISPLACEMENT IN CM (POSITIVE NORTHWARDS).
C     3. LLON   = EAST-WEST DISPLACEMENT IN CM (POSITIVE WESTWARDS).
C
C     EXTERNALS
C     =========
C
C     1. SUBROUTINE TIDE COMPUTES THE PARTIAL OCEAN TIDAL HEIGHT FOR
C        EACH OF THE FIRST SIX LEADING CONSTITUENTS OF THE TIDAL
C        SPECTRUM.
C
C     2. SUBROUTINE AREA COMPUTES THE AREA OF THE MESH CELL UNDER
C        CONSIDERATION.
C
C     3. SUBROUTINE PSI0 COMPUTES THE GEOCENTRIC ANGLE BETWEEN THE POINT
C        OF INTEREST AND THE POINT OF LOAD.
C
C     4. SUBROUTINE KERNEL EVALUATES THE INTEGRATION KERNEL
C        CORRESPONDING TO THE GEOCENTRIC ANGLE PSI DETERMINED BY
C        SUBROUTINE PSI0.
C
C     5. SUBROUTINE AZMTH COMPUTES THE AZIMUTH CONNECTING THE POINT OF
C        INTEREST AND THE POINT OF LOAD.
```

```
C
C     VARIABLES
C     =========
C
C     AI1       = DAYS ELAPSED SINCE THE BEGINNING OF THE YEAR IYEAR
C                 UP TO THE TIME OF OBSERVATION.
C     NA        = LONGITUDE NUMBER.
C     K         = CO-LATITUDE NUMBER.
C     LAT       = CO-LATITUDE OF THE POINT OF LOAD IN DEGREES.
C     LON       = EAST LONGITUDE OF THE POINT OF LOAD IN DEGREES.
C
C     WRITTEN BY SPIROS D. PAGIATAKIS, DECEMBER 1981.
C
C-----------------------------------------------------------------------
ISN 0003        REAL *8 AI1,TZ,VOL,LOAD,LOADUP,COLAT,ELONG,LATA,LONA,LAT,LON,
               *        DZ1,KER,D0,AMJD,AJD1,LLAT,LLON,AZ,RKER
ISN 0004        REAL *4 PSI,AMJDN
ISN 0005        INTEGER N
ISN 0006        DIMENSION TABL(361),TABL2(361),L1(30),L11(30),M1(30),M11(30)
ISN 0007        DATA L1/23,20,21,64,47,47,64,30,28,40,27,12,8,64,64,17,64,36,58,
               *        8,51,58,32,84,84,110,84,80,94,160/
ISN 0008        DATA M1/65,29,31,85,65,65,72,52,53,48,48,22,21,73,71,24,78,48,72,
               *        13,60,66,46,119,108,123,126,106,113,168/
ISN 0009        DATA L11/14,120,196,0,0,354,345,236,120,0,10,244,306,43,73,68,98,
               *         137,255,272,243,248,286,15,33,118,290,284,307,0/
ISN 0010        DATA M11/120,181,285,43,15,361,361,287,138,11,15,281,339,57,86,
               *        121,107,143,263,307,281,256,296,34,40,152,308,291,319,165/
ISN 0011        D0=180.D0/3.14159265358979D0
ISN 0012        LOADUP=0.D0
ISN 0013        LLAT=0.D0
ISN 0014        LLON=0.D0
ISN 0015        LATA=COLAT*D0
ISN 0016        LONA=ELONG*D0
ISN 0017        N=1976
C-----------------------------------------------------------------------
C
C     EVALUATE THE DISPLACEMENT OF THE EARTH'S CRUST BY INTEGRATING
C     THE TIDAL HIGHT ALL OVER THE OCEANS WITH GREEN'S FUNCTIONS
C     (INTEGRATION KERNELS).
C
ISN 0018        DO 70 NA=2,168
ISN 0019        DO 60 K=1,360
ISN 0020        DO 10 I=1,30
ISN 0021        IF (NA.GT.L1(I).AND.NA.LT.M1(I)) GO TO 20
ISN 0023     10 CONTINUE
ISN 0024        GO TO 30
```

```
ISN 0025          20 IF (K.GT.L11(I).AND.K.LT.M11(I)) GO TO 60
ISN 0027          30 CALL TIDE (NA,K,N,A11,TZ,I1)
ISN 0028             IF (TZ.EQ.0.0) GO TO 40
ISN 0030             LAT=(NA-0.5)*1.0D0
ISN 0031             LON=(K-0.5)*1.0D0
ISN 0032             CALL AREA (LAT,DZ1)
ISN 0033             VOL=TZ*DZ1*1.0D6
ISN 0034             CALL PSI0 (LATA,LONA,LAT,LON,PSI)
ISN 0035             CALL KERNEL (KER,RKER,PSI)
ISN 0036             LOAD=KER*VOL
ISN 0037             RLOAD=RKER*VOL
ISN 0038             GO TO 50
ISN 0039          40 LOAD=0.D0
ISN 0040             RLOAD=0.D0
ISN 0041          50 CALL AZMTH (LATA,LONA,LAT,LON,PSI,AZ)
ISN 0042             LLAT=LLAT+LOAD*DCOS(AZ/D0)
ISN 0043             LLON=LLON-LOAD*DSIN(AZ/D0)
ISN 0044             LOADUP=LOADUP+RLOAD
ISN 0045          60 CONTINUE
ISN 0046          70 CONTINUE
                C-------------------------------------------------------------------
ISN 0047             RETURN
ISN 0048             END
```

```
ISN 0002            SUBROUTINE PSI0 (LATA,LONA,LAT,LON,PSI)
                C-----------------------------------------------------------------
                C
                C     SUBROUTINE PSI0 DETERMINES THE SPHERICAL ANGLE PSI, DEFINED BY THE
                C     THE POINT OF INTEREST AND THE POINT OF LOAD.
                C
                C     CALLED FROM: LOAD.
                C
                C     INPUT
                C     =====
                C
                C     LATA  = CO-LATITUDE OF THE POINT OF INTEREST.
                C     LONA  = EAST LONGITUDE OF THE POINT OF INTEREST.
                C     LAT   = CO-LATITUDE OF THE POINT OF LOAD.
                C     LON   = EAST LONGITUDE OF THE POINT OF LOAD.
                C
                C     OUTPUT
                C     ======
                C
                C     PSI   = GEOCENTRIC SPHERICAL ANGLE IN DEGREES.
                C
                C     VARIABLES
                C     =========
                C
                C     LATA0 = LATITUDE OF THE POINT OF INTEREST (NORTH OR SOUTH).
                C     LONA0 = LONGITUDE OF THE POINT OF INTEREST (EAST OR WEST).
                C     LAT0  = LATITUDE OF THE POINT OF LOAD ( NORTH OR SOUTH ).
                C     LON0  = LONGITUDE OF THE POINT OF LOAD ( EAST OR WEST ).
                C
                C     NOTICES
                C     =======
                C
                C     ALL THE INPUT ANGLES AS WELL AS THE VARIABLES ARE IN DEGREES.
                C
                C     NORTH LATITUDE AND EAST LONGITUDE ARE CONSIDERED POSITIVE WHILE
                C     SOUTH LATITUDE AND WEST LONGITUDE ARE CONSIDERED NEGATIVE.
                C
                C     WRITTEN BY: SPIROS D. PAGIATAKIS, DECEMBER  1981.
                C
                C-----------------------------------------------------------------
ISN 0003            REAL *8 LATA,LATA0,LONA,LONA0,LAT,LAT0,LON,LON0,D0,P1,P2
ISN 0004            REAL *4 PSI
ISN 0005            D0=3.14159265358979D0/180.0D0
ISN 0006            LATA0=90-LATA
ISN 0007            LAT0=90-LAT
```

```
ISN 0008            IF (LONA.LE.180) LONA0=LONA
ISN 0010            IF (LONA.GT.180) LONA0=180-LONA
ISN 0012            IF (LON.LE.180) LON0=LON
ISN 0014            IF (LON.GT.180) LON0=180-LON
ISN 0016           P1=DSIN(LATA0*D0)*DSIN(LAT0*D0)
ISN 0017           P2=DCOS(LATA0*D0)*DCOS(LAT0*D0)*DCOS((LON0-LONA0)*D0)
ISN 0018           PSI=DARCOS(P1+P2)/D0
ISN 0019           RETURN
ISN 0020           END
```

```
ISN 0002            REAL FUNCTION SEVALS (N,U,X,Y,B,C,D)
                   C-----------------------------------------------------------------------
                   C
                   C     REAL FUNCTION SEVALS EVALUATES THE KERNELS COMPUTED BY FARRELL
                   C     (1972) FROM THE COEFFICIENTS OF A CUBIC POLYNOMIAL.
                   C
                   C     CALLED FROM: KERNEL.
                   C
                   C-----------------------------------------------------------------------
ISN 0003            INTEGER N
ISN 0004            REAL U,X(N),Y(N),B(N),C(N),D(N)
ISN 0005            REAL DX
ISN 0006            INTEGER I,J,K
ISN 0007            DATA I/1/
ISN 0008            IF (I.GE.N) I=1
ISN 0010            IF (U.LT.X(I)) GO TO 10
ISN 0012            IF (U.LE.X(I+1)) GO TO 30
ISN 0014         10 I=1
ISN 0015            J=N+1
ISN 0016         20 K=(I+J)/2
ISN 0017            IF (U.LT.X(K)) J=K
ISN 0019            IF (U.GE.X(K)) I=K
ISN 0021            IF (J.GT.I+1) GO TO 20
ISN 0023         30 DX=U-X(I)
ISN 0024            SEVALS=Y(I)+DX*(B(I)+DX*(C(I)+DX*D(I)))
ISN 0025            RETURN
ISN 0026            END
```

```
ISN 0002            SUBROUTINE TIDE (NA,K,N,AII,TZ,II)
C-----------------------------------------------------------------------
C
C     SUBROUTINE TIDE COMPUTES THE PARTIAL OCEAN TIDE ALL OVER THE GLOBE
C     FOR EACH OF THE FIRST SIX LEADING CONSTITUENTS OF THE TIDAL
C     SPECTRUM.
C
C     THE MODEL IN USE IS THE N.S.W.C. HYDRODYNAMICALLY INTERPOLATED
C     MODEL DEVELOPED BY SCHWIDERSKI (1978).
C
C     THE TIDAL CONSTANTS (AMPLITUDES AND PHASES) ON A 1X1 DEGREE GRID
C     ARE STORED ON THE SURVEYING ENGINEERING DISK (SE0002, UNB
C     COMPUTING CENTRE) UNDER THE FOLLOWING CHARACTERISTICS:
C
C     FILE 1(2016,2888,L,N1), DSN=SPIROS.SEADATA,UNIT=M3330.
C
C     CALLED FROM: LOAD.
C
C     CONSTITUENTS
C     ============
C
C     I=1  M2
C       2  S2
C       3  K1
C       4  O1
C       5  N2
C       6  P1
C
C     INPUT
C     =====
C
C     1. NA   = LONGITUDE NUMBER.
C     2. K    = CO-LATITUDE NUMBER.
C     3. N    = YEAR OF THE OBSERVATION.
C     4. AII  = DAYS ELAPSED SINCE THE BEGINNING OF THE YEAR N UP TO THE
C               TIME OF OBSERVATION.
C     5. II   = I
C
C     OUTPUT
C     ======
C
C     1. TZ   = TOTAL TIDAL HEIGHT IN METRES.
C
C     EXTERNALS
C     =========
C
C     FILE 1(2016,2888,L,N1) DISK=SE0002.
C
```

```
C      VARIABLES
C      =========
C
C      F(I)    = THE FREQUENCY OF THE CONSTITUENT I IN RADIANS/HOUR.
C      V1,V2,V3,V4,V5,V6  = THE ASTRONOMICAL ARGUMENTS OF THE SIX
C                           CONSTITUENTS CORRESPONDING TO 1ST JAN. 1976
C                           AT 00 HOURS U.T.
C      F1,F2,F3,F4,F5,F6  = THE NODAL CORRECTIONS TO THE AMPLITUDES FOR
C                           THE YEAR 1976.
C      TABL (K) = TABLE OF AMPLITUDES IN METRES FOR THE CO-LATITUDE
C                 NUMBER K.
C      TABL2(K) = TABLE OF GREENWICH PHASES FOR THE CO-LATITUDE NUMBER K
C                 IN DEGREES (0-360).
C      Z(II)    = PARTIAL OCEAN TIDE OF THE CONSTITUENT II IN METRES.
C      ARG      = THE ARGUMENT OF THE COSINE TERM OF THE PARTIAL TIDE.
C
C      WRITTEN BY SPIROS D. PAGIATAKIS OCTOBER, 1981
C
C-----------------------------------------------------------------------
ISN 0003        REAL*8 F,D,AB1,B1,TD,H0,S0,P0,X,Z,TZ,A11,V1,V2,V3,V4,V5,V6,F1,F2,
               *F3,F4,F5,F6,ARG
ISN 0004        INTEGER N,NREC
ISN 0005        DIMENSION F(6),Z(6),TABL(361),TABL2(361),V(6),F1(6)
ISN 0006        DEFINE FILE 1(2016,2888,L,N1)
ISN 0007        DATA F/.5058684,.5235984,.2625156,.2433528,.496368,.2610828/
ISN 0008        DATA V/26.1,359.9,16.1,6.3,305.3,350.6/
ISN 0009        DATA F1/1.029,0.998,0.916,0.862,1.026,1.009/
ISN 0010        D=3.14159265358979D0/180.D0
C-----------------------------------------------------------------------
C
C      COMPUTE THE PARTIAL OCEAN TIDE
C
ISN 0011        NREC=NA+(II-1)*168
ISN 0012        READ (1'NREC) TABL,TABL2
ISN 0013        IF (TABL(K).GT.3.0) GO TO 50
ISN 0015        ARG=F(II)*A11*24.D0+V(II)*D-TABL2(K)*D
ISN 0016        Z(II)=F1(II)*TABL(K)*DCOS(ARG)
ISN 0017        TZ=Z(II)
ISN 0018        GO TO 60
ISN 0019     50 TZ=0.0D0
ISN 0020     60 RETURN
ISN 0021        END
```

OCEAN TIDE LOADING DEFORMATIONS OF THE LITHOSPHERE

STATION NAME = DIONYSSOS SATELLITE TRACKING CENTER
CO-LATITUDE = 51 55 14.000 (D MIN SEC)
EAST LONGITUDE = 23 56 1.000 (D MIN SEC)

CONSTITUENT	RADIAL DISP. (CM) (OUTWARDS +)		N-S DISP. (CM) (NORTH +)		E-W DISP. (CM) (WEST +)	
	AMP.	PHASE	AMP.	PHASE	AMP.	PHASE
M2	0.36	41.1	0.11	255.0	0.09	333.4
S2	0.11	48.0	0.03	275.3	0.05	348.2
K1	0.15	171.3	0.03	307.5	0.06	250.6
O1	0.07	168.6	0.02	279.2	0.04	250.3
N2	0.06	33.7	0.03	250.3	0.02	331.7
P1	0.05	156.9	0.01	311.1	0.02	253.5

REFERENCES

Alterman, Z., H. Jarosch and C.L. Pekeris (1961), "Propagation of Rayleigh waves in the earth", Geophysical Journal of the Royal Astronomical Society, 4, 219-241.

Altmann, W., H.J. Dittfeld and C. Eistner (1977), Results of gravimetric earth-tide observations 1970-1976. Presented at the 8th International Symposium on Earth Tides, Institut fur Theoretische Geodasie der Universitat Bonn, 19-24 Sept.

Apostol, T.M. (1962), Calculus, Vol. 1, Blaisdell Publishing Company, New York.

Beaumont, C. and A. Lambert (1972), "Coastal structure from surface load tilts, using a finite element model", Geophysical Journal of the Royal Astronomical Society, 29, 203-226.

Boussinesq, J. (1885), Application des Potentiels a l' Étude de l'Équilibre et du Mouvement des Solides Élastiques, Gauthier-Villars, Paris.

Bretreger, K. and R.S. Mather (1978), "Modelling ocean loading effects on tidal gravity in Australia", Geophysical Journal of the Royal Astronomical Society, 52, 241-257.

Bullen, K.E. (1975), The Earth's Density, John Wiley and Sons, New York.

Bureau Internatinal de l' Heure (1980), Annual Report for 1979, Paris.

Cannon, W.H. (1978), "The classical analysis of the response of a long baseline interferometer", Geophysical Journal of the Royal Astronomical Society, 53, 503-530.

Cathles, L.M. (1971), The viscosity of the earth's mantle, Ph.D Thesis, Princeton University, Princeton, N.J.

Chiaruttini, C. and E. Livieratos (1978), "Oceanic loading on European laser ranging sites", Geophysical Journal of the Royal Astronomical Society, 54, 593-600.

Courant, R. and D. Hilbert (1970), Methods of Mathematical Physics, Interscience Publishers Inc., New York.

Davidson, D.A. (1980), A least squares adjustment for long baseline interferometry, M.Sc. Thesis, Dept. of Surveying Engineering, U.N.B., Fredericton N.B.

Eirich, R.F. (1950), Rheology, Vol 1, Academic Press, New York.

Farrell, W. E. (1972), "Deformation of the earth under surface mass loads", Reviews of Geophysics and Space Physics, Vol. 10, 3, 761-797.

Goad, C. C. (1979), Gravimetric tidal loading computed from integrated Green's functions, NOAA Technical Memorandum NOS NGS 22, Rockville, MD.

Godin, G. (1972), The Analysis of Tides, University of Toronto Press, Toronto, Ontario.

Godin, G. (1980), Cotidal charts for Canada, Manuscript report series No 55, Marine Sciences and Information Directorate, Dept. of Fisheries and Oceans, Ottawa, Ontario.

Haddon, R.A.W. and K.E. Bullen (1969), "An earth model incorporating free earth oscillation data", Physics of the Earth and Planetary Interiors, 2, 35-49.

Henriksen, S.W. (1977), Systems for the determination of polar motion, NOAA Technical Report NOS 72 NGS 7, Rockville, MD.

Hosoyama, K. (1977), On the tidal constant of gravity at Mizusawa. Proceedings of the 8th International Symposium on Earth Tides, Institut für Theoretische Geodäsie der Universitat Bonn, 19-24 Sept., 593-596.

Improved Lunar Ephemeris 1952-1959 (1954): A Joint Supplement to the American Ephemeris and the (British) Nautical Almanac, United States Government Printing Office, Washington.

Jeffreys, H. (1976), The Earth, Cambridge University Press, London.

Kuo, J.T. (1977), Tidal corrections at McDonald and Haleakala, Scientific Applications of Lunar Laser Ranging, 241-254, Reidel Publishing Company, Holland.

Langley, R.B. (1979), Precision geodesy and astrometry with a three station long baseline interferometer, Ph.D Thesis, York University, Toronto, Ontario.

Longman, I.M. (1962), "A Green's function for determining the deformation of the earth under surface mass loads. 1. Theory", Journal of Geophysical Research, Vol. 67, 2, 845-850.

Longman, I.M. (1963), "A Green's function for determining the deformation of the earth under surface mass loads. 2. Computational results", Journal of Geophysical Research, Vol. 68, 2, 485-496.

Melchior, P. (1966), The Earth Tides, Pergamon Press, Oxford.

Melchior, P. (1978), The Tides of the Planet Earth, Pergamon Press, Oxford.

Melchior, P., J.T. Kuo and B. Ducarme (1976), "Earth tide gravity maps for western Europe", Physics of the Earth and Planetary Interiors, 13, 184-196.

Merriam, J.B. (1978), A parametarized earth tide model for advanced geodynamics, Technical Report, Department of Earth and Environmental Sciences, York University, Toronto, Ontario.

Merriam, J.B. (1980), "The series computation of the gravitational perturbation due to an ocean tide", Physics of the Earth and Planetary Interiors, 23, 81-86.

Merriam, J.B. (1981), "An investigation of dispersive effects on tidal gravity measurements at Alice Springs", Physics of the Earth and Planetary Interiors, 27, 187-193.

Mikhlin, S.G. (1967), Linear Equations of Mathematical Physics, Holt, Rinehart and Winston, Inc., New York.

Moens, M. (1976), "Solid earth tide and Arctic oceanic loading tide at Longyearbyen (Spitsbergen)", Physics of the Earth and Planetary Interiors, 13, 197-211.

Moens, M. (1980), "About the relation between Love numbers and load numbers in earth tides theory", Manuscripta Geodaetica, Vol. 5, 217-233.

Munk, W.H. and G.J.F. MacDonald (1960), The Rotation of the Earth, Cambridge University Press, London.

Nadeau, G. (1964), Introduction to Elasticity, Rinehart and Winston, New York.

Pekeris, C.L. (1978), "The bodily tide and the yielding of the earth due to tidal loading", Geophysical Journal of the Royal Astronomical Society, 52, 471-478.

Pekeris, C.L. and H. Jarosch (1958), The free oscillation of the earth, in Contributions in Geophysics in honour of Beno Gutenberg, Vol. 1. Edited by H. Benioff, M. Ewing, B. Howell and F. Press, Pergamon Press, New York.

Rectorys, K. (editor) (1969), Survey of Applicable Mathematics, M.I.T. Press, Cambridge, MA.

Shapiro, I.I. (1978), Principles of very long baseline interferometry in Dept. of Geodetic Science Report No 280, The Ohio State University, Colombus, Ohio.

Schwiderski, E.W. (1978), Global ocean tides, part I: A detailed hydrodynamical interpolation model, NSWC/DL TR-3866, Naval Surface Weapons Center, Dahlgren, VA.

Schwiderski, E.W. (1979), Global ocean tides, part II: The semidiurnal principal lunar tide (M2), Atlas of tidal charts and maps, NSWC TR 79-414, Naval Surface Weapons Center, Dalhgren, VA.

Schwiderski, E.W. (1981a), Global ocean tides, part III: The semidiurnal principal solar tide (S2), Atlas of tidal charts and maps, NSWC TR 81-122, Naval Surface Weapons Center, Dalhgren, VA.

Schwiderski, E.W. (1981b), Global ocean tides, part IV: The diurnal luni-solar declination tide (K1), Atlas of tidal charts and maps, NSWC TR 81-142, Naval Surface Weapons Center, Dalhgren, VA.

Schwiderski, E.W. (1981c), Global ocean tides, part V: The diurnal principal lunar tide (O1), Atlas of tidal charts and maps, NSWC TR 81-144, Naval Surface Weapons Center, Dalhgren, VA.

Schwiderski, E.W. (1981d), Global ocean tides, part VI: The semidiurnal elliptical lunar tide (N2), Atlas of tidal charts and maps, NSWC TR 81-218, Naval Surface Weapons Center, Dalhgren, VA.

Schwiderski, E.W. (1981e), Global ocean tides, part VII: The diurnal principal solar tide (P1), Atlas of tidal charts and maps, NSWC TR 81-220, Naval Surface Weapons Center, Dalhgren, VA.

Schwiderski, E.W. (1981f), Global ocean tides, part VIII: The semidiurnal luni-solar declination tide (K2), Atlas of tidal charts and maps, NSWC TR 81-222, Naval Surface Weapons Center, Dalhgren, VA.

Schwiderski, E.W. and L.T. Szeto (1981), The NSWC Global Ocean Tide Data Tape (GOTD), its features and application, random-point tide program, NSWC TR 81-254, Naval Surface Weapons Center, Dalhgren, VA.

Suklje, L. (1969), Rheological Aspects of Soil Mechanics, Wiley-Interscience, London.

Torge, W. and H.G. Wenzel (1977), Comparison of tide observations with nine different gravimeters at Hannover, Proceedings of the 8th International Symposium on Earth Tides, Institut für Theoretische Geodäsie der Universitat Bonn, 19-24 Sept., 632-640.

Vaníček, P. (1978), Loading effects, personal notes, (unpublished).

Vaníček, P. (1980), Tidal corrections to geodetic quantities, NOAA Technical Report, NOS 83 NGS 14, Rockville, MD.

Vaníček, P. and E. Krakiwsky (1982), Geodesy: The Concepts, North Holland, Amsterdam.

Wahr, J.M. and T. Sasao (1981), "A diurnal resonance in the ocean tide and in the earth's load response due to the resonant free 'core nutation'", Geophysical Journal of the Royal Astronomical Society, 64, 747-765.

Warburton, R.J., C. Beaumont and J.M. Goodkind (1975), "The effect of ocean tide loading on tides of the solid earth observed with a superconducting gravimeter", Geophysical Journal of the Royal Astronomical Society, 43, 707-720.

Zschau, J. (1976), "Tidal sea load tilt of the crust and its application to the study of crustal and upper mantle structure", Geophysical Journal of the Royal Astronomical Society, 44, 577-593.